Electronic Supplementary Material (ESI) for Dalton Transactions.

Supplementary Information

Non-symmetric benzo[b]-fused BODIPYs as a versatile fluorophore platform reaching the NIR: A systematic study of the underlying structure–property relationship

André Bessette,[1,2] Thomas Auvray,[1] Dr Denis Désilets[2] Prof. Garry S. Hanan[1].*

[1] Département de Chimie, Université de Montréal, Pavillon J.-A. Bombardier, 5155 Decelles Avenue, Montréal, Québec, H3T-2B1, Canada

[2] PCAS Canada Inc., 725 Trotter street, Saint-Jean-sur-Richelieu, Québec, J3B 8J8, Canada.

Table of Contents

Materials and Instrumentation

Asymmetric benzo[b]-fused BODIPYs (BbF) **1** – **10** were obtained by adaptation of the synthetic procedure first reported by Wakamiya *et al.* for a similar derivative.[1] The synthesis of aryl-pyrrole derivatives **11** – **20** was done by palladium-catalyzed cross-coupling of pyrrole anions with aryl halides following an adapted procedure from Sadighi *et al*.[2, 3] and all characterizations matched previously reported literature for compounds **11** – **18**.[2, 4-6] The compound (1*H*-indol-2-yl)(phenyl)methanone **21** was synthesized following the procedure from Zhang *et al*.[7] Reagents and solvents were obtained commercially and used without further purification. Reactions were carried out under ambient atmosphere unless otherwise stated. Solvents were removed under reduced pressure using a rotary evaporator unless otherwise stated.

Nuclear magnetic resonance (NMR) spectra were recorded in $CDCl_3$ at room temperature (r.t.). 300 MHz ^{1}H and 75 MHz ^{13}C NMR of BbF **1** – **4** and **7** – **10** along with aryl-pyrrole **19** and **20** were recorded on a Bruker Avance 300 spectrometer. 400 MHz ^{1}H and 100 MHz ^{13}C NMR of BbF **5** and **6** were recorded on a Bruker Avance 400 spectrometer. Chemical shifts are reported in part per million (ppm) relative to residual solvent protons (7.27 ppm) and carbon resonance (77.00 ppm) of the solvent.

High-Resolution Electro Spray Ionization Mass Spectrometry (HR-ESIMS) was performed on a Bruker micrOTOF II for BbF **1** – **10**. Low resolution Electronic Ionization (EI) mass spectrometry for compounds **19** and **20** was performed on a Agilent 6890 Series GC equipped with a 5973 Network Mass Selective Detector module.

Absorption spectra were measured in CH_2Cl_2 (DCM) at concentrations obeying Beer-Lambert's law at r.t. on a Cary 6000i UV-vis-NIR Spectrophotometer. Luminescence measurements were done on a Perkin LS 55 Fluorescence Spectrometer.

Full details on crystal structure determination and refinement data for compounds **1**, **5**, **8** and **9** are reported in corresponding section and on the Cambridge Crystallographic Data Centre (CCDC numbers 1418610 – 1418613).

Electrochemical measurements were carried out in argon-purged CH_2Cl_2 at room temperature with a BAS CV50W multipurpose potentiostat. The working electrode used was a glassy carbon electrode for every compound. The counter electrode was a Pt wire, and the pseudo-reference electrode was a silver wire. The reference was set using an internal 1 mM ferrocene/ferrocenium sample at 0.46 V vs SCE in CH_2Cl_2.[8] The concentration of the compounds was about 1 mM. Tetrabutylammonium hexafluorophosphate (TBAP) was used as supporting electrolyte and its concentration was 0.10 M. Cyclic voltammograms (CV) were obtained at scan rates of 50, 100, 200, and 500 mV/s. For reversible processes, half-wave potentials (vs. SCE) from CV were used. To establish the potential of irreversible processes, differential pulse voltammetry (DPV) experiments were performed with a step rate of 4 mV, a pulse height of 50 mV, and a frequency of 5 Hz. Criteria for reversibility were the separation of 60 mV between cathodic and anodic peaks, the close to unity ratio of the intensities of the cathodic and anodic currents, and the constancy of the peak potential on changing scan rate.

Experimental uncertainties are as follows: absorption maxima, ±2 nm; molar absorption coefficient, 10%; redox potentials, ± 10 mV.

Computational Methods

Computational modelization of BbF **1** – **10** was achieved following the general procedure depicted by Jacquemin and coworkers for Aza-BODIPYs.[9] All calculations were performed with the Gaussian 09 software (G09).[10] Crystallographic coordinates of **1** were used as starting points for construction of the various derivatives before geometry optimizations. Geometry optimizations, frequency calculations and molecular orbital (MO) calculations were performed by DFT method using the PBE0[11-13] / 6-311G(2d,p) basis set using the Polarization Continuum Model (PCM)[14] of dichloromethane. Tight convergence criteria and no symmetry constraints were imposed during the optimization process. Only positive frequencies were found for the optimized structures. The 40 first absorption bands were calculated by TD-DFT using the BMK[15] / 6-311+G(2d,p) level of theory with the PCM of dichloromethane. MOs were visualized (isovalue = 0.02) with GaussView 3 software.[16] GaussSum 3.0 was employed to extract from TD-DFT results the absorption energies and oscillator strengths, while molecular orbital energies were obtained from DFT.[17] Chemissian 4.23 program was used to represent MO's energy levels (Figure S.62) and determine the electronic distribution (in %) of the various parts of the fluorophores from DFT results and calculate the natural transition orbitals (NTO) (isovalue = 0.02) associated with absorption bands in the visible (> 400 nm) range obtained from TD-DFT results.[18]

Synthetic Methods

General procedure for non-symmetric benzo[b]-fused BODIPYs **1** – **7**, **9** and **10**.

(1*H*-Indol-2-yl)(phenyl)methanone **21** (1 equiv.) and the corresponding aryl-pyrrole (1 equiv.) were dissolved in CH_2Cl_2 under magnetic stirring. The reaction mixture was cooled to 0°C under an inert atmosphere and phosphoryl chloride ($POCl_3$; 2.1 equiv.) was added dropwise. After 0.5 hours, the cooling bath was removed and the reaction stirred at r.t. overnight. Water was added and the organic phase washed, dried over anhydrous $MgSO_4$ and the solvent was removed under reduced pressure. The crude intermediate obtained was dried *in vacuo* at 45°C overnight. A portion of the solid was than dissolved in dry CH_2Cl_2 in a flamed dried flask, triethylamine (TEA; 6.5 equiv.) was added under inert atmosphere, followed by boron trifluoride diethyl etherate (**(**$BF_3{\cdot}OEt_2$; 9 equiv.), and the reaction mixture was stirred at r.t. for 4 hours or upon completion by TLC analysis. Water was added and the organic phase washed, dried over anhydrous $MgSO_4$ and the solvent removed under reduced pressure. Purification by silica gel chromatography, isolation by solvent evaporation and *in vacuo* drying afforded the entitled product as a deeply coloured solid.

BbF **1** (Ar_{Prox} = Ph)

21 (886 mg; 4.00 mmol), 2-phenyl-1*H*-pyrrole **11** (573 mg; 4.00 mmol) and $POCl_3$ (0.79 mL; 8.41 mmol) in 25 mL of CH_2Cl_2. 1.56 g of a dark red solid was recovered as the crude intermediate; 96 mg used for next step with TEA (0.25 mL; 1.80 mmol) and $BF_3{\cdot}OEt_2$ (0.31 mL; 2.49 mmol) in 5 mL of dry CH_2Cl_2. Yield = 28.4 mg of dark red powder (29 % over 2 steps). Dark red needles suitable for X-ray structural analysis crystallized from slow diffusion of heptane in a concentrated $CDCl_3$ solution. ^{1}H NMR ($CDCl_3$, 400 MHz) δ/ppm: 8.15 - 8.09 (m, 2 H), 7.81

(d, J = 8.6 Hz, 1 H), 7.69 - 7.51 (m, 9 H), 7.34 (m, 1 H), 7.14 (d, J = 4.6 Hz, 1 H), 7.09 - 7.00 (m, 2 H), 6.89 (d, J = 4.6 Hz, 1 H). ^{13}C NMR ($CDCl_3$, 100 MHz) δ/ppm: 164.5, 147.5, 146.3, 140.6, 136.9, 134.6, 134.16, 131.4, 131.0, 130.9, 130.5, 129.9, 129.9, 129.6, 128.5, 128.4, 124.4, 123.4, 122.3, 121.8, 115.7. Mass Spec (*m/z*); HRMS calcd for $C_{25}H_{17}BF_2N_2$: [$(M + Na)^+$] 417.1349, found: 417.1347 (-0.48 ppm).

BbF **2** (Ar_{Prox} = *p*-Me-Ph)

21 (1.23 g; 5.55 mmol), 2-(*p*-tolyl)-1*H*-pyrrole **12** (873 mg; 5.55 mmol) and $POCl_3$ (0.79 mL; 8.41 mmol) in 50 mL of CH_2Cl_2. 2.70 g of a dark red solid was recovered as the crude intermediate; 200 mg used for next step with TEA (0.50 mL; 3.61 mmol) and $BF_3{\cdot}OEt_2$ (0.62 mL; 4.99 mmol) in 10 mL of dry CH_2Cl_2. Yield = 79.6 mg of dark purple crystals (47 % over 2 steps). ^{1}H NMR ($CDCl_3$, 400 MHz) δ/ppm: 8.05 (d, J = 8.3 Hz, 2 H), 7.84 (d, J = 8.6 Hz, 1 H), 7.67 - 7.50 (m, 6 H), 7.41 - 7.31 (m, 3 H), 7.11 (d, J = 4.6 Hz, 1 H), 7.08 - 7.00 (m, 2 H), 6.89 (d, J = 4.6 Hz, 1 H), 2.48 (s, 3 H). ^{13}C NMR ($CDCl_3$, 100 MHz) δ/ppm: 164.7, 147.2, 145.4, 141.9, 140.8, 136.9, 134.7, 134.2, 130.9, 130.4, 130.1, 130.0, 129.9, 129.4, 129.3, 128.5, 128.3, 124.5, 123.2, 121.6, 115.6, 21.7. Mass Spec (*m/z*); HRMS calcd for $C_{26}H_{19}BF_2N_2$: [$(M + Na)^+$] 431.1506, found: 431.1502 (-0.93 ppm).

BbF **3** (Ar_{Prox} = *p*-^{i}Pr-Ph)

21 (896 mg; 4.05 mmol), 2-(4-isopropylphenyl)-1*H*-pyrrole **13** (750 mg; 4.05 mmol) and $POCl_3$ (0.80 mL; 8.50 mmol) in 50 mL of CH_2Cl_2. 1.75 g of a dark red solid was recovered as the crude intermediate; 200 mg used for next step with TEA (0.47 mL; 3.35 mmol) and $BF_3{\cdot}OEt_2$ (0.57 mL; 4.63 mmol) in 10 mL of dry CH_2Cl_2. Yield = 136 mg of gold-red powder (67 % over 2 steps). ^{1}H NMR ($CDCl_3$, 400 MHz) δ/ppm: 8.13 - 8.07 (m, 2 H), 7.84 (d, J = 8.6 Hz, 1 H), 7.67 -

7.51 (m, 6 H), 7.43 (d, J = 8.3 Hz, 2 H), 7.34 (m, 1 H), 7.12 (d, J = 4.6 Hz, 1 H), 7.08 - 7.00 (m, 2 H), 6.91 (d, J = 4.6 Hz, 1 H), 3.03 (quin, J = 6.9 Hz, 1 H), 1.34 (d, J = 6.9 Hz, 6 H). ^{13}C NMR ($CDCl_3$, 100 MHz) δ/ppm: 164.8, 152.5, 147.2, 145.3, 140.8, 136.9, 134.6, 134.2, 130.9, 130.8, 130.4, 130.2 (t, J = 6 Hz), 129.2, 128.8, 128.3, 126.8, 124.6, 123.2, 121.6, 121.5, 115.6, 34.2, 23.7. Mass Spec (*m/z*); HRMS calcd for $C_{28}H_{23}BF_2N_2$: $[(M + Na)^+]$ 459.1819, found: 459.1837 (3.92 ppm).

BbF **4** (Ar_{Prox} = *p*-^{t}Bu-Ph)

21 (833 mg; 3.76 mmol), 2-(4-(*tert*-butyl)phenyl)-1*H*-pyrrole **14** (750 mg; 3.76 mmol) and $POCl_3$ (0.74 mL; 7.90 mmol) in 50 mL of CH_2Cl_2. 1.79 g of a dark red solid was recovered as the crude intermediate; 200 mg used for next step with TEA (0.45 mL; 3.23 mmol) and $BF_3{\cdot}OEt_2$ (0.55 mL; 4.47 mmol) in 10 mL of dry CH_2Cl_2. Yield = 103 mg of gold-red powder (54 % over 2 steps). ^{1}H NMR ($CDCl_3$, 400 MHz) δ/ppm: 8.14 - 8.08 (m, 2 H), 7.84 (d, J = 8.8 Hz, 1 H), 7.68 - 7.51 (m, 8 H), 7.34 (m, 1 H), 7.13 (d, J = 4.6 Hz, 1 H), 7.07 - 7.00 (m, 2 H), 6.92 (d, J = 4.6 Hz, 1 H), 1.41 (s, 9 H). ^{13}C NMR ($CDCl_3$, 100 MHz) δ/ppm: 164.7, 154.8, 147.2, 145.3, 140.9, 136.9, 134.6, 134.3, 130.9, 130.8, 130.0 (t, J = 6 Hz), 129.9, 129.2, 128.4, 128.4, 125.7, 124.7, 123.2, 121.6, 121.5, 115.6, 35.1, 31.1. Mass Spec (*m/z*); HRMS calcd for $C_{29}H_{25}BF_2N_2$: $[(M + Na)^+]$ 473.1976, found: 473.1954 (-4.65 ppm).

BbF **5** (Ar_{Prox} = *p*-OMe-Ph)

21 (2.32 g; 10.5 mmol), 2-(4-methoxyphenyl)-1*H*-pyrrole **15** (1.50 g; 10.5 mmol) and $POCl_3$ (2.07 mL; 22.0 mmol) in 60 mL of CH_2Cl_2. 4.14 g of a dark red solid was recovered as the crude intermediate; 135 mg used for next step with TEA (0.32 mL; 2.33 mmol) and $BF_3{\cdot}OEt_2$ (0.40 mL; 3.23 mmol) in 5 mL of dry CH_2Cl_2. Yield = 52.1 mg dark purple powder (36 % over 2

steps). Dark red needles suitable for X-ray structural analysis crystallized from slow diffusion of heptane in a concentrated CH_2Cl_2 solution. ^{1}H NMR ($CDCl_3$, 400 MHz) δ/ppm: 8.22 - 8.16 (m, 2 H), 7.85 (d, *J* = 8.5 Hz, 1 H), 7.65 - 7.51 (m, 6 H), 7.34 (m, 1 H), 7.13 - 7.07 (m, 3 H), 7.04 (m, 1 H), 7.00 (s, 1 H), 6.91 (d, *J* = 4.8 Hz, 1 H), 3.93 (s, 3 H). ^{13}C NMR ($CDCl_3$, 100 MHz) δ/ppm: 164.4, 162.3, 146.9, 144.3, 141.0, 136.9, 134.6, 134.3, 132.2 (t, *J* = 6 Hz), 130.9, 130.8, 130.3, 128.9, 128.3, 124.5, 123.6, 123.1, 121.5, 120.8, 115.5, 114.2, 55.4. Mass Spec (*m/z*); HRMS calcd for $C_{26}H_{19}BF_2N_2O$: [(M + Na)$^+$] 447.1455, found: 447.1453 (-0.45 ppm).

BbF **6** (Ar_{Prox} = *m*-OMe-Ph)

21 (825 mg; 3.73 mmol), 2-(3-methoxyphenyl)-1*H*-pyrrole **16** (646 mg; 3.73 mmol) and $POCl_3$ (0.74 mL; 7.83 mmol) in 50 mL of CH_2Cl_2. 1.71 g of a dark red solid was recovered as the crude intermediate; 250 mg used for next step with TEA (0.60 mL; 4.32 mmol) and $BF_3{\cdot}OEt_2$ (0.74 mL; 5.98 mmol) in 10 mL of dry CH_2Cl_2. Yield = 132 mg of dark red powder (57% over 2 steps). ^{1}H NMR ($CDCl_3$, 500 MHz) δ/ppm: 7.82 (d, *J* = 8.7 Hz, 1 H), 7.81 - 7.78 (m, 1 H), 7.66 - 7.61 (m, 4 H), 7.60 - 7.51 (m, 3 H), 7.46 (t, *J* = 7.9 Hz, 1 H), 7.35 (m, 1 H), 7.14 - 7.09 (m, 2 H), 7.08 - 7.01 (m, 2 H), 6.88 (d, *J* = 4.6 Hz, 1 H), 3.95 (s, 3 H). ^{13}C NMR ($CDCl_3$, 125 MHz) δ/ppm: 164.3, 159.52, 159.47, 146.2, 140.6, 136.9, 134.6, 134.1, 132.6, 130.9, 130.49 (d, *J* = 2 Hz), 129.6, 129.5, 128.4, 124.4, 123.4, 122.4 (t, *J* = 4 Hz), 122.3, 121.8, 117.4, 115.7, 114.9 (t, *J* = 5 Hz), 114.8, 55.5. Mass Spec (*m/z*); HRMS calcd for $C_{26}H_{19}BF_2N_2O$: [(M + Na)$^+$] 447.1455, found: 447.1460 (1.12 ppm).

BbF **7** (Ar_{Prox} = di-*m*-OMe-Ph)

21 (1.09 g; 4.92 mmol), 2-(3,5-dimethoxyphenyl)-1*H*-pyrrole **17** (999 mg; 4.92 mmol) and $POCl_3$ (0.97 mL; 10.3 mmol) in 50 mL of CH_2Cl_2. 2.13 g of a dark red solid was recovered as the

crude intermediate; 254 mg used for next step with TEA (0.57 mL; 4.06 mmol) and $BF_3 \cdot OEt_2$ (0.69 mL; 5.62 mmol) in 10 mL of dry CH_2Cl_2. Yield = 134 mg (50 % over 2 steps). ^{1}H NMR ($CDCl_3$, 400 MHz) δ/ppm: 7.82 (d, *J* = 8.8 Hz, 1 H), 7.67 - 7.49 (m, 6 H), 7.35 (m, 1 H), 7.31 (d, *J* = 2.4 Hz, 2 H), 7.11 (d, *J* = 4.6 Hz, 1 H), 7.08 - 6.99 (m, 2 H), 6.87 (d, *J* = 4.6 Hz, 1 H), 6.67 (t, *J* = 2.2 Hz, 1 H), 3.91 (s, 6 H). ^{13}C NMR ($CDCl_3$, 100 MHz) δ/ppm: 164.3, 160.6, 147.6, 146.3, 140.6, 136.9, 134.6, 134.2, 133.0, 130.9 (2C), 130.5, 129.7, 128.4, 124.4, 123.4, 122.4, 121.8, 115.7, 108.0 (t, *J* = 6 Hz), 103.7, 55.6. Mass Spec (*m/z*); HRMS calcd for $C_{27}H_{21}BF_2N_2O_2$: [$(M + Na)^+$] 477.1561, found: 477.1544 (-3.56 ppm).

BbF **8** (Ar_{Prox} = *p*-NMe_2-Ph)

21 (245 mg; 1.07 mmol; 1 equiv.) and *N*,*N*-dimethyl-4-(1*H*-pyrrol-2-yl)aniline **18** (200 mg; 1.07 mmol; 1 equiv.) were dissolved in CH_2Cl_2 (50 mL) under magnetic stirring. The reaction mixture put under an inert atmosphere and triethylamine (0.17 mL; 1.18 mmol; 1.1 equiv.) followed by phosphoryl chloride ($POCl_3$; 0.21 mL; 2.25 mmol; 2.1 equiv.) were added dropwise. After 0.5 hours at r.t., the reaction was heated at reflux overnight. The reaction mixture was than exposed to air for 36 hours under reflux were a colour change from brown to deep purple was observed. Water was added and the organic phase washed, dried over anhydrous MgSO4 and the solvent removed under reduced pressure. The crude intermediate obtained as a dark blue solid was dried *in vacuo* at 45°C overnight, than dissolved in dry CH_2Cl_2 in a flamed dried flask. Triethylamine (0.85 mL; 6.11 mmol; 6.5 equiv.) was added under inert atmosphere, followed by boron trifluoride diethyl etherate (1.04 mL; 8.46 mmol; 9 equiv.), and the reaction mixture was stirred at r.t. for 3 hours. Water was added and the organic phase washed, dried over anhydrous MgSO4 and the solvent removed under reduced pressure. Purification by silica gel chromatography, isolation by solvent evaporation and *in vacuo* drying afforded the entitled

product as a deep blue solid. Gold blue needles suitable for X-ray structural crystallized from diffusion of heptane in a concentrated CH_2Cl_2 solution. Yield = 337 mg (72 %). ^{1}H NMR ($CDCl_3$, 300 MHz) δ/ppm: 8.27 (d, *J* = 9.3 Hz, 2 H), 7.88 (d, *J* = 8.3 Hz, 1 H), 7.65 - 7.48 (m, 6 H), 7.31 (m, 1 H), 7.09 - 6.99 (m, 3 H), 6.89 - 6.79 (m, 3 H), 3.15 (s, 6 H). ^{13}C NMR ($CDCl_3$, 75 MHz) δ/ppm: 164.8, 152.6, 145.6, 141.8, 140.0, 137.0, 134.8, 134.2, 132.9 (t, *J* = 6 Hz), 130.8, 130.6, 129.7, 128.2, 127.4, 124.7, 122.5, 121.0, 117.7, 117.5, 115.3, 111.6, 40.0. Mass Spec (*m/z*); HRMS calcd for $C_{27}H_{22}BF_2N_3$: $[(M + Na)^+]$ 460.1772, found: 460.1773 (0.22 ppm).

BbF **9** (Ar_{Prox} = *p*-OMe-Naphtyl)

Compound **21** (843 mg; 4.92 mmol), 2-(6-methoxynaphthalen-2-yl)-1H-pyrrole **19** (850 mg; 3.81 mmol) and $POCl_3$ (0.75 mL; 7.99 mmol) in 50 mL of CH_2Cl_2. 1.82 g of a dark purple solid was recovered as the crude intermediate; 200 mg used for next step with TEA (0.42 mL; 3.05 mmol) and $BF_3{\cdot}OEt_2$ (0.52 mL; 4.22 mmol) in 10 mL of dry CH_2Cl_2. Yield = 35 mg of dark green powder (18 % over 2 steps). Dark purple needles suitable for X-ray structural analysis crystallized from slow diffusion of heptane in a concentrated CH_2Cl_2 solution. ^{1}H NMR ($CDCl_3$, 500 MHz) δ/ppm: 8.64 (s, 1 H), 8.22 (dd, *J* = 8.7, 1.8 Hz, 1 H), 7.98 - 7.81 (m, 3 H), 7.69 - 7.49 (m, 6 H), 7.41 - 7.30 (m, 1 H), 7.26 - 7.14 (m, 3 H), 7.08 - 7.00 (m, 3 H), 3.98 (s, 3 H). ^{13}C NMR ($CDCl_3$, 125 MHz) δ/ppm: 164.7, 159.6, 147.2, 145.0, 141.1, 137.0, 136.1, 134.6, 134.3, 131.1, 131.03, 131.91, 130.4, 129.2, 128.40, 128.37, 127.1 (t, *J* = 6 Hz), 127.0, 126.4, 124.8, 123.2, 121.6, 121.4, 119.6, 115.6, 105.8, 55.5. Mass Spec (*m/z*); HRMS calcd for $C_{30}H_{21}BF_2N_2O$: $[(M + Na)^+]$ 497.1612, found: 497.1626 (2.82 ppm).

BbF **10** (Ar_{Prox} = Phen)

21 (227 mg; 1.03 mmol), 2-(phenanthren-9-yl)-1H-pyrrole **20** (250 mg; 1.03 mmol) and $POCl_3$ (0.20 mL; 2.16 mmol) in 25 mL of CH_2Cl_2. 459 mg of a dark red solid was recovered as the crude intermediate and used for the next step with TEA (0.93 mL; 6.68 mmol) and $BF_3 \cdot OEt_2$ (1.14 mL; 9.25 mmol) in 40 mL of dry CH_2Cl_2. Yield = 127 mg of dark purple powder (25 % over 2 steps). ^{1}H NMR ($CDCl_3$, 400 MHz) δ/ppm: 8.79 (dd, *J* = 14.2, 8.3 Hz, 2 H), 8.37 (s, 1 H), 8.07 (dd, *J* = 7.9, 1.1 Hz, 1 H), 7.88 (d, *J* = 8.1 Hz, 1 H), 7.82 - 7.48 (m, 11 H), 7.32 - 7.21 (m, 2 H), 7.13 (s, 1 H), 7.00 (t, *J* = 7.5 Hz, 1 H), 6.86 (d, *J* = 4.6 Hz, 1 H). ^{13}C NMR ($CDCl_3$, 100 MHz) δ/ppm: 163.4, 147.7, 146.9, 139.4, 137.1, 134.1, 133.4, 131.1, 130.9, 130.8, 130.63, 130.58, 130.4, 130.3 (t, *J* = 5 Hz), 130.2, 130.0, 129.9, 128.4, 128.03, 127.98, 127.1, 126.93, 126.87, 126.6, 126.0, 123.4, 123.13, 123.09, 122.6, 121.8, 115.6. Mass Spec (*m/z*); HRMS calcd for $C_{33}H_{21}BF_2N_2$: [$(M + Na)^+$] 517.1664, found: 517.1663 (-0.19 ppm).

*General procedure for aryl-pyrroles **19** and **20**.*

Pyrrole (1.6 equiv.) was slowly added under an inert atmosphere to a cooled (0°C) suspension of sodium hydride (NaH 60 % dispersion in mineral oil; 1.6 equiv.) in anhydrous THF (20 mL) and stirring was continued for 0.5 h at r.t. After cooling to 0°C, a solution of zinc chloride ($ZnCl_2$; 1.6 equiv.) in anhydrous THF (80 mL) was syringed. After stirring for 10 min at r.t., di-*tert*-butyl-*o*-biphenylphosphine (JohnPhos; 1.5 - 2 mol %) and $Pd(OAc)_2$ (1.5 -2 mol %) were added in one portion and the resulting mixture was degassed with N_2. The corresponding aryl halide (1 equiv.) was subsequently added to the reaction mixture and the resulting brown solution was refluxed for 72 hours. After cooling to r.t., a saturated solution of sodium thiosulfate ($Na_2S_2O_3$, 100 mL) was added, stirring was continued for 15 min, followed by concentration of the reaction mixture under reduced pressure and filtration. The filter cake was repeatedly washed with ethyl acetate (5 x 50 mL) and the filtrate was transferred to a separatory funnel. After

separation of both phases, the aqueous layer was extracted with ethyl acetate (2 x 50 mL) and the combined organic phase was washed with water (100 mL). Drying over anhydrous $MgSO_4$, followed by filtration and removal of the solvent under reduced pressure afforded a yellow-brown solid which was purified by column chromatography giving the title compound.

2-(6-methoxynaphthalen-2-yl)-1H-pyrrole **19**

Pyrrole (2.34 mL; 33.1 mmol), NaH (1.32 g; 33.1 mmol), $ZnCl_2$ (4.55 g; 33.1 mmol), JohnPhos (127 mg; 0.413 mmol), $Pd(OAc)_2$ (94.7 mg; 0.413 mmol) and 2-bromo-6-methoxynaphtalene (5.00 g; 20.7 mmol). Yield = 1.09 g of dark yellow crystals (24 %). ^{1}H NMR ($CDCl_3$, 300 MHz) δ/ppm: 8.55 (br. s., 1 H), 7.83 - 7.57 (m, 4 H), 7.20 - 7.06 (m, 2 H), 6.96 - 6.85 (m, 1 H), 6.63 - 6.60 (m, 1 H), 6.39 - 6.30 (m, 1 H), 3.94 (s, 3 H). ^{13}C NMR ($CDCl_3$, 75 MHz) δ/ppm: 157.4, 133.2, 132.3, 129.2, 128.2 (2C), 127.4, 123.7, 121.2, 119.2, 118.8, 110.2, 106.0, 105.8, 55.3. Mass Spec (*m/z*); MS calcd for $C_{15}H_{13}NO$: [M^+] 223.1, found: 223.1.

2-(phenanthren-9-yl)-1H-pyrrole **20**

Pyrrole (2.16 mL; 30.5 mmol), NaH (1.22 g; 30.5 mmol), $ZnCl_2$ (4.20 g; 30.5 mmol), JohnPhos (87.9 mg; 0.286 mmol), $Pd(OAc)_2$ (65.5 mg; 0.286 mmol) and 9-bromo-phenanthrene (5.00 g; 19.1 mmol). Yield = 0.37 g of an off-white solid (8 %). ^{1}H NMR ($CDCl_3$, 300 MHz) δ/ppm: 8.78 (d, J = 8.3 Hz, 1 H), 8.71 (d, J = 8.1 Hz, 1 H), 8.47 (br. s., 1 H), 8.36 (dd, J = 8.2, 1.1, 1 H), 7.92 - 7.84 (m, 1 H), 7.82 - 7.57 (m, 5 H), 7.04 - 6.97 (m, 1 H), 6.63 - 6.56 (m, 1 H), 6.47 (m, 1 H). ^{13}C NMR ($CDCl_3$, 75 MHz) δ/ppm: 131.5, 130.8, 130.7, 130.4, 130.2, 129.8, 128.5, 126.9, 126.9, 126.8, 126.6 (2C), 126.5, 123.0, 122.5, 118.3, 109.7, 109.4. Mass Spec (*m/z*); MS calcd for $C_{18}H_{13}N$: [M^+] 243.1, found: 243.1.

NMR Characterization

Figure S.1 – ^{1}H (top) and ^{13}C (bottom) of BbF **1** ($CDCl_3$; 400 MHz and 100 MHz, respectively)

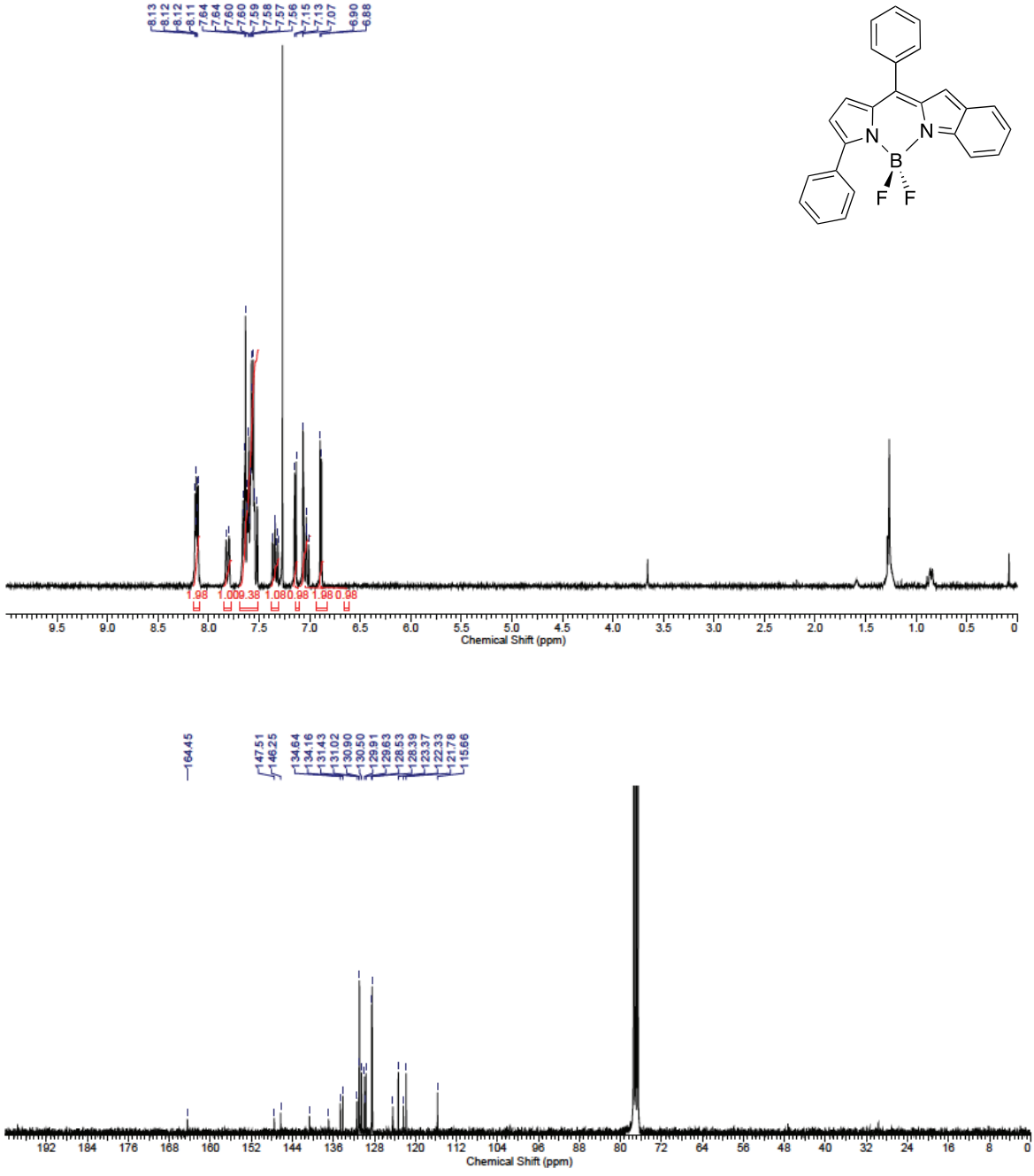

Figure S.2 – ^{1}H (top) and ^{13}C (bottom) of BbF **2** ($CDCl_3$; 400 MHz and 100 MHz, respectively)

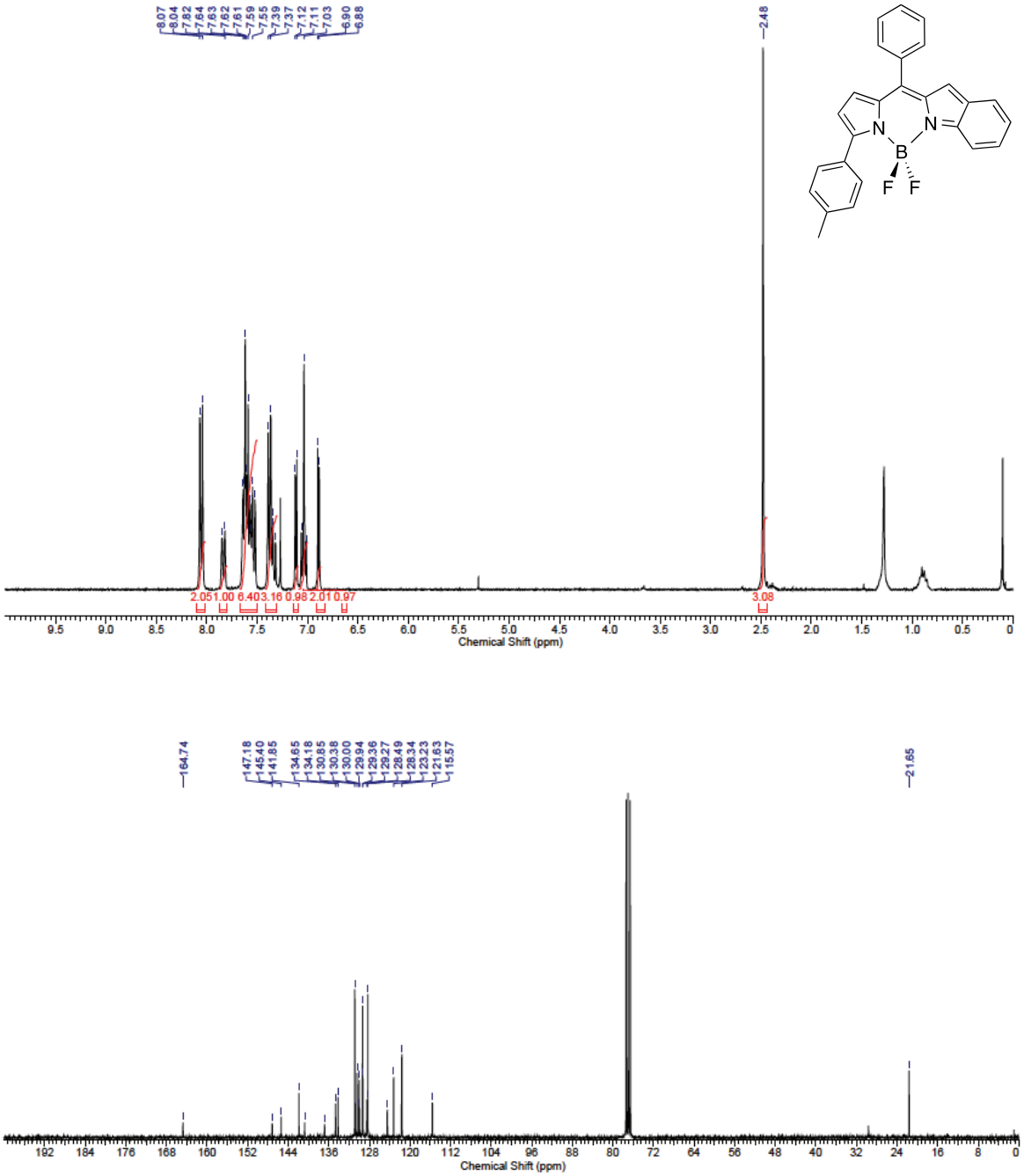

Figure S.3 – ^{1}H (top) and ^{13}C (bottom) of BbF **3** ($CDCl_3$; 400 MHz and 100 MHz, respectively)

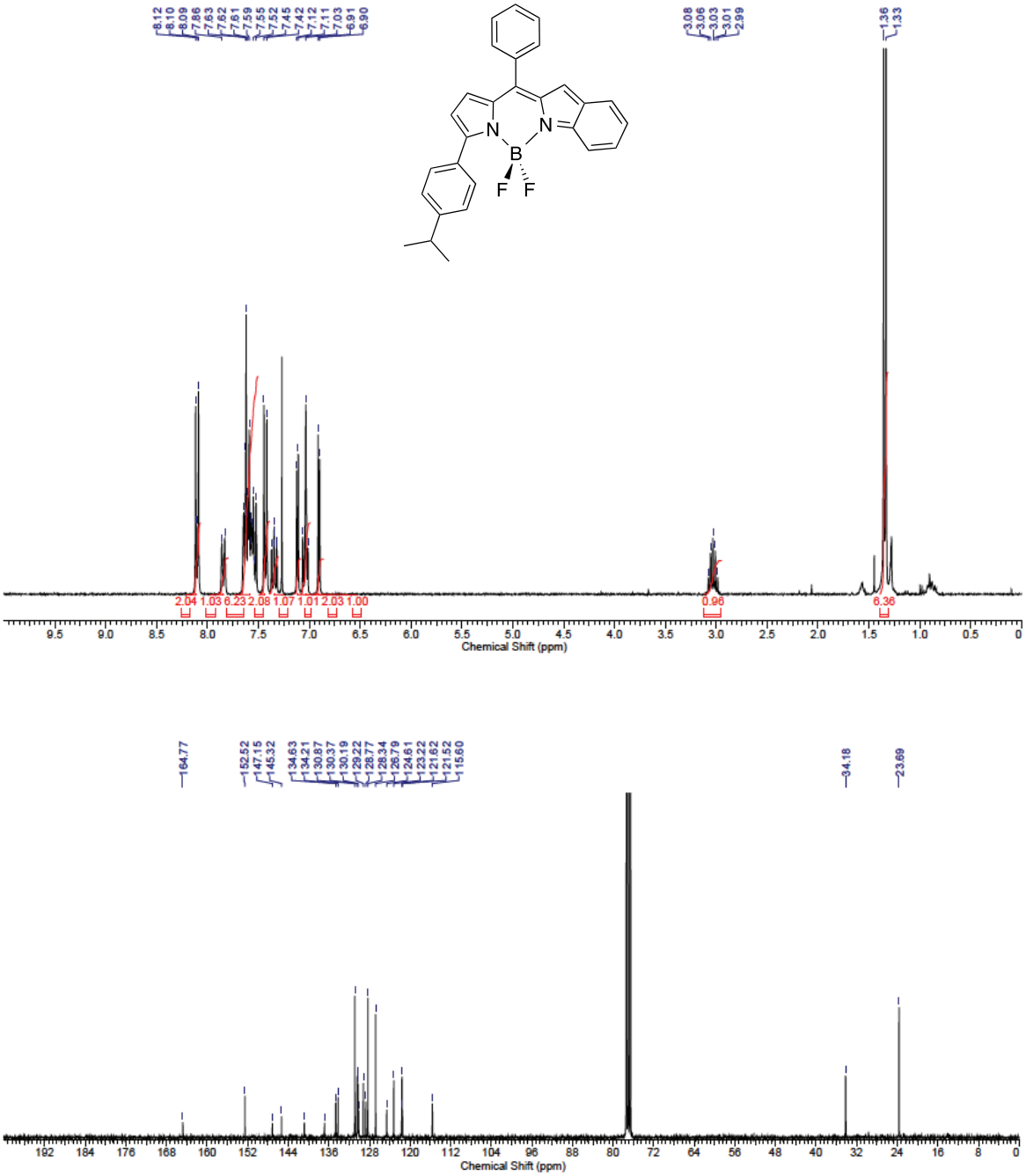

Figure S.4 – ^{1}H (top) and ^{13}C (bottom) of BbF **4** ($CDCl_3$; 400 MHz and 100 MHz, respectively)

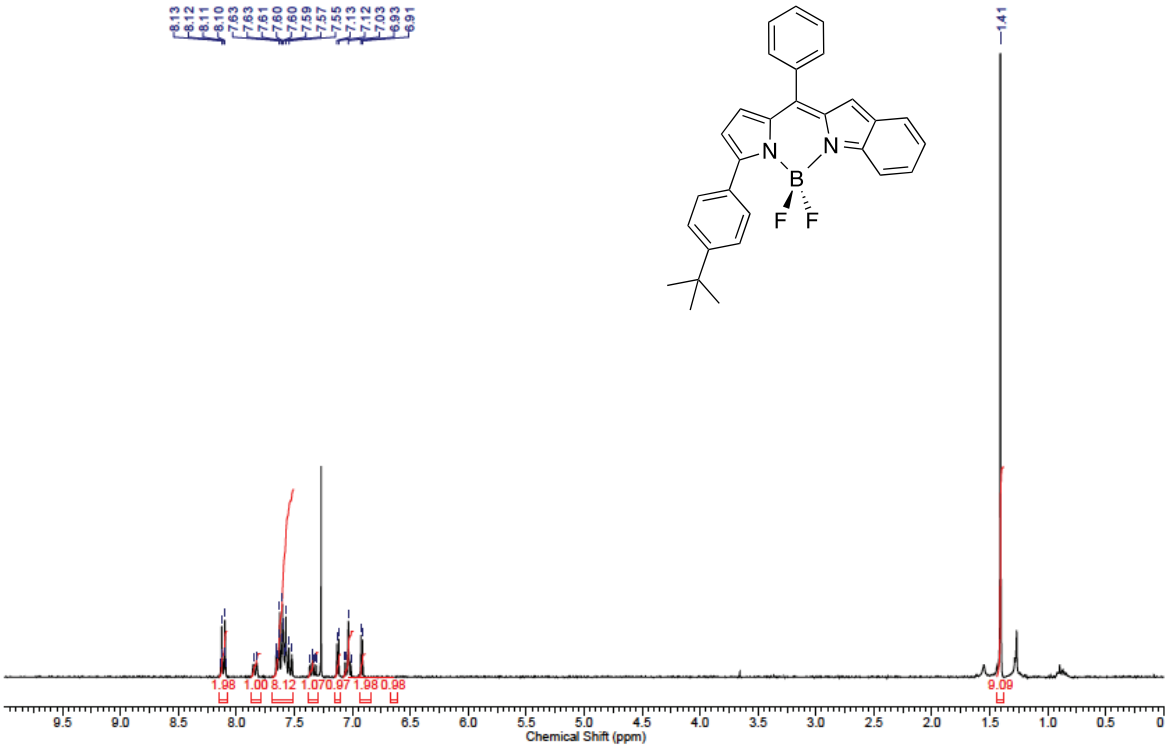

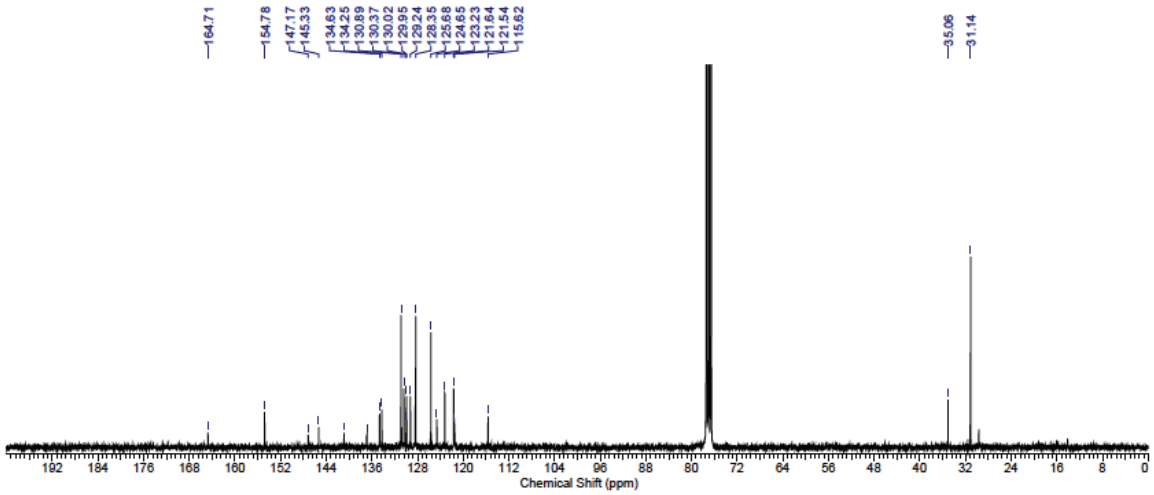

Figure S.5 – ^{1}H (top) and ^{13}C (bottom) of BbF **5** ($CDCl_3$; 500 MHz and 125 MHz, respectively)

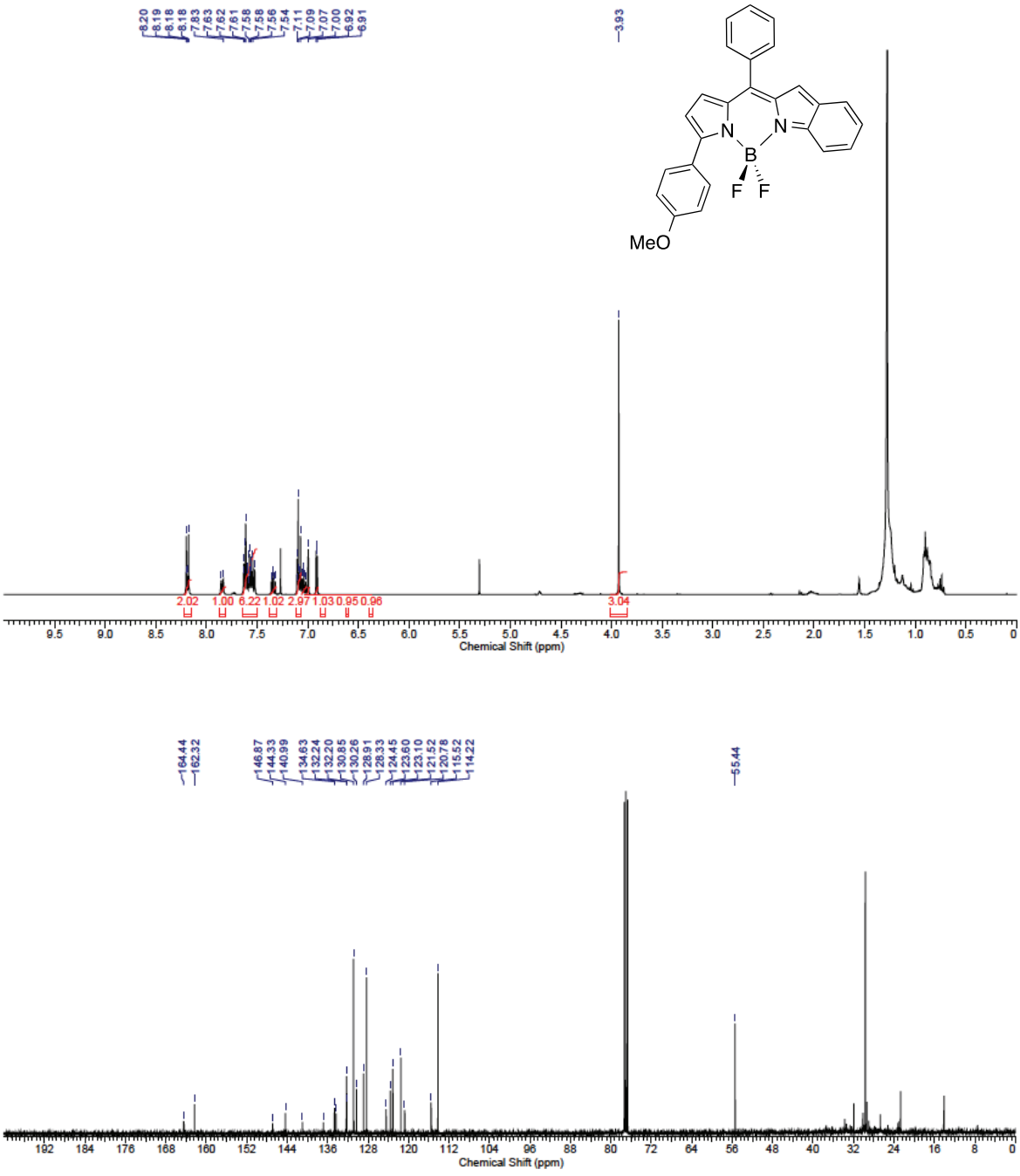

Figure S.6 – ^{1}H (top) and ^{13}C (bottom) of BbF **6** ($CDCl_3$; 500 MHz and 125 MHz, respectively)

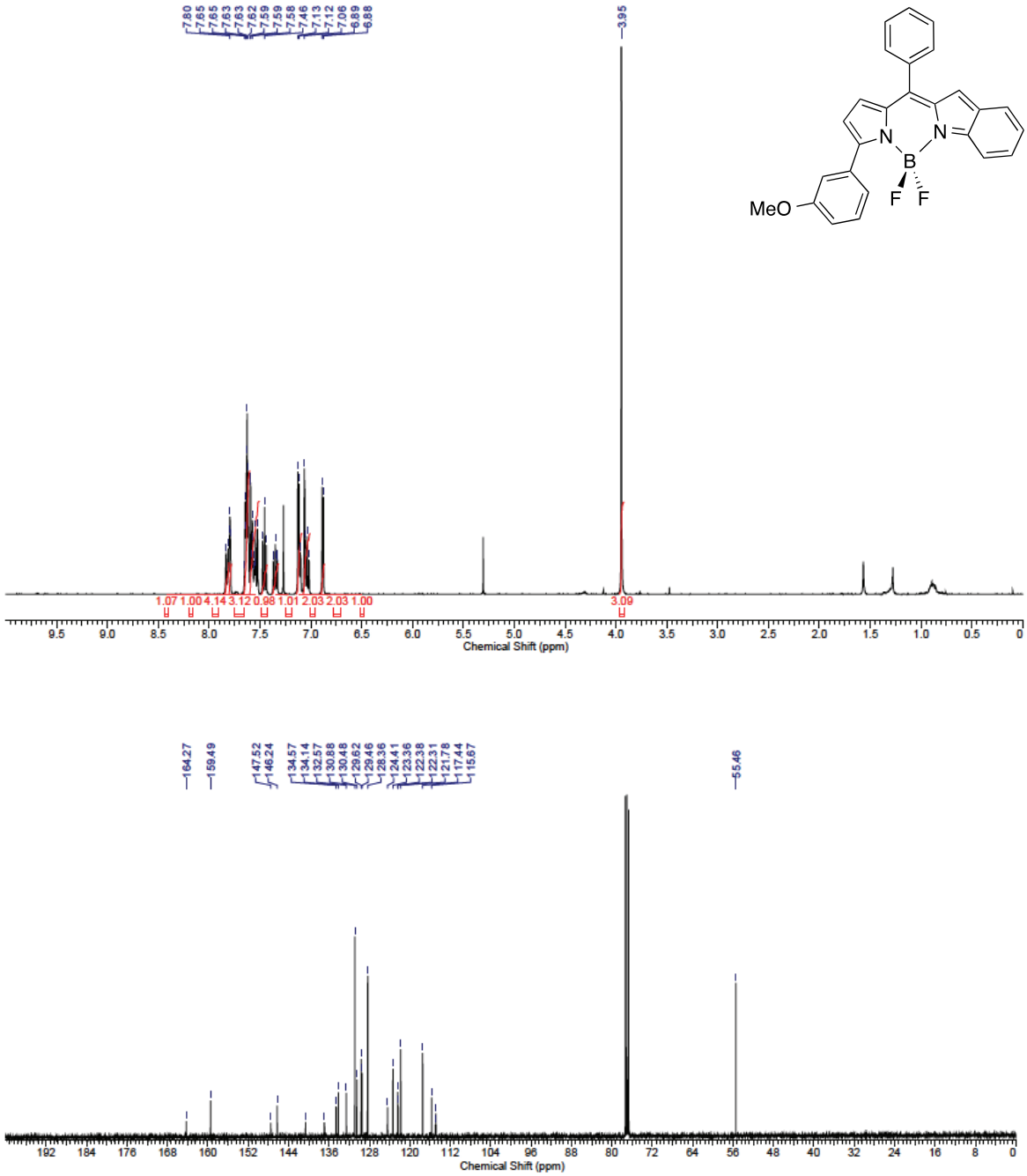

Figure S.7 – ^{1}H (top) and ^{13}C (bottom) of BbF **7** ($CDCl_3$; 400 MHz and 100 MHz, respectively)

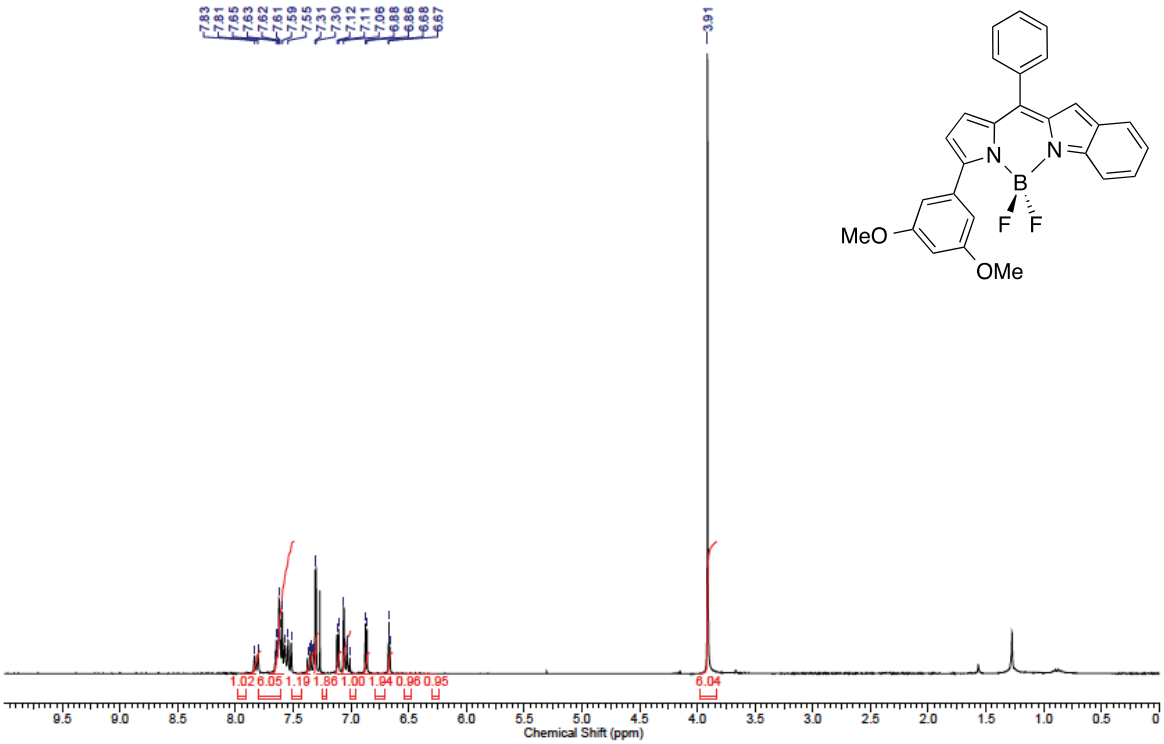

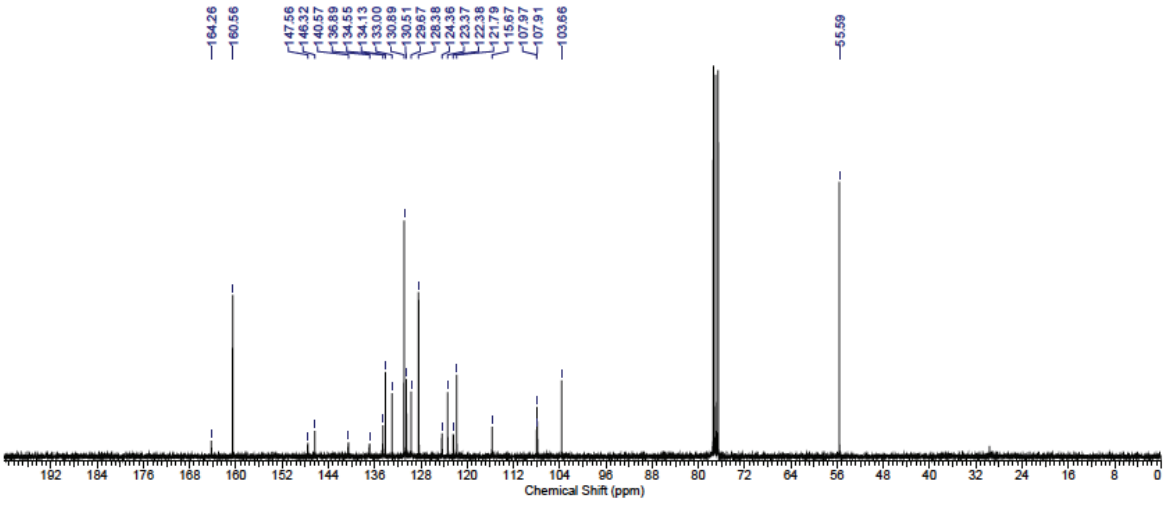

Figure S.8 – ^{1}H (top) and ^{13}C (bottom) of BbF **8** ($CDCl_3$; 300 MHz and 75 MHz, respectively)

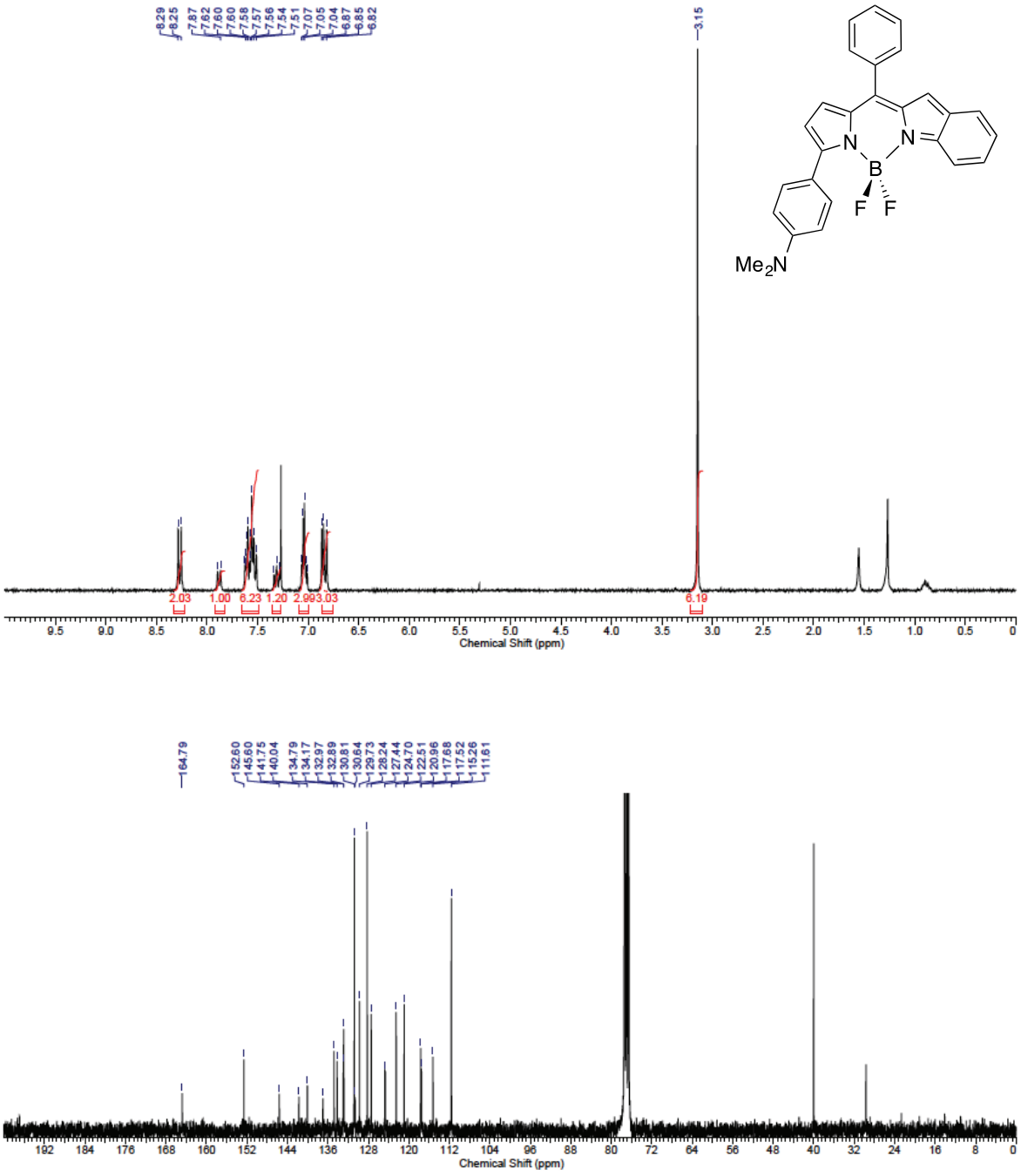

Figure S.9 – ^{1}H (top) and ^{13}C (bottom) of BbF **9** ($CDCl_3$; 500 MHz and 125 MHz, respectively)

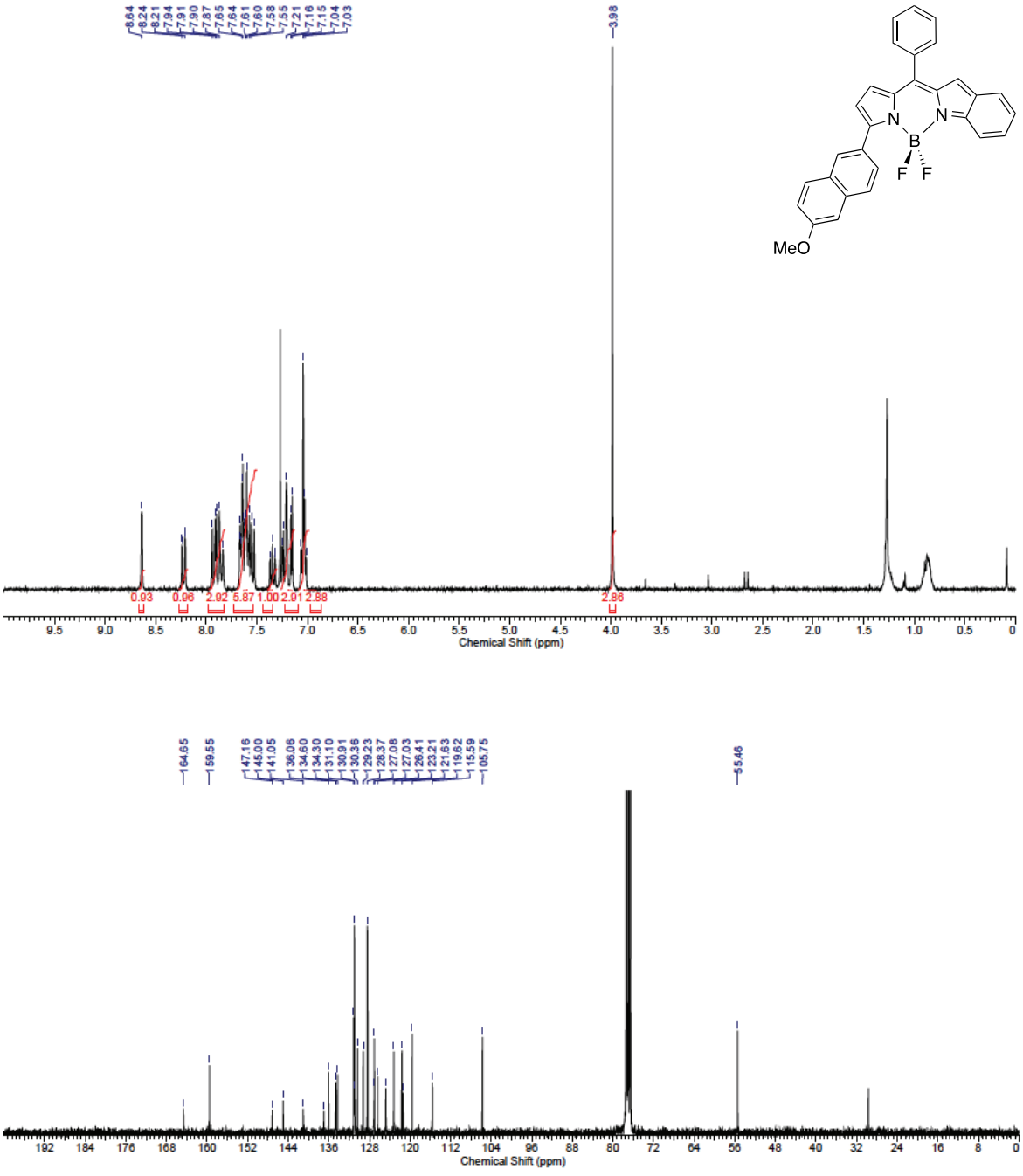

Figure S.10 – ^{1}H (top) and ^{13}C (bottom) of BbF **10** ($CDCl_3$; 400 MHz and 100 MHz, respectively)

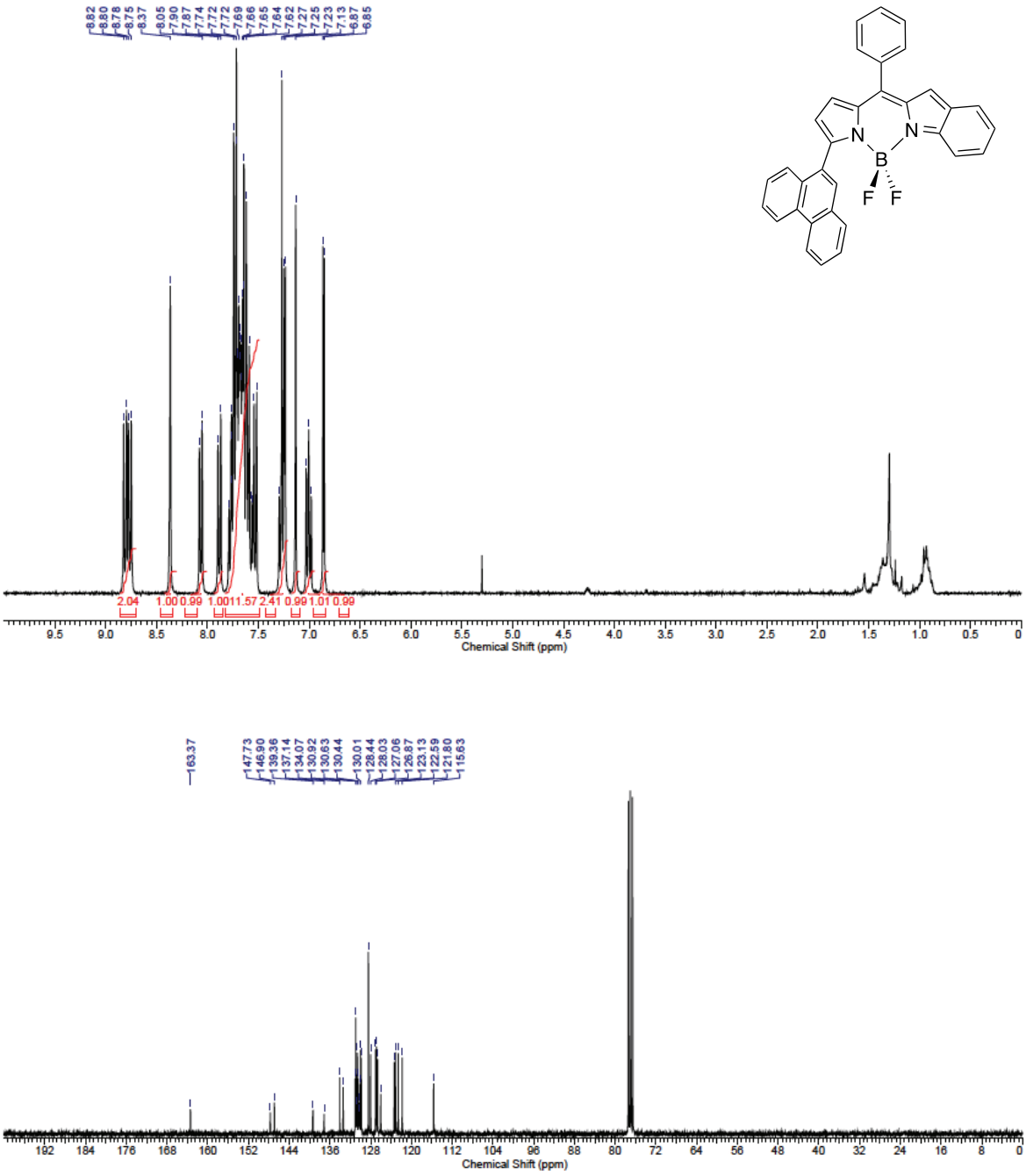

Figure S.11 – ^{1}H (top) and ^{13}C (bottom) of 2-(6-methoxynaphthalen-2-yl)-1H-pyrrole **19** ($CDCl_3$; 300 MHz and 75 MHz, respectively)

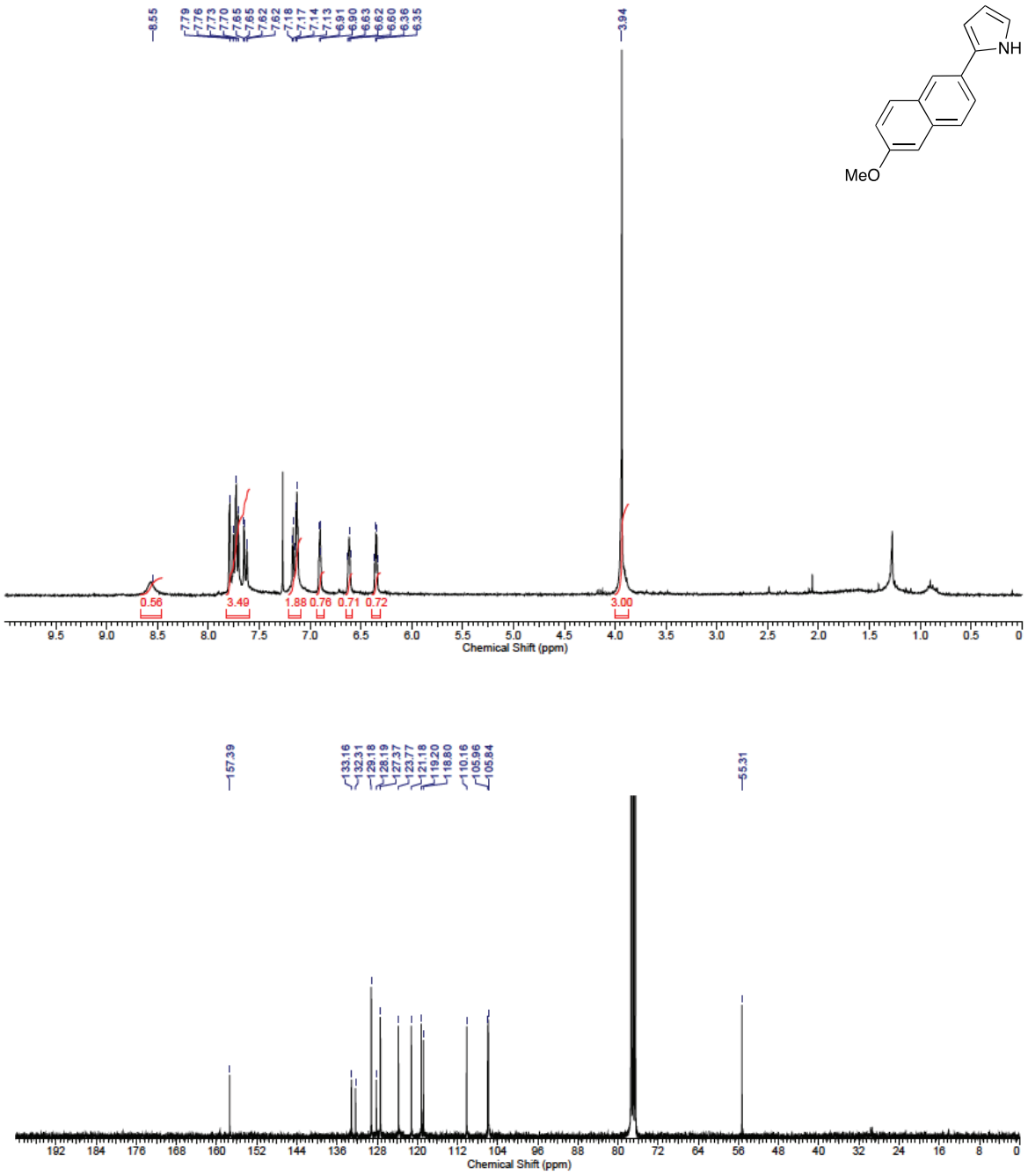

Figure S.12 – ^{1}H (top) and ^{13}C (bottom) of 2-(phenanthren-9-yl)-1H-pyrrole **20** ($CDCl_3$; 300 MHz and 75 MHz, respectively)

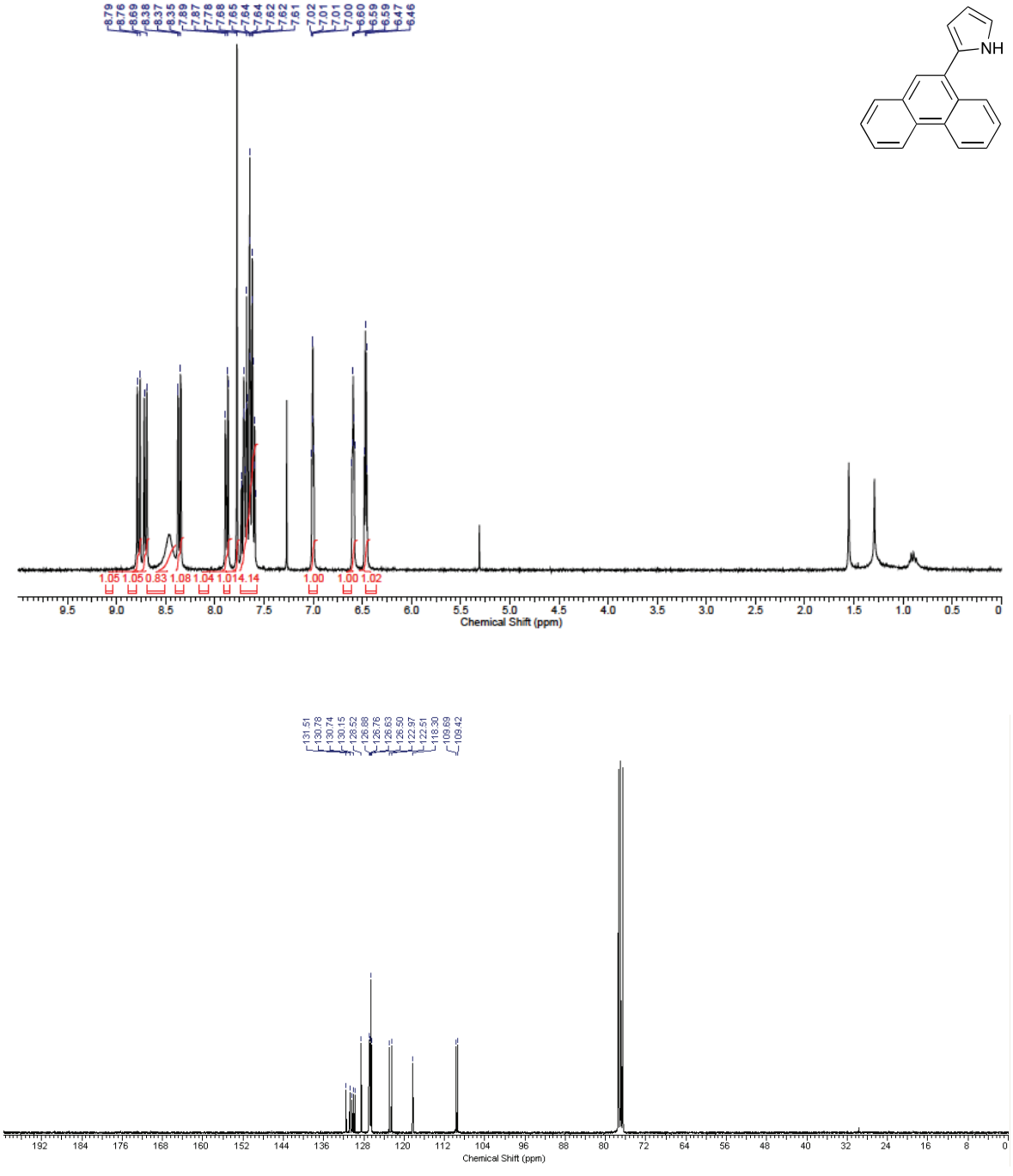

Mass Spectrometry

Figure S.13 – HRMS of BbF **1**

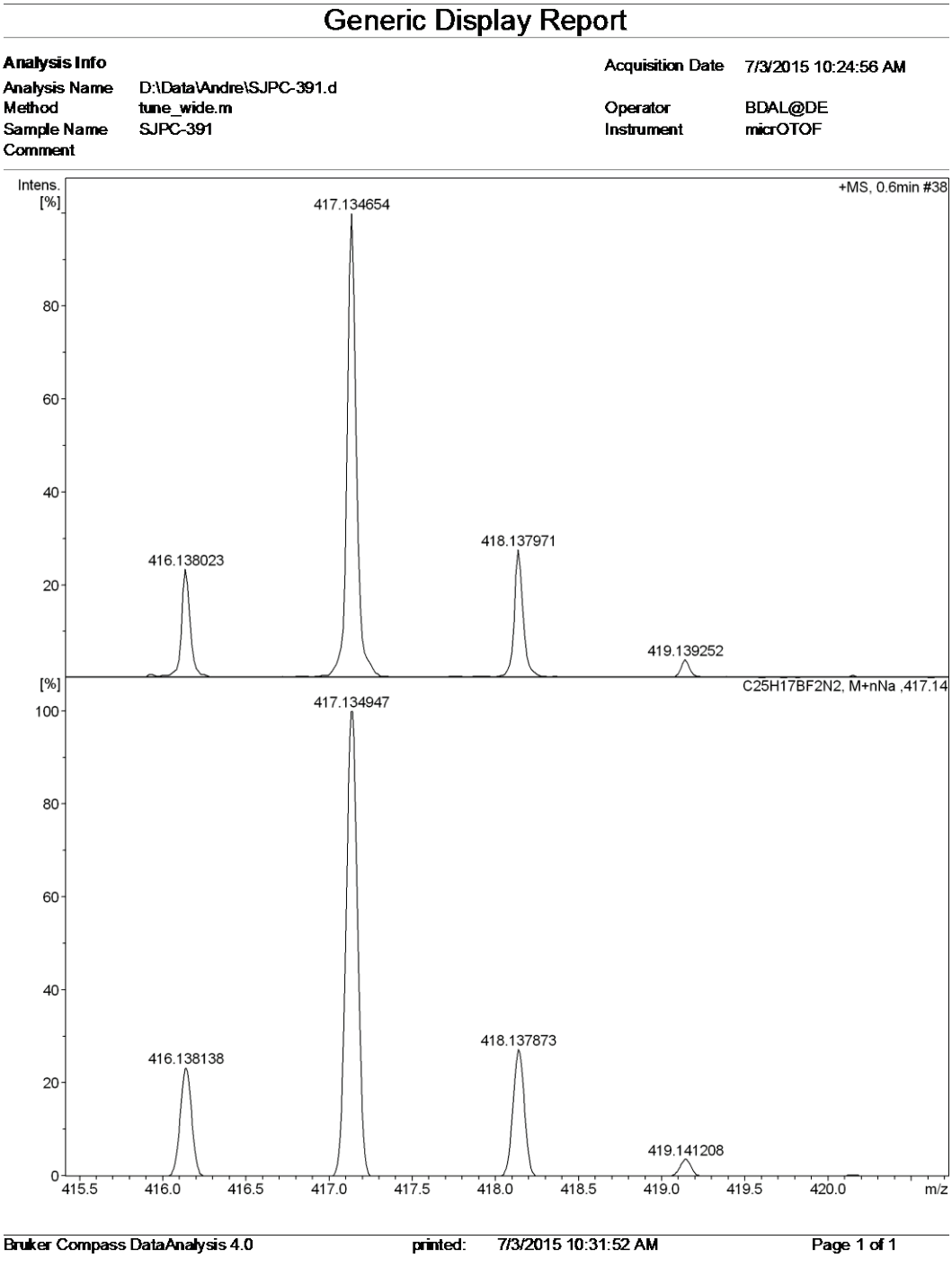

Figure S.14 – HRMS of BbF **2**

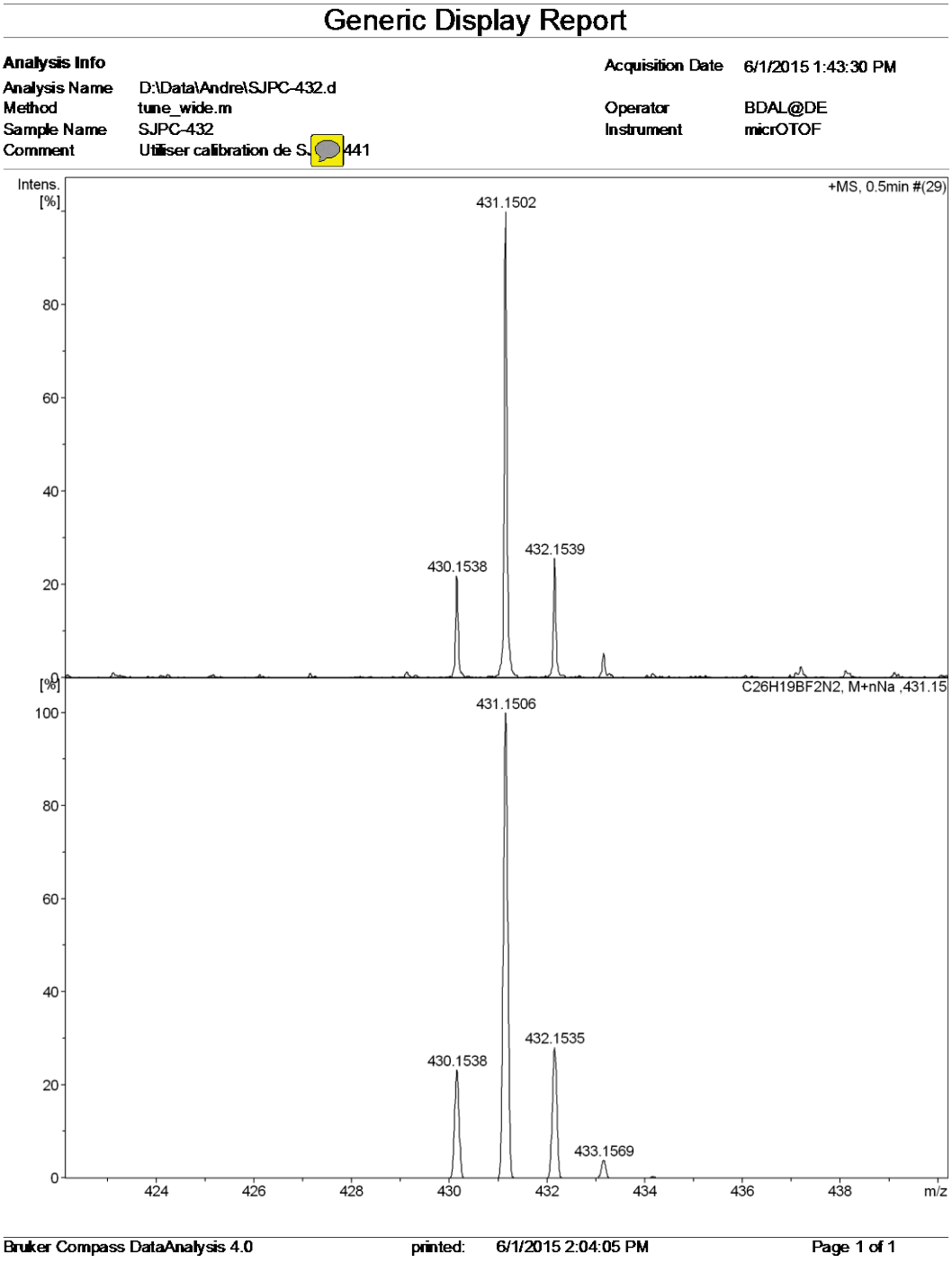

Figure S.15 – HRMS of BbF **3**

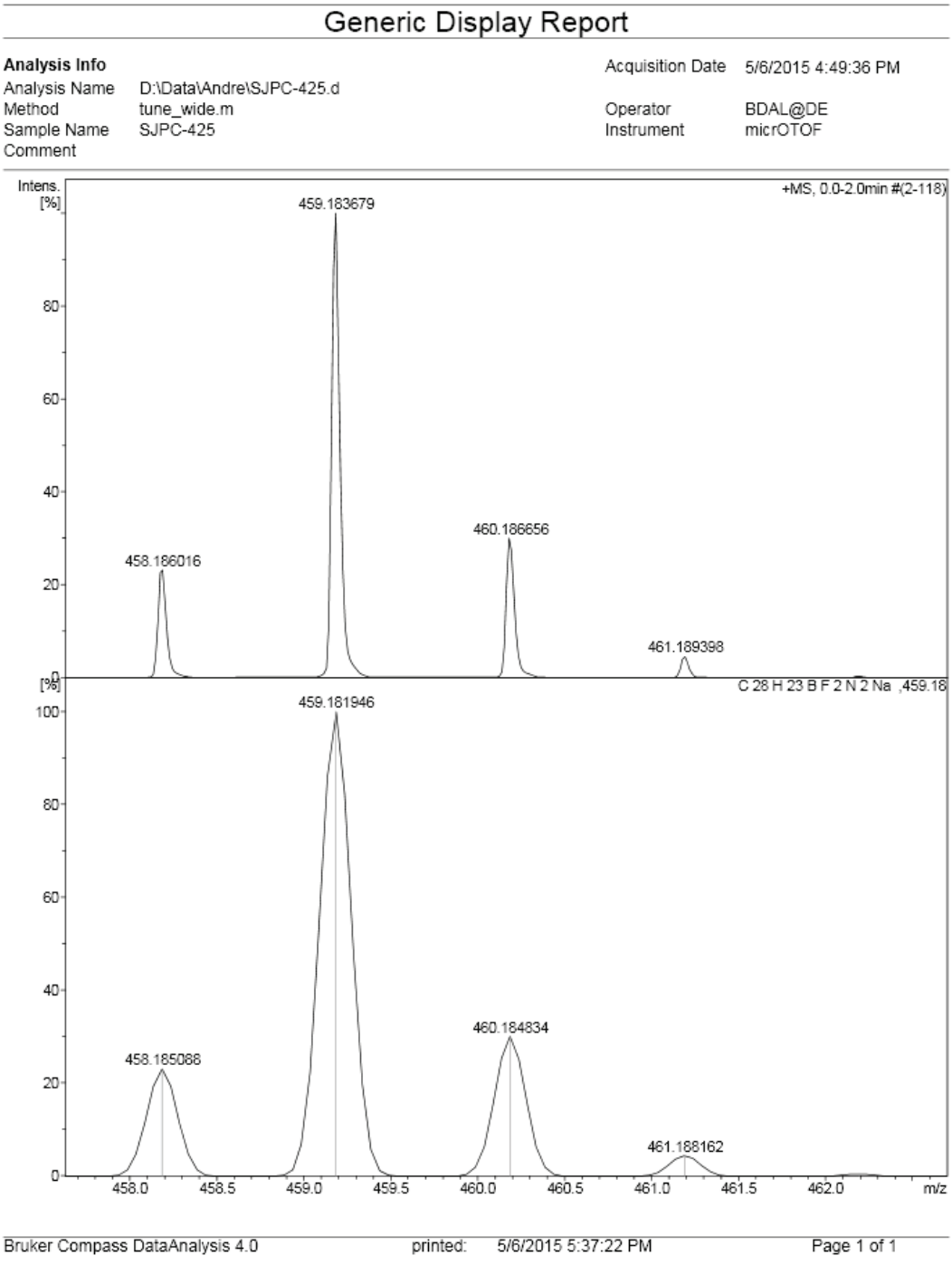

Figure S.16 – HRMS of BbF **4**

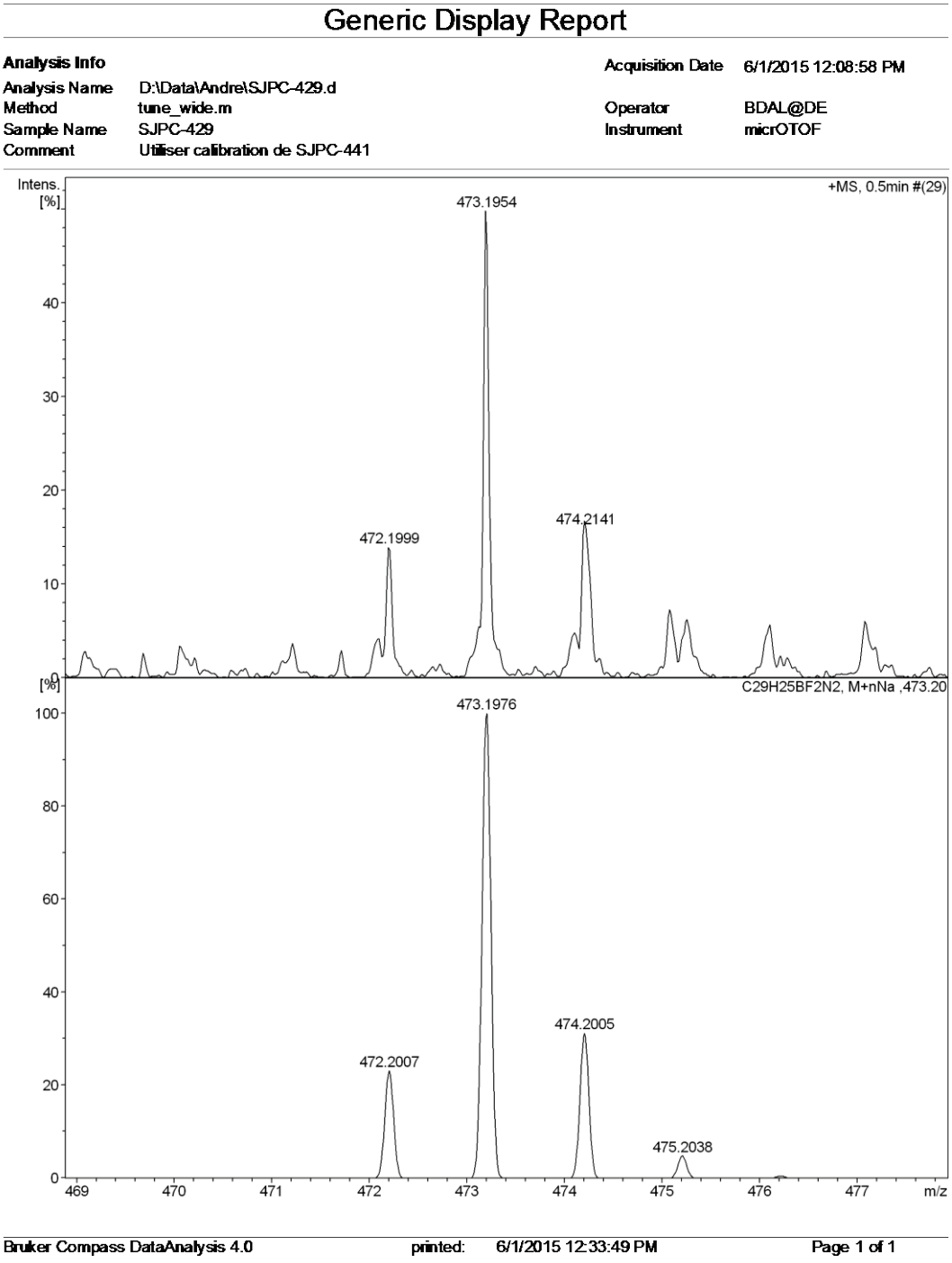

Figure S.17 – HRMS of BbF **5**

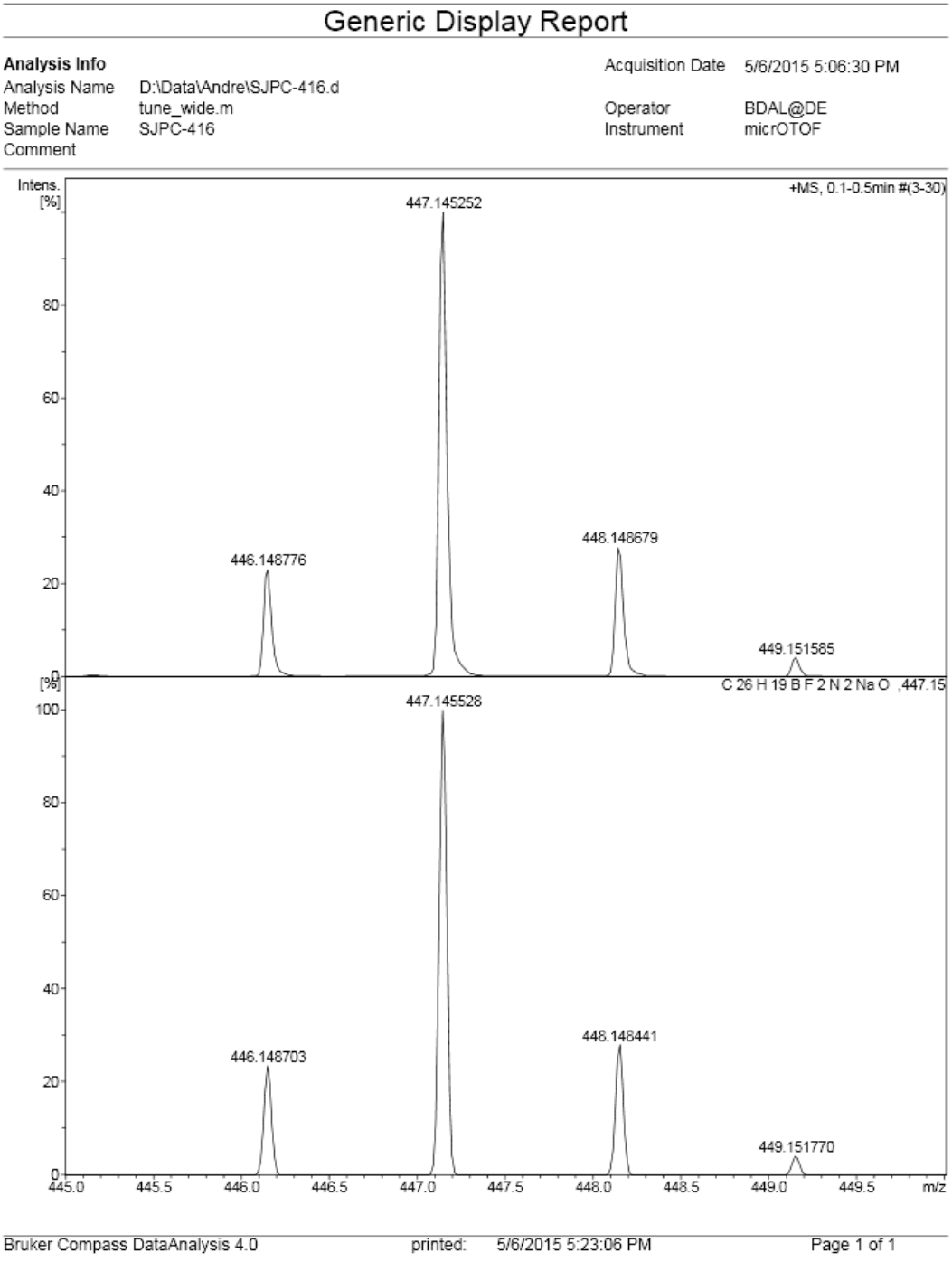

Figure S.18 – HRMS of BbF **6**

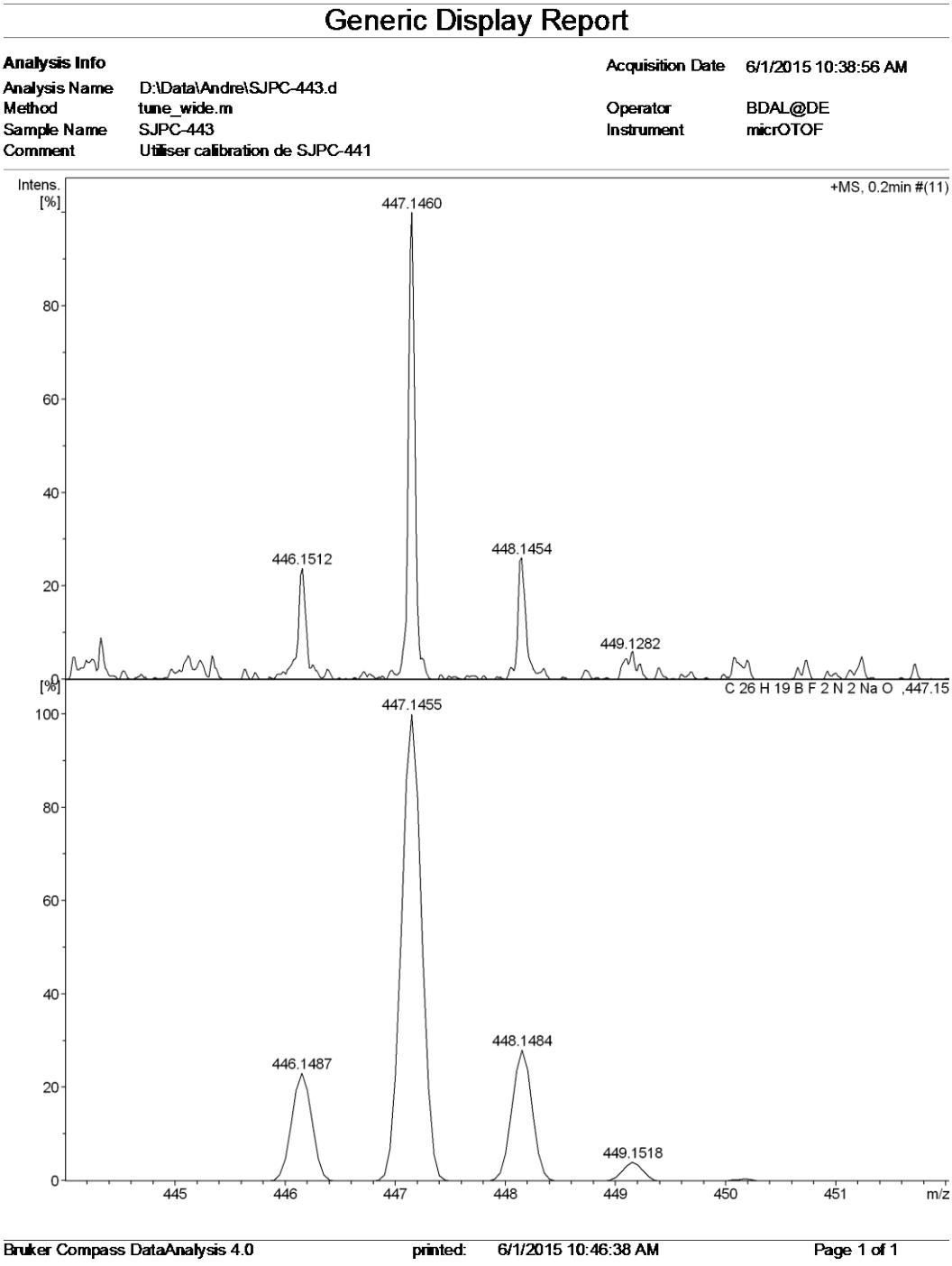

Figure S.19 – HRMS of BbF **7**

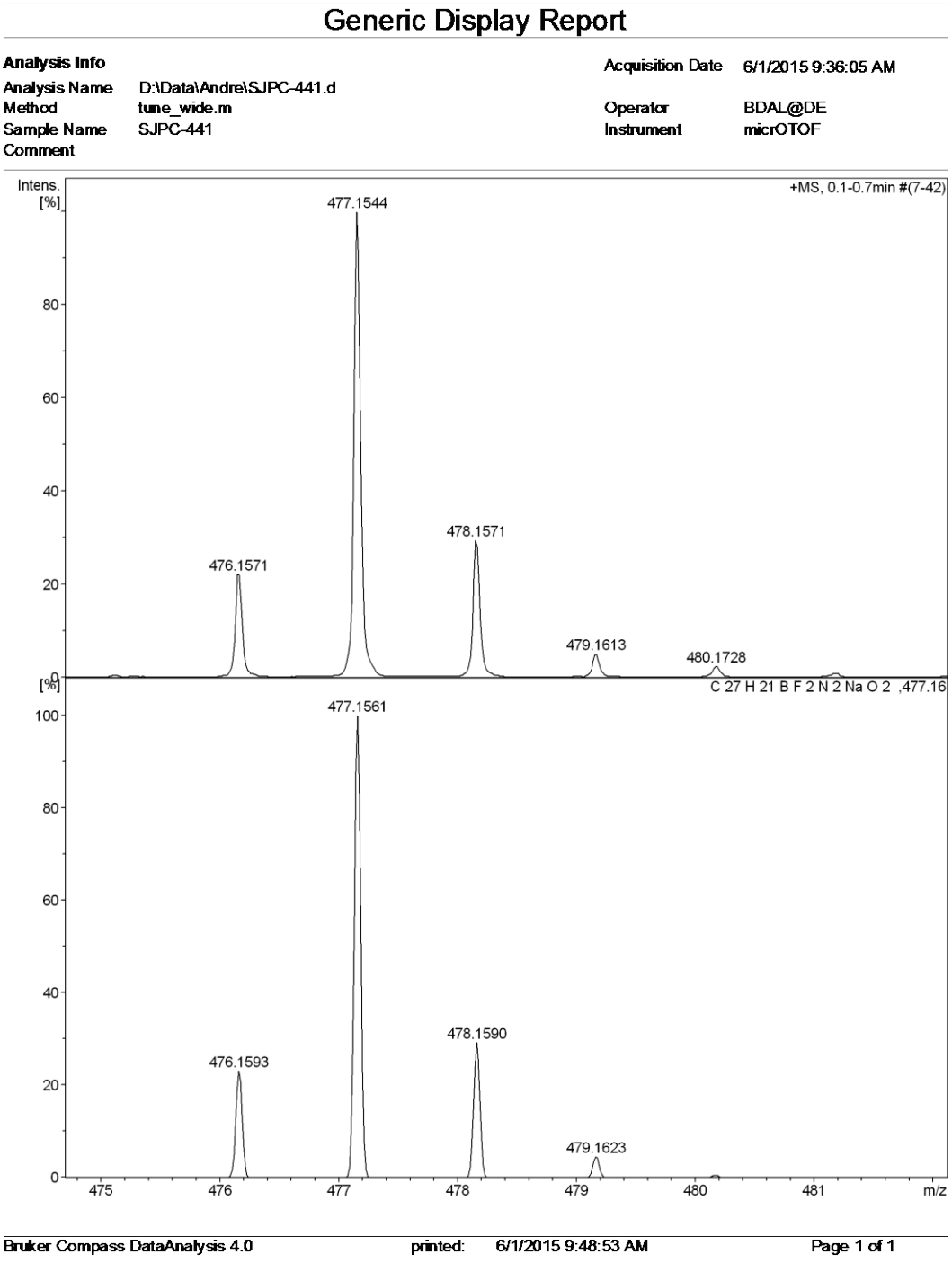

Figure S.20 – HRMS of BbF **8**

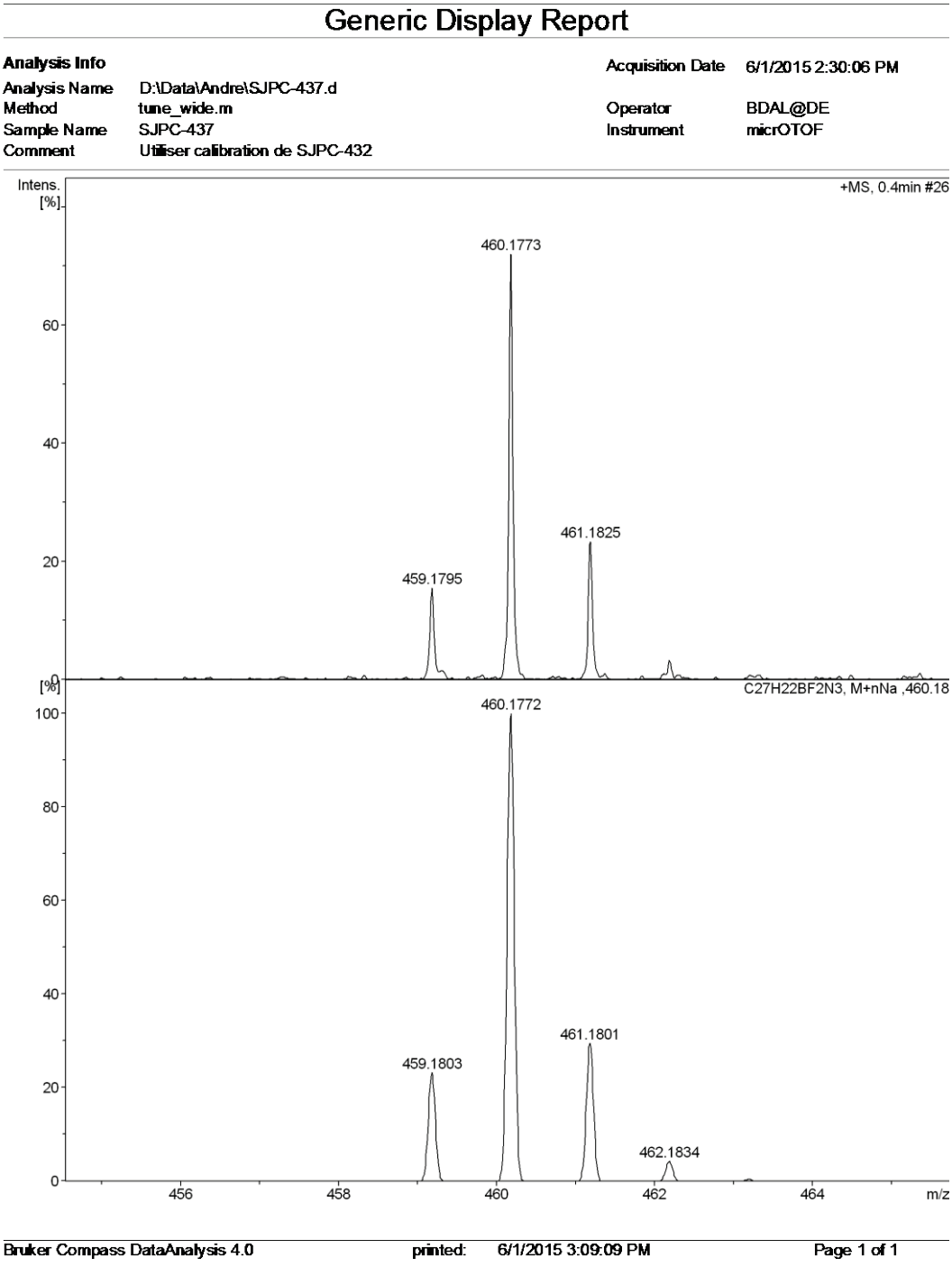

Figure S.21 – HRMS of BbF **9**

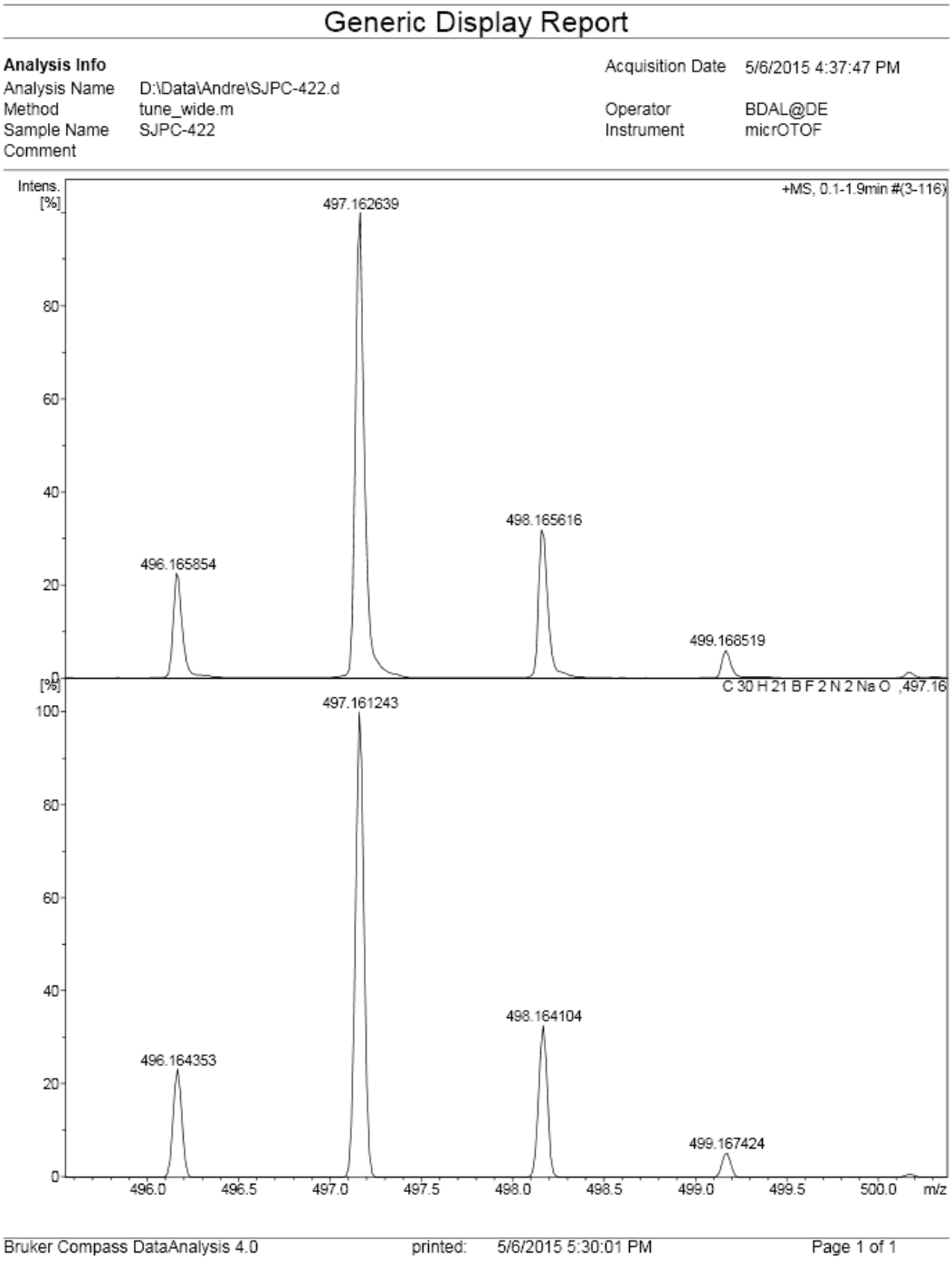

Figure S.22 – HRMS of BbF **10**

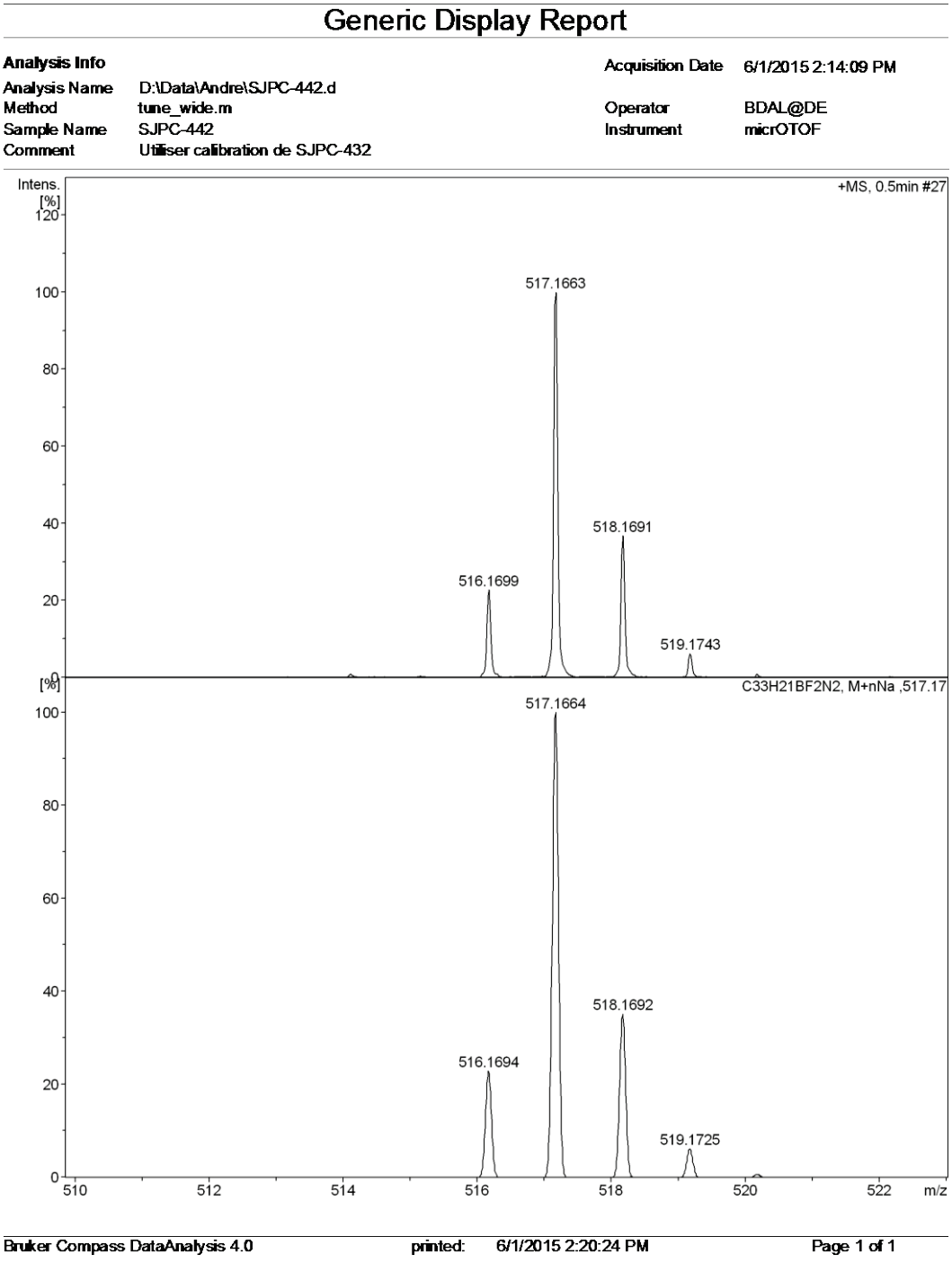

Figure S.23 – GC-MS of 2-(6-methoxynaphthalen-2-yl)-1H-pyrrole **19**

```
File       :C:\msdchem\1\DATA\PCAB\SJPC-413-1.D
Operator   : AB7
Acquired   : 28 Apr 2015  10:09     using AcqMethod NITROKETONE MODIFIE.M
Instrument :    GCMS
Sample Name: SJPC-413-1
Misc Info  :
Vial Number: 7
```

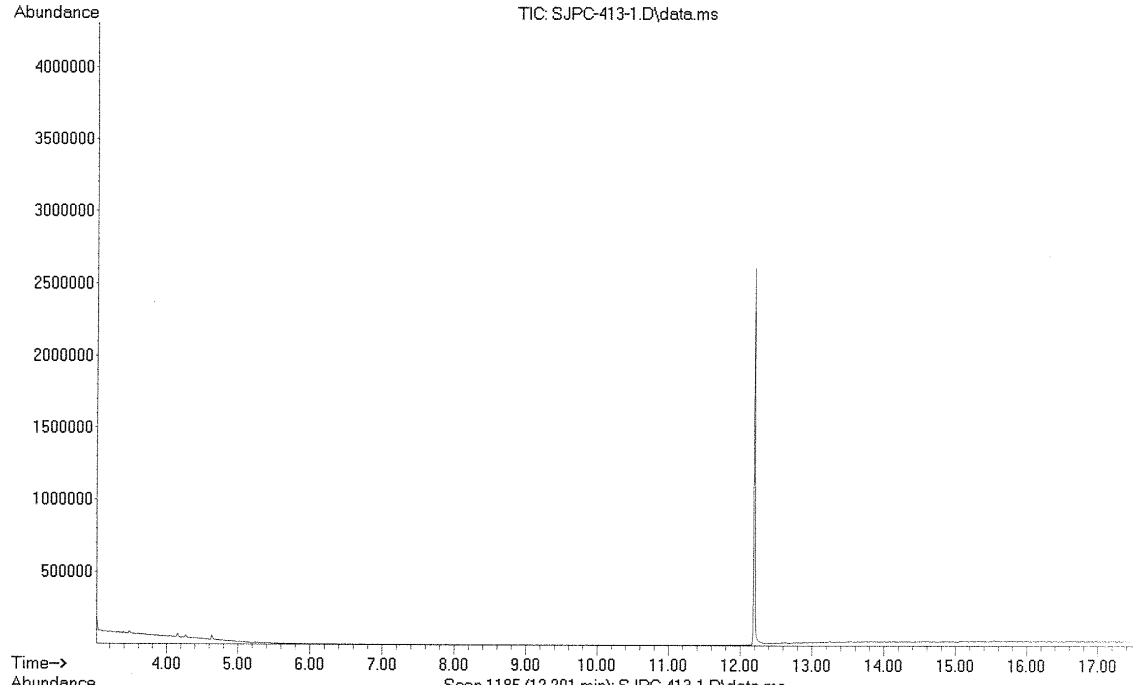

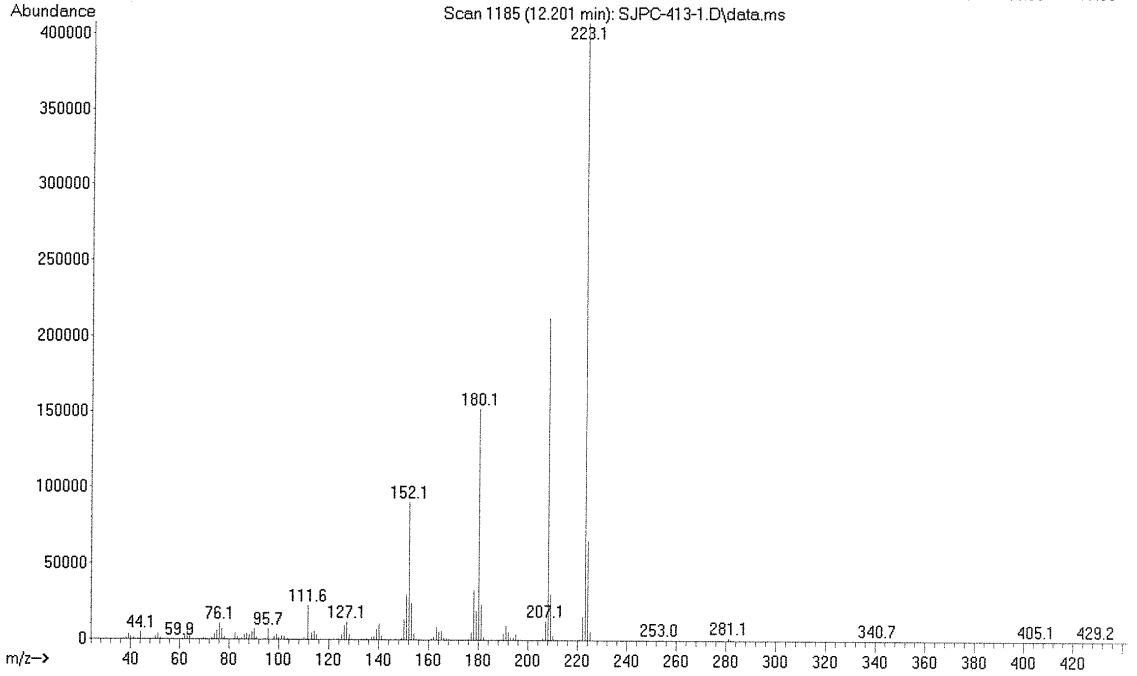

Figure S.24 – GC-MS of 2-(phenanthren-9-yl)-1H-pyrrole **20**

```
File       :C:\msdchem\1\DATA\PCAB\SJPC-436-OWE.D
Operator   : AB7
Acquired   : 19 May 2015  10:01     using AcqMethod NITROKETONE MODIFIE.M
Instrument :    GCMS
Sample Name: SJPC-436-OWE
Misc Info  :
Vial Number: 8
```

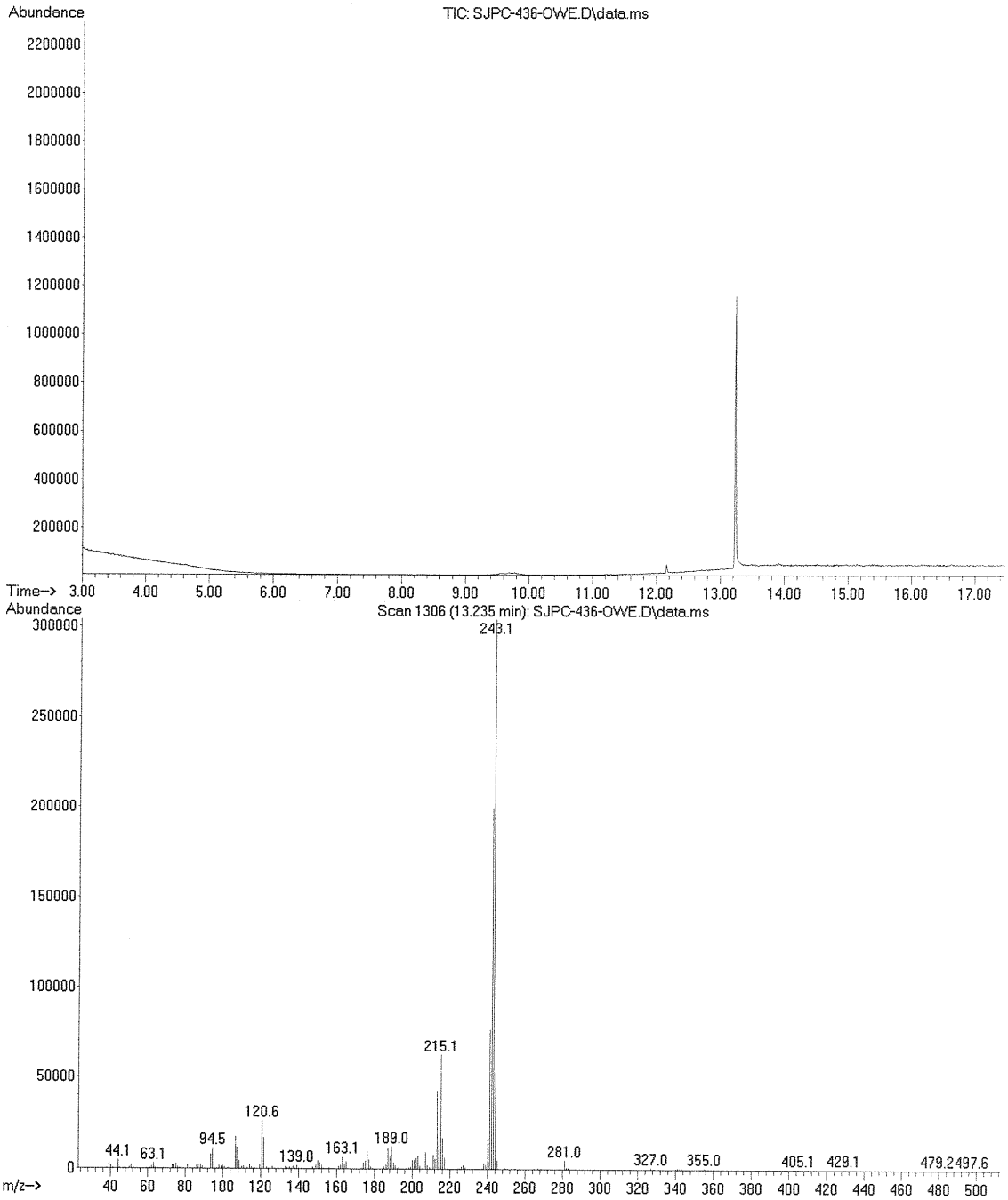

Spectroscopy

Figure S.25 – UV/vis absorption spectrum of BbF **1**, **5** and **8** – **10** in ACN solution.

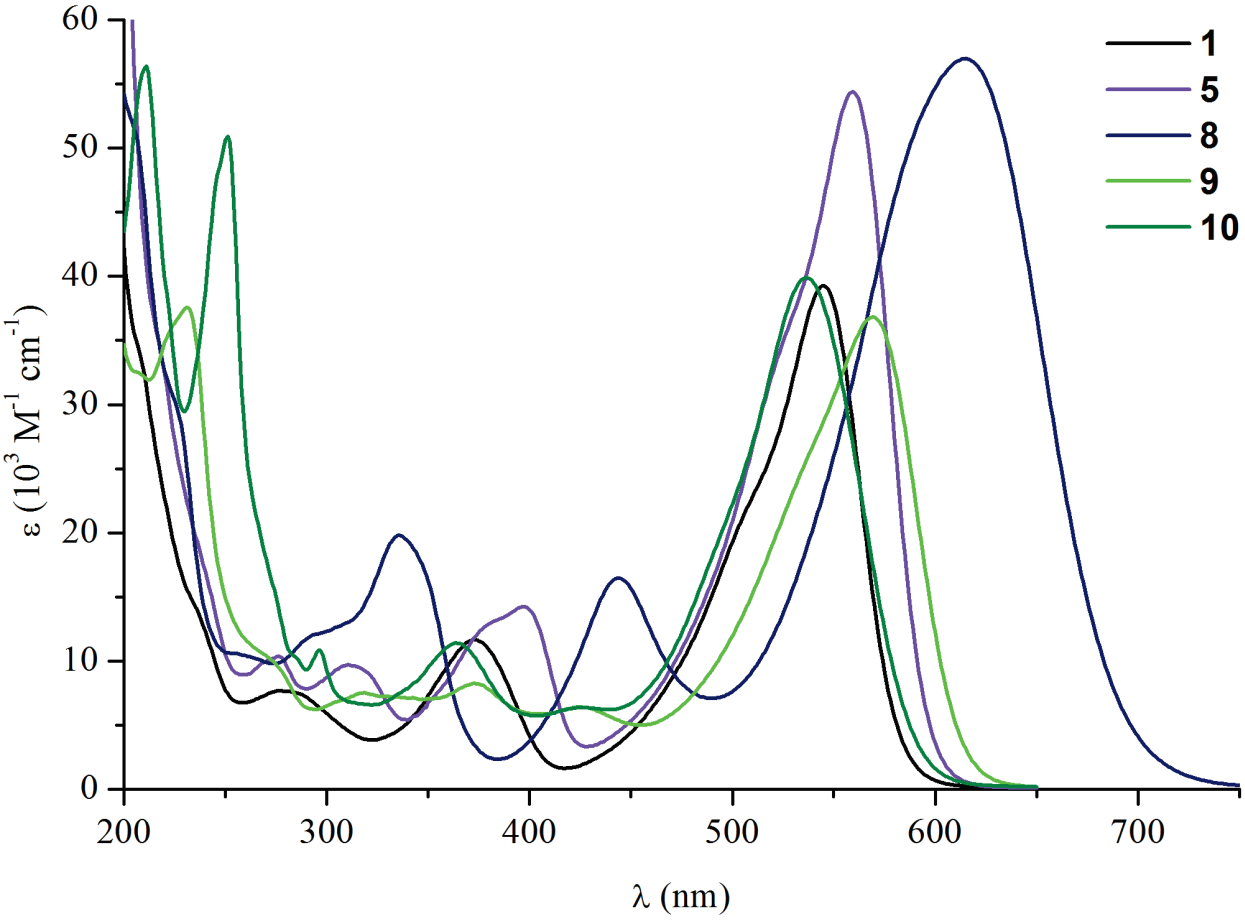

Figure S.26 – Absorption (solid) and emission spectrum (dash; excitation = 553 nm) of BbF **1** in DCM solution.

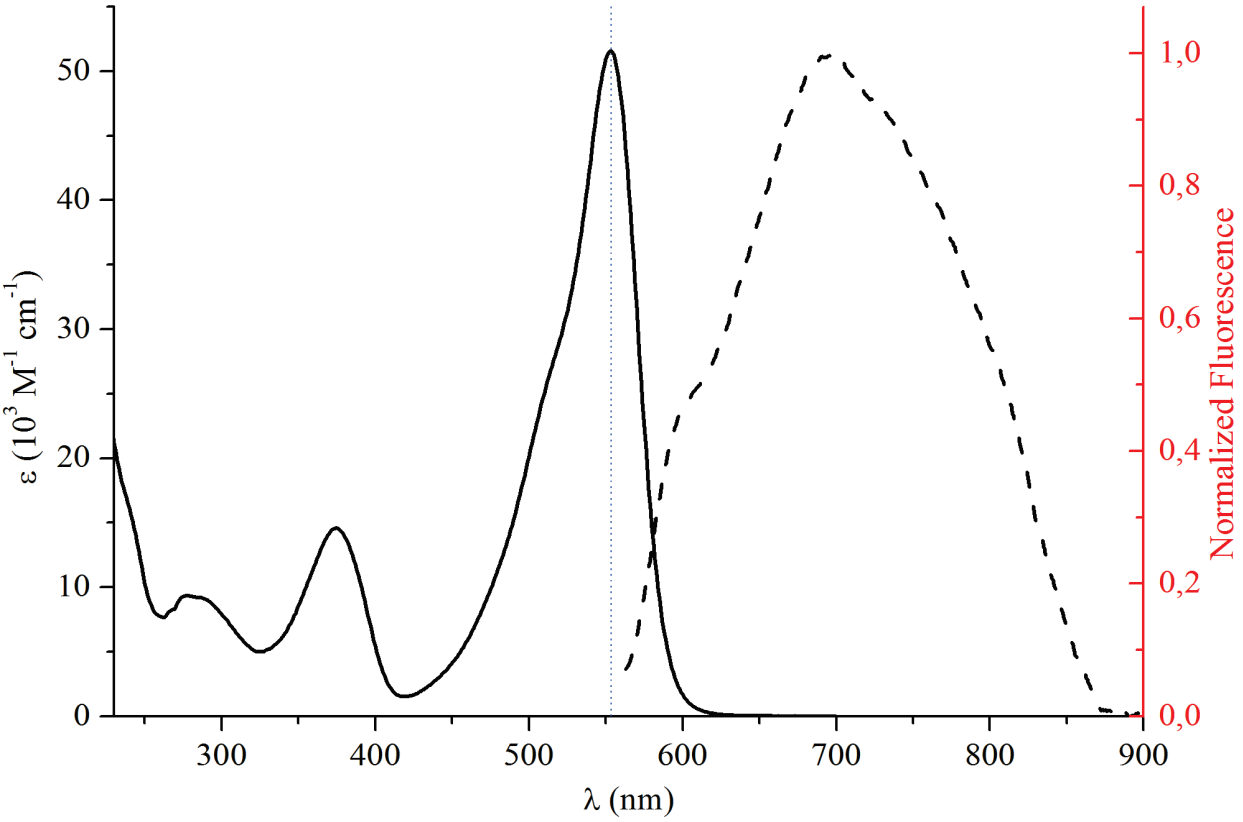

Figure S.27 – Absorption (solid) and emission spectrum (dash; excitation = 545 nm) of BbF **1** in ACN solution.

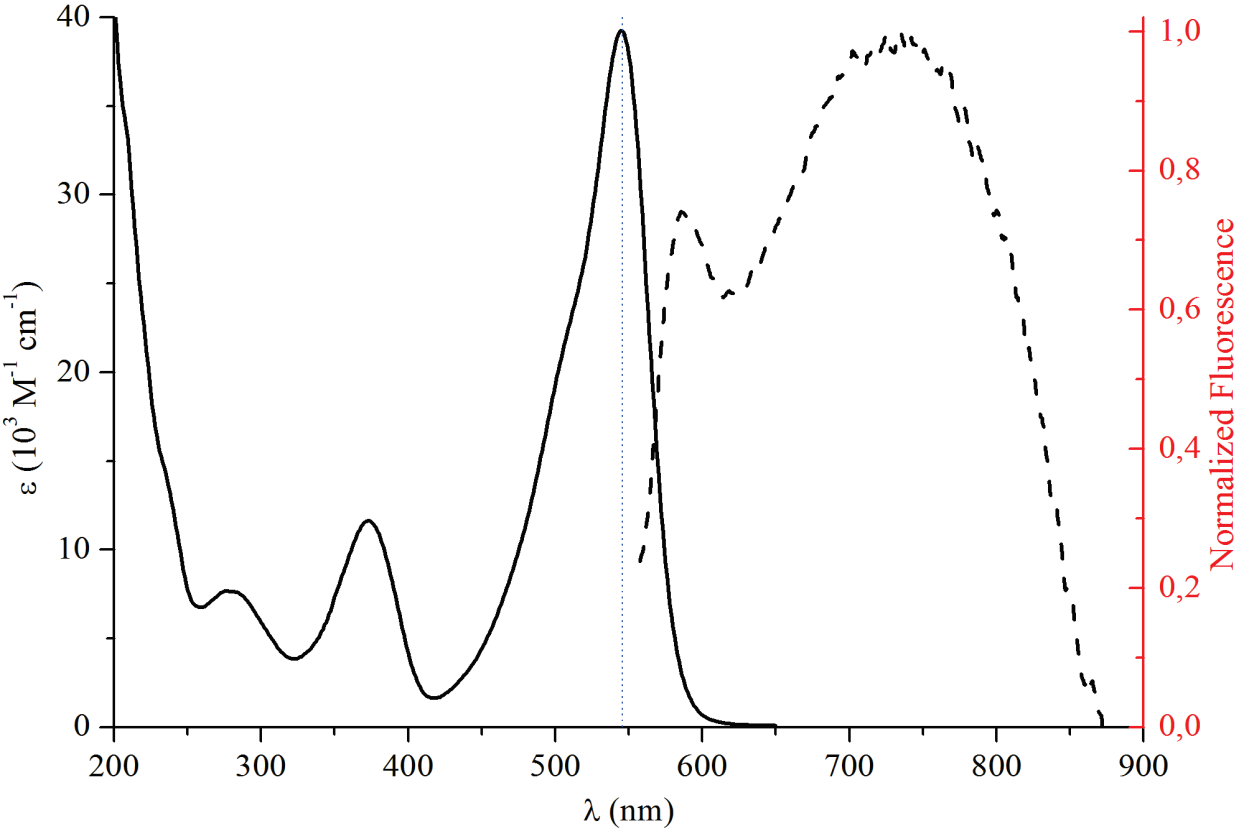

Figure S.28 – Absorption (solid) and emission spectrum (dash; excitation = 557 nm) of BbF **2** in DCM solution.

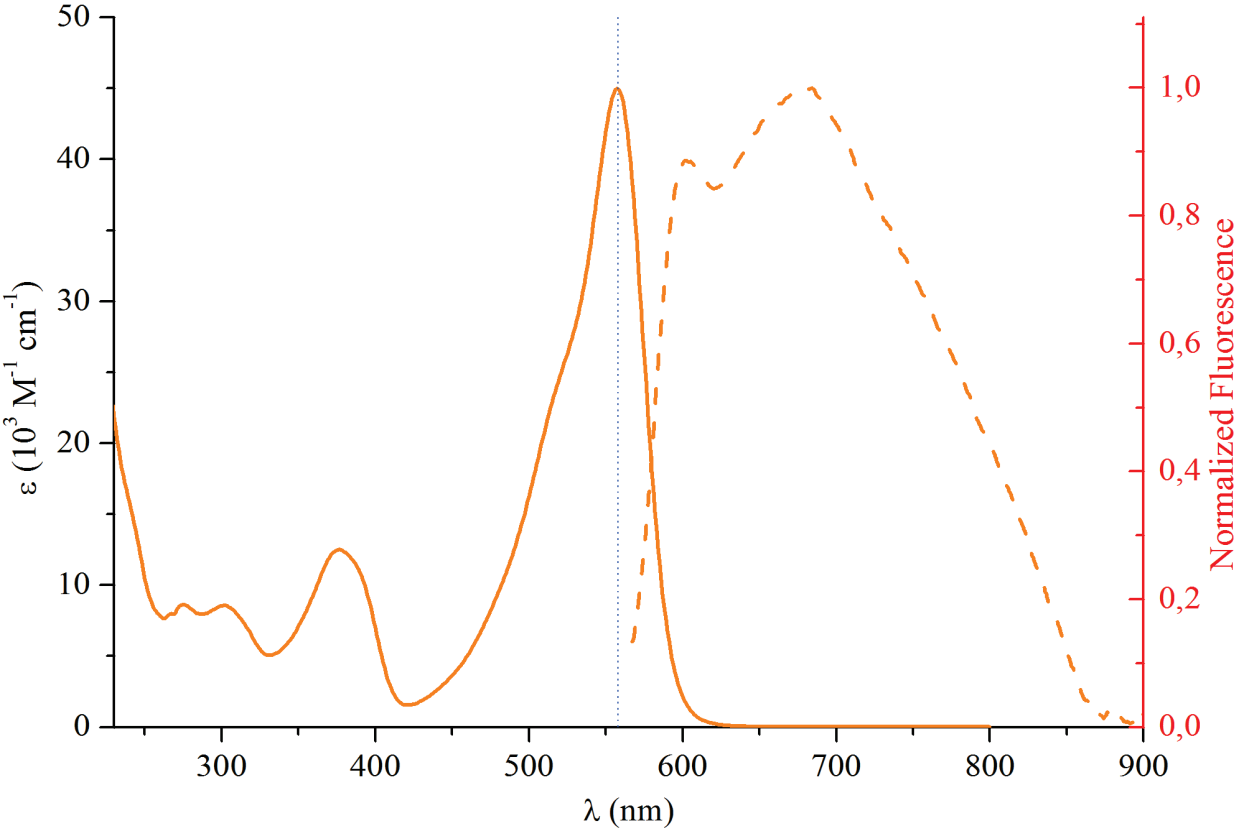

Figure S.29 – Absorption (solid) and emission spectrum (dash; excitation = 558 nm) of BbF **3** in DCM solution.

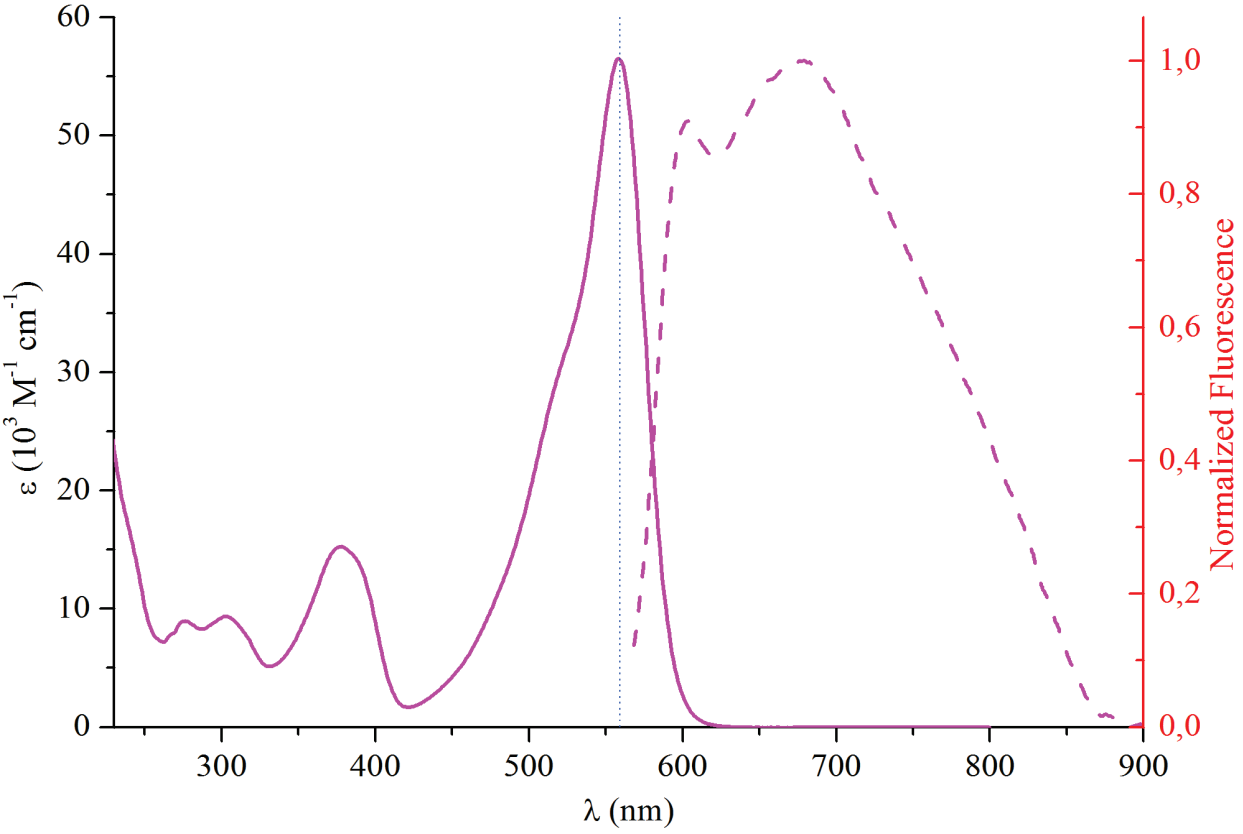

Figure S.30 – Absorption (solid) and emission spectrum (dash; excitation = 559 nm) of BbF **4** in DCM solution.

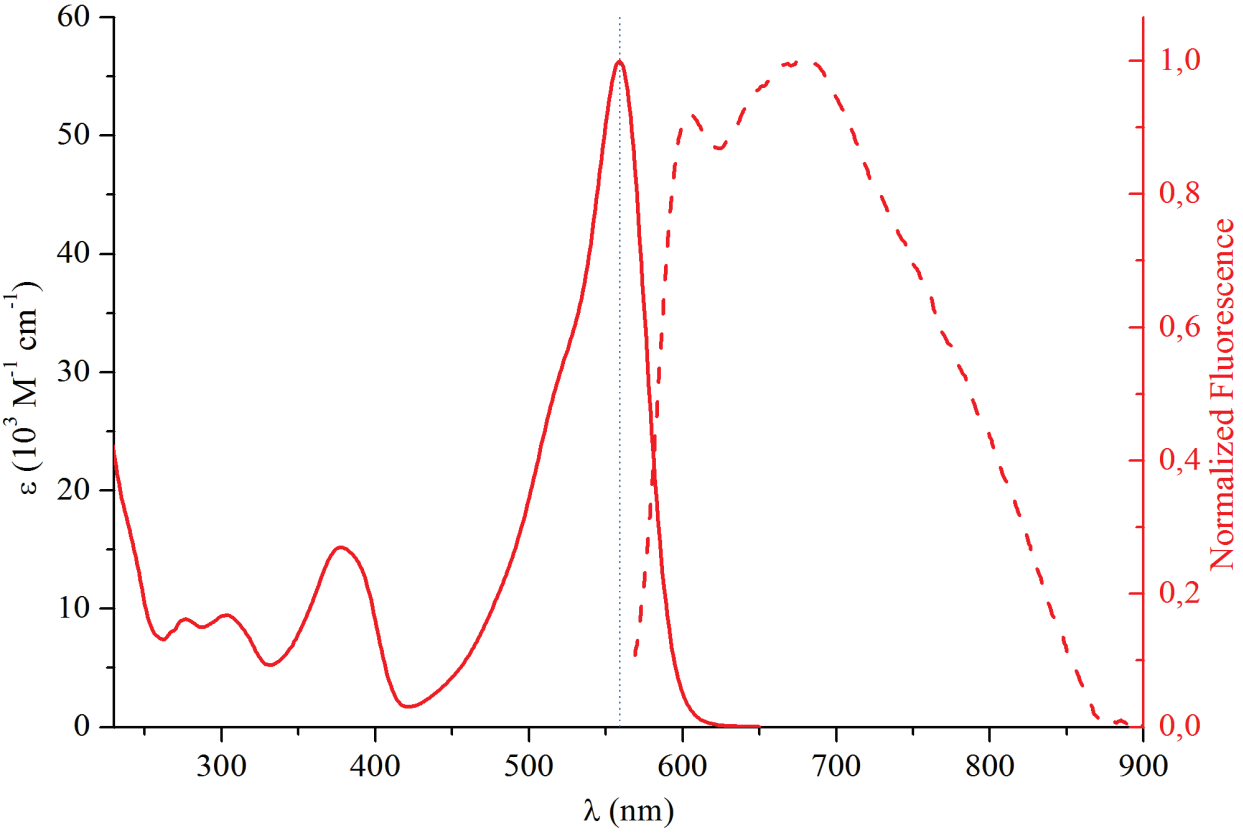

Figure S.31 – Absorption (solid) and emission spectrum (dash; excitation = 567 nm) of BbF **5** in DCM solution.

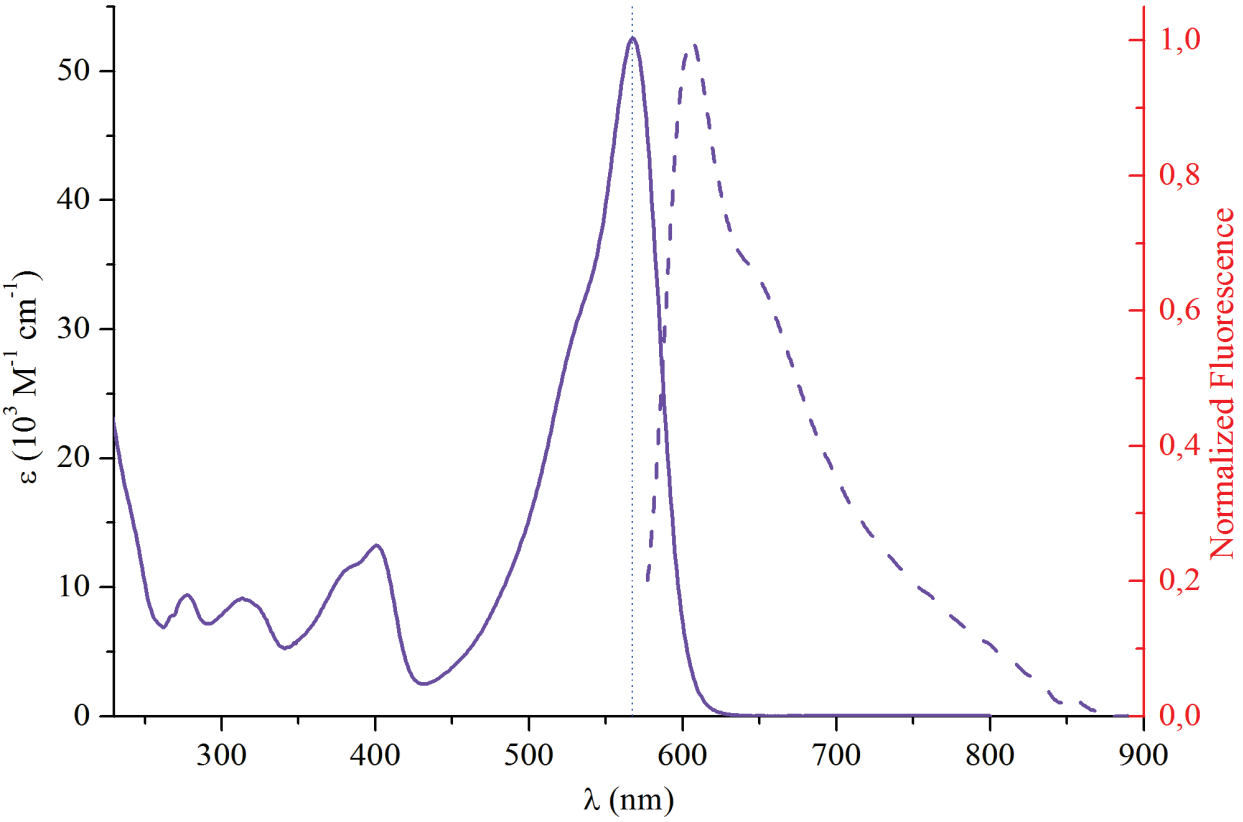

Figure S.32 – Absorption (solid) and emission spectrum (dash; excitation = 559 nm) of BbF **5** in ACN solution.

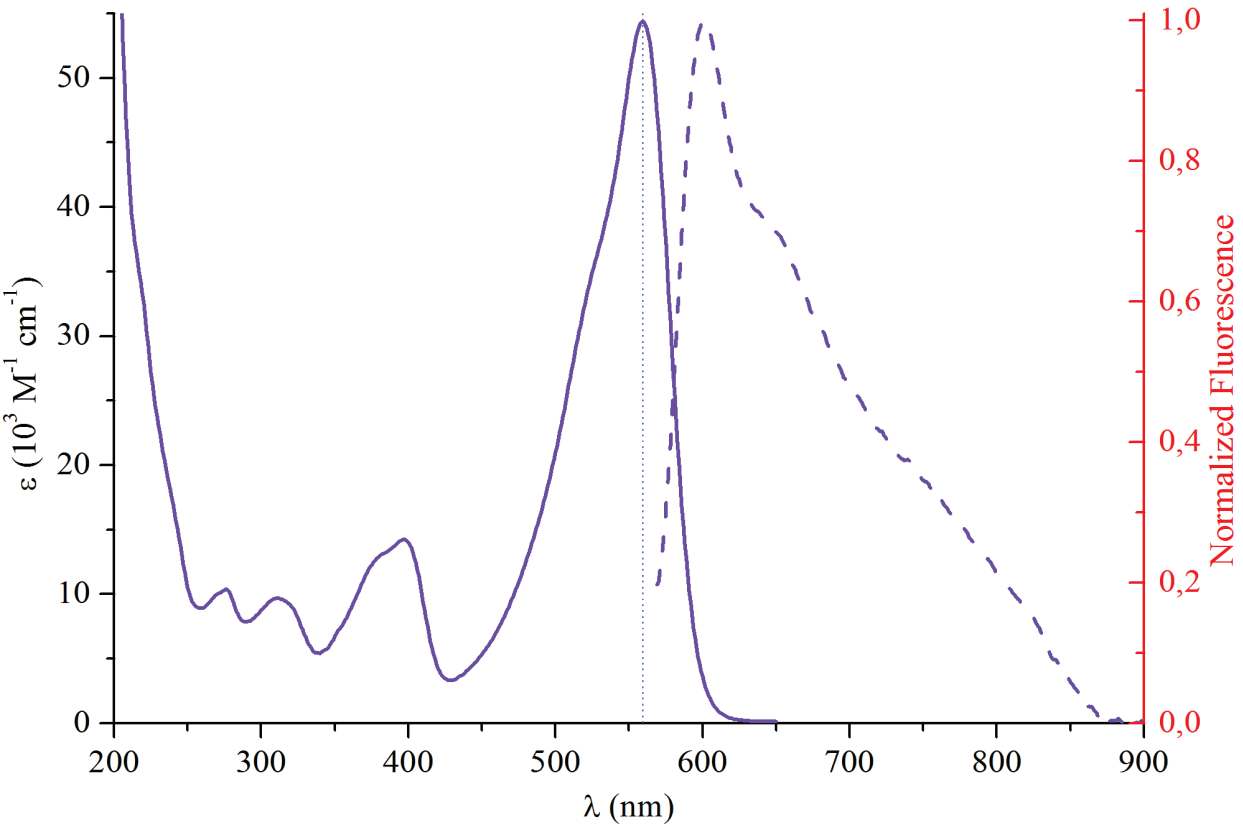

Figure S.33 – Absorption (solid) and emission spectrum (dash; excitation = 556 nm) of BbF **6** in DCM solution.

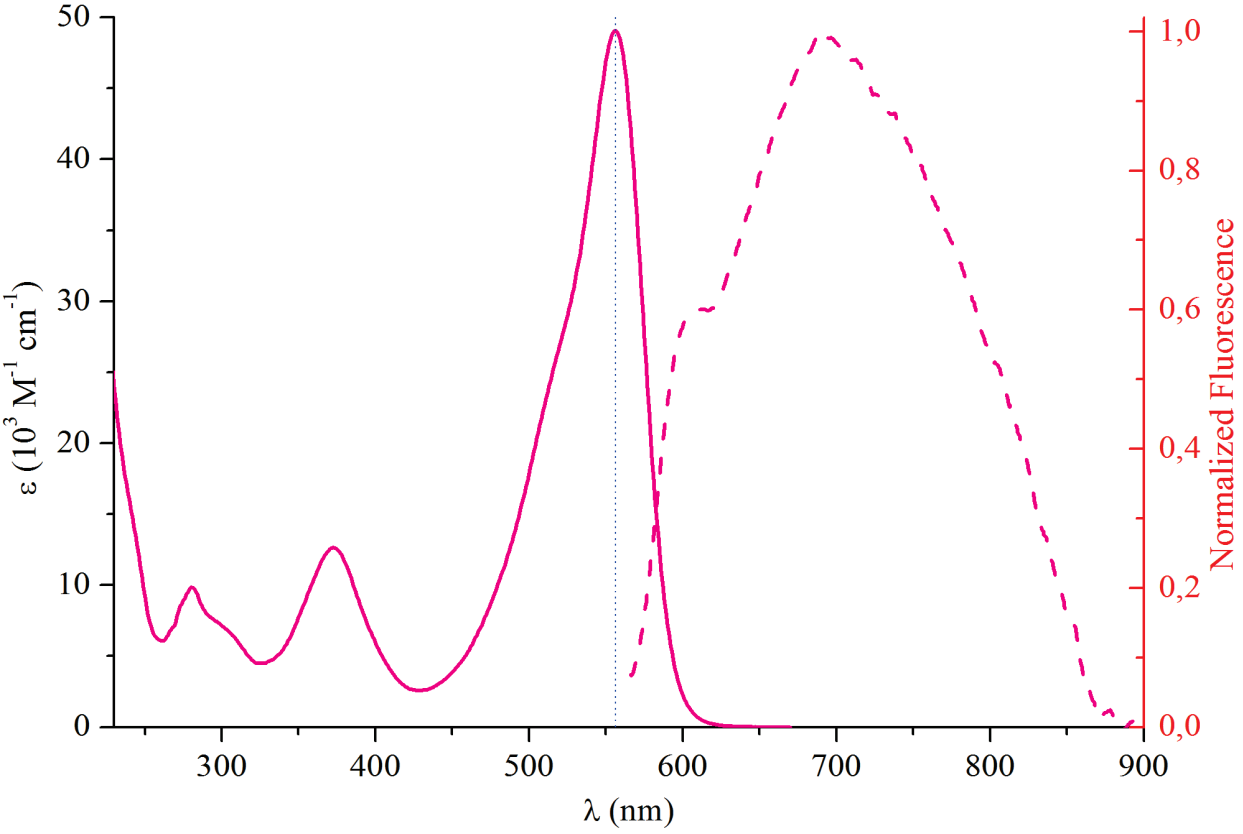

Figure S.34 – Absorption (solid) and emission spectrum (dash; excitation = 557 nm) of BbF **7** in DCM solution.

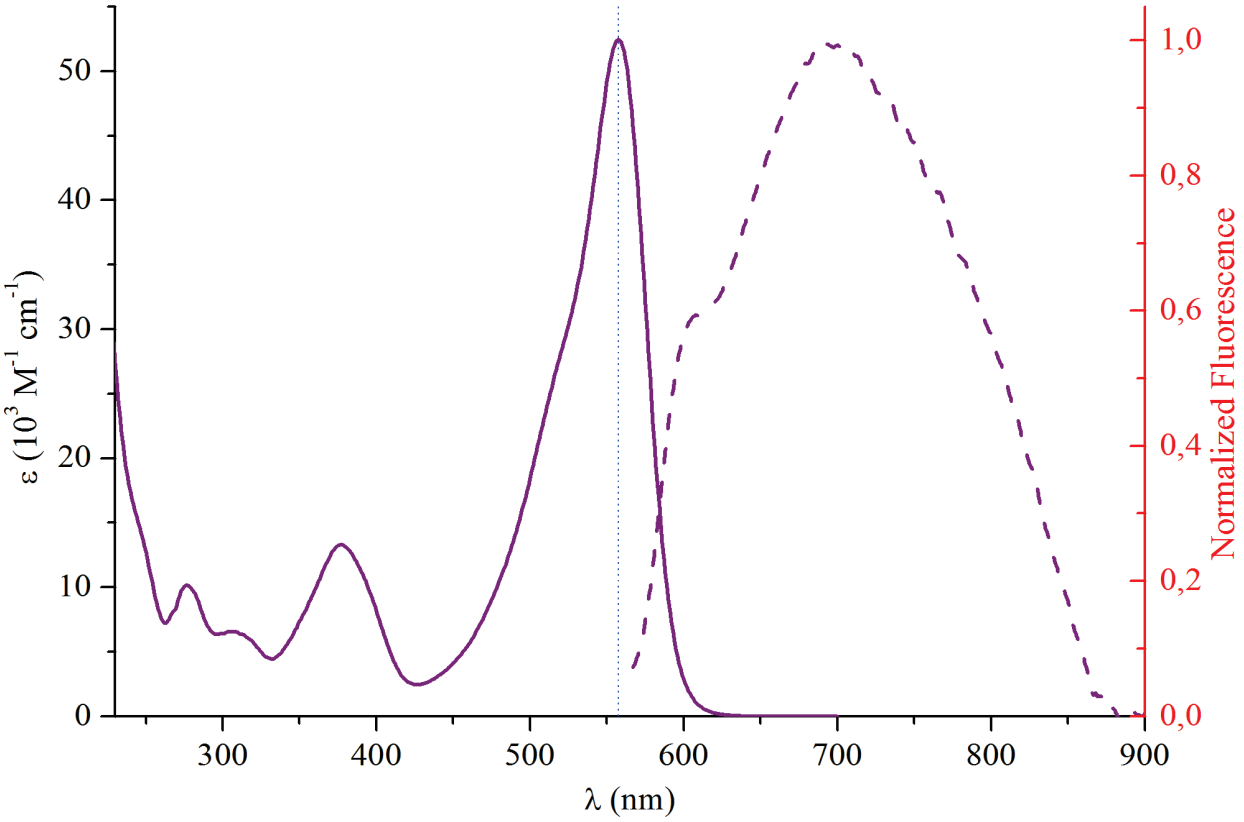

Figure S.35 – Absorption (solid) and emission spectrum (dash; excitation = 626 nm) of BbF **8** in DCM solution.

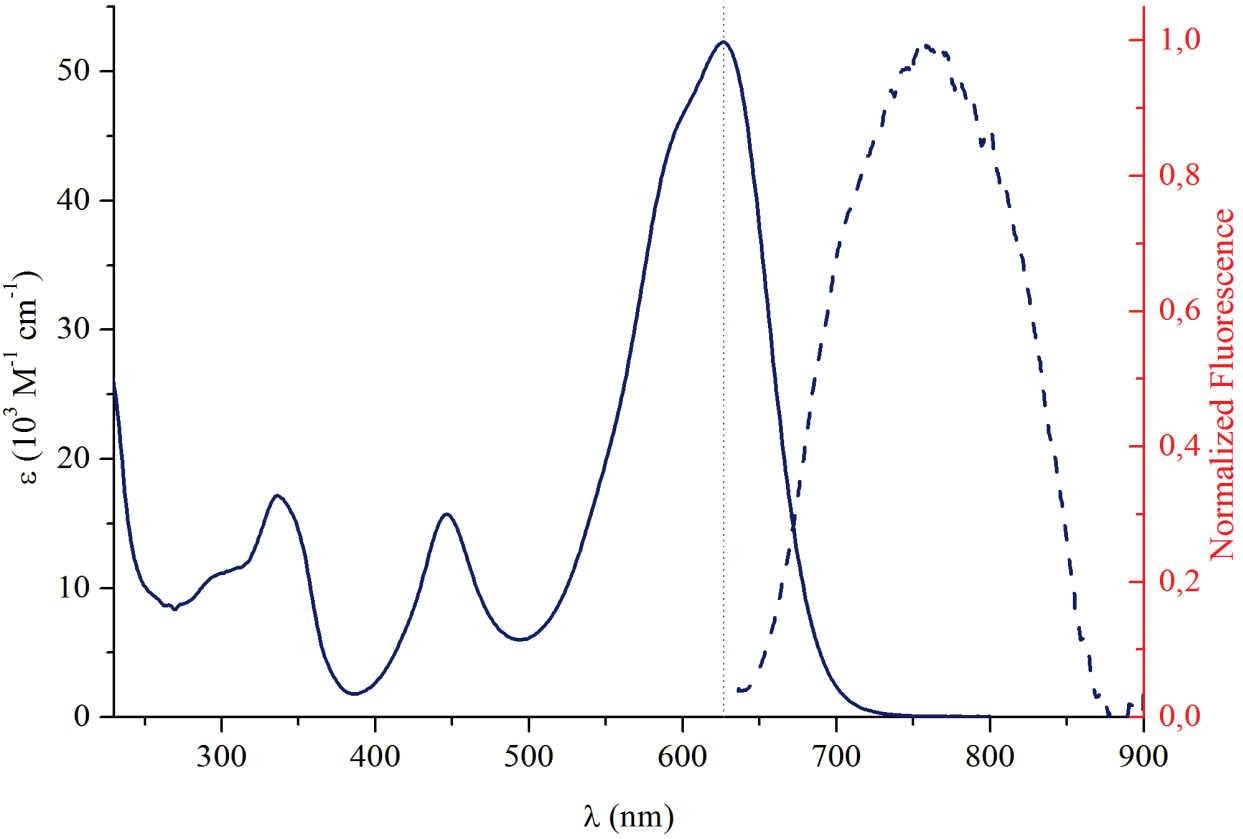

Figure S.36 – UV/vis absorption spectrum of BbF **8** before (blue) and after (orange) addition of an excess of $HClO_4$ in DCM solution.

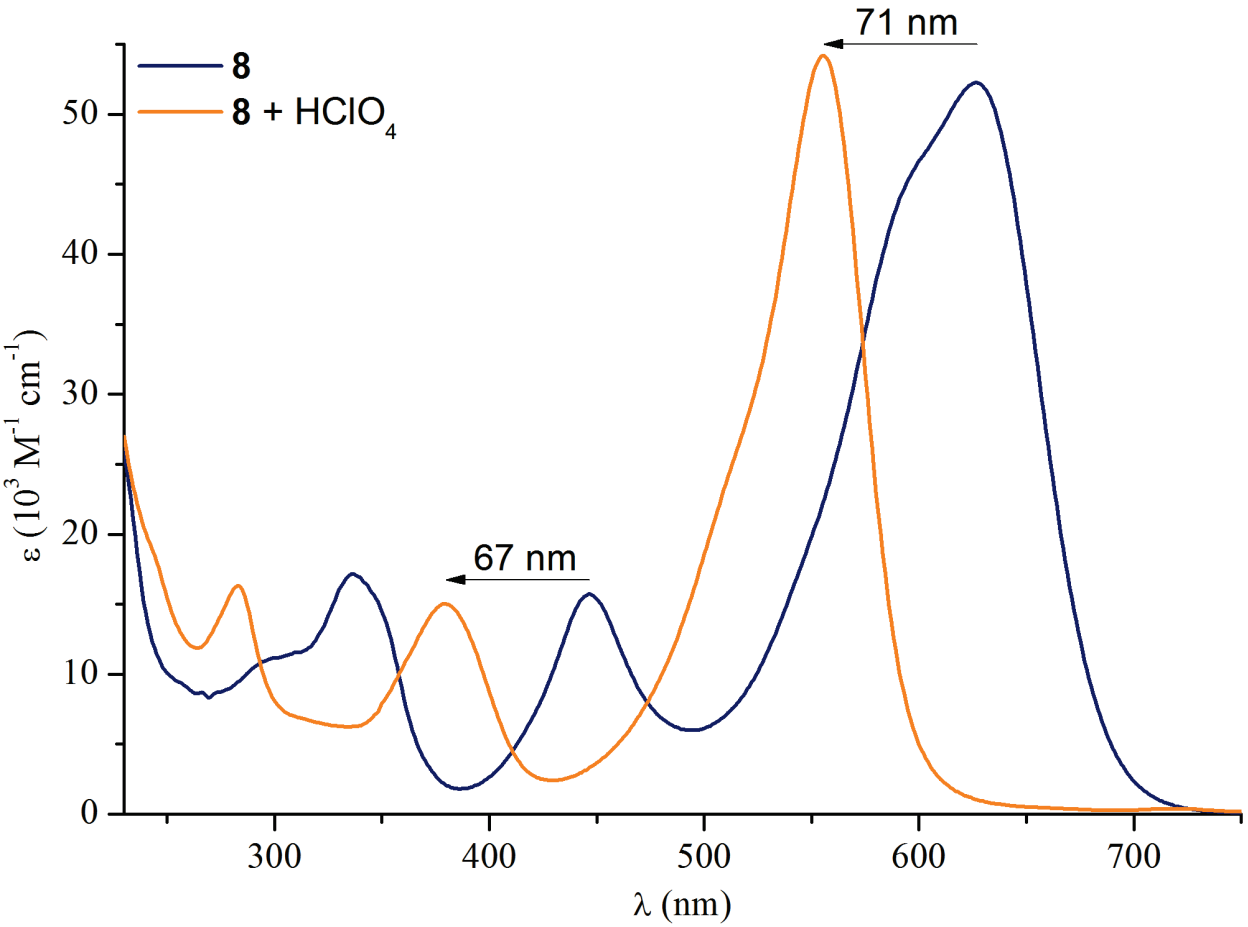

Figure S.37 – UV/vis absorption spectrum of BbF **8** before (blue) and after (orange) addition of an excess of $HClO_4$ in ACN solution.

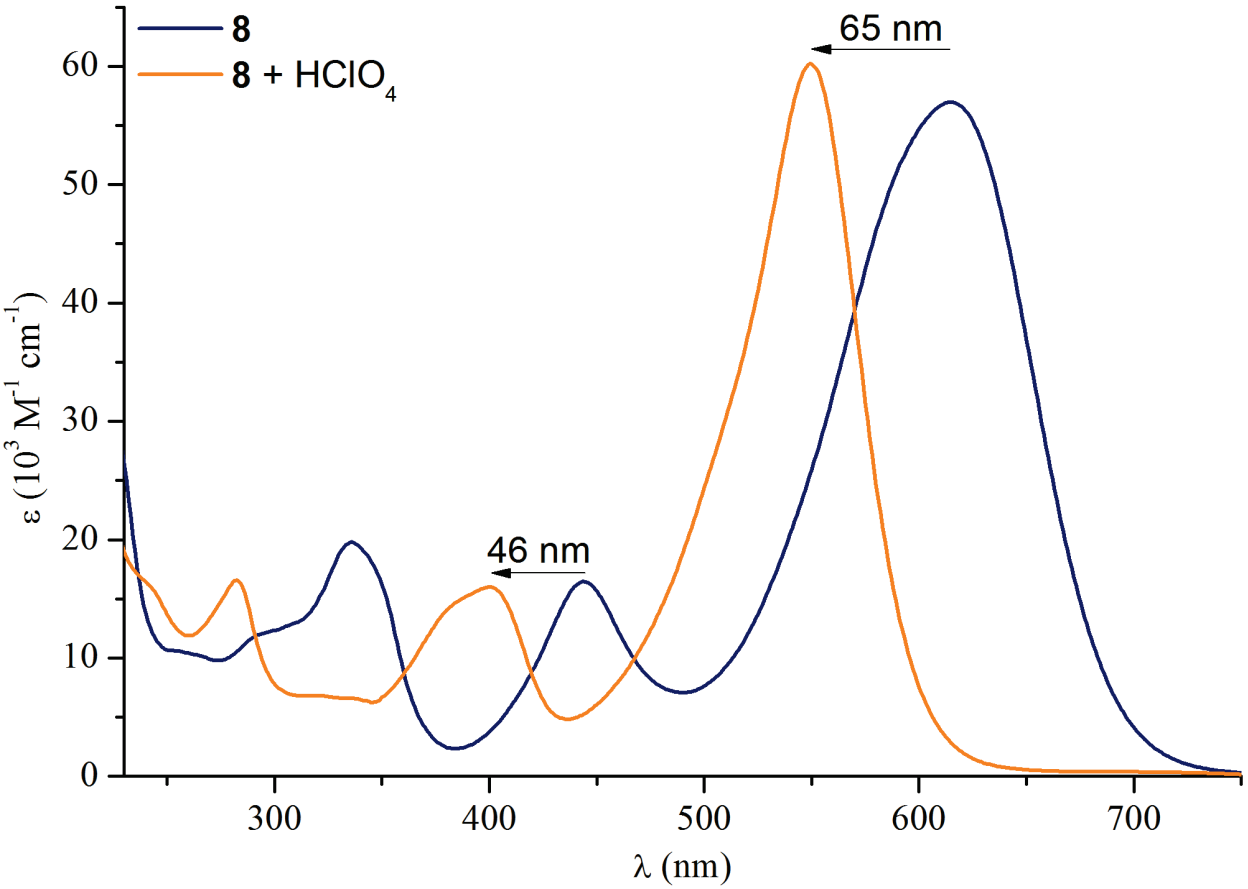

Figure S.38 – Absorption (solid) and emission spectrum (dash; excitation = 578 nm) of BbF **9** in DCM solution.

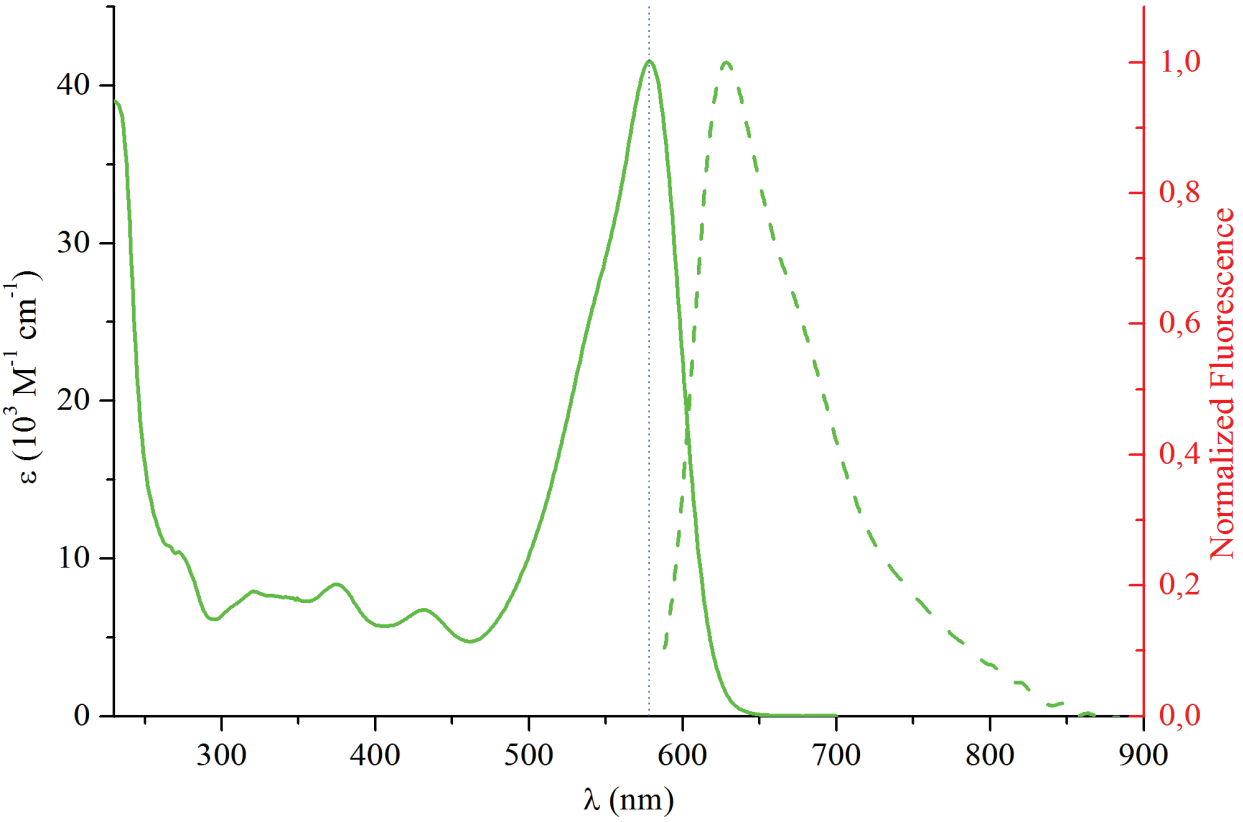

Figure S.39 – Absorption (solid) and emission spectrum (dash; excitation = 569 nm) of BbF **9** in ACN solution.

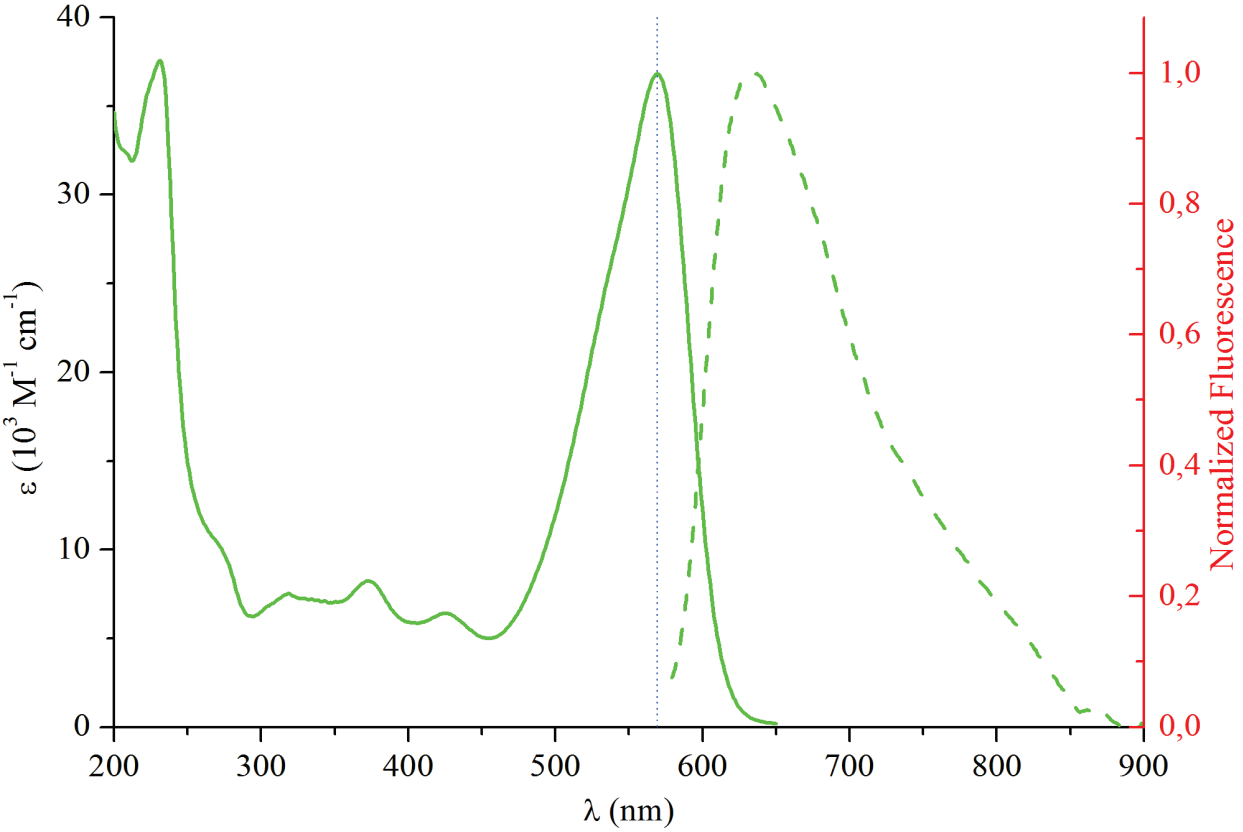

Figure S.40 – Absorption (solid) and emission spectrum (dash; excitation = 547 nm) of BbF **10** in DCM solution.

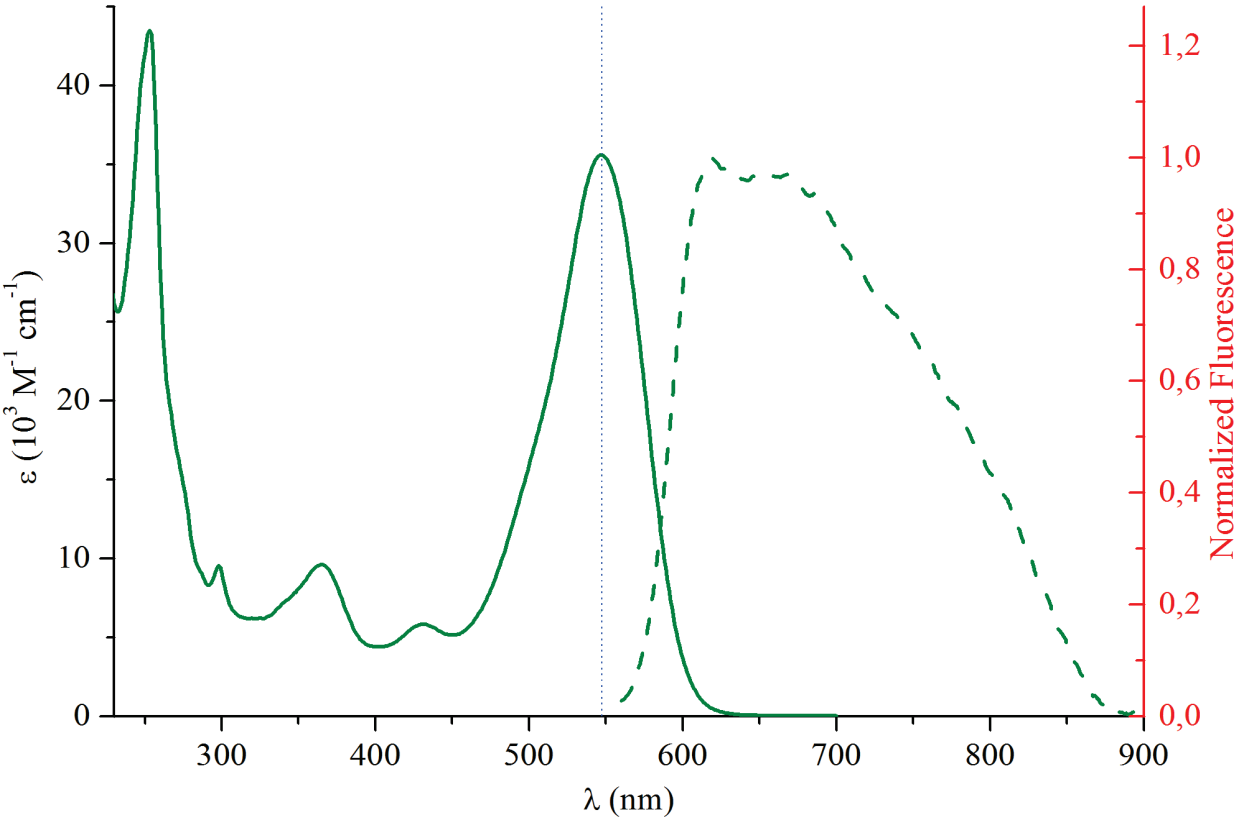

Figure S.41 – Absorption (solid) and emission spectrum (dash; excitation = 536 nm) of BbF **10** in ACN solution.

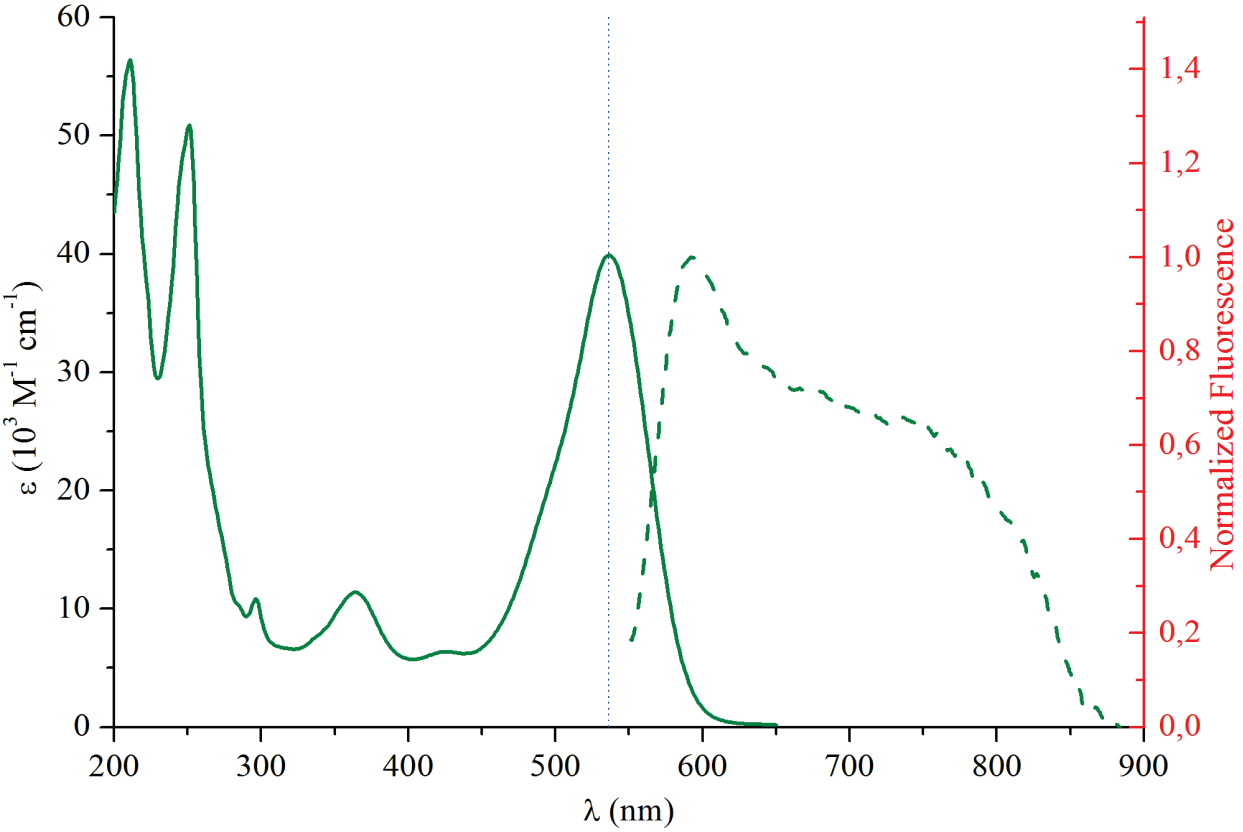

Table S.1 – Compilation of the optoelectronic properties for related BODIPYs of interest previously reported in literature.

	Spectroscopy [a]							Electrochemistry [b]						
	Solvent	**$\lambda_{Abs\ max}$**	**λ_{Em}**	**Δ_{Stoke} (cm^{-1})**	**Φ_F**	**τ (ns)**	**Ref**	**Solvent**	**E_{Ox}**	**E_{Red}**	**HOMO redox**	**LUMO redox**	**ΔE_{Ox}**	**Ref**
22	$CHCl_3$	504 (14)	512	311	0.70	5.0	[19]	DCM	1.61*	-0.73*	-6.56	-4.22	2.34	[19]
23	$CHCl_3$	504 (58)	521	620	0.06	0.45	[19]	DCM	1.65*	-0.73; -1.71*	-6.60	-4.22	2.38	[20]
	DCM	500 (33)	527	1025	0.03	NA	[21]							
24	DCM	501 (87)	513	467	0.67	3.51	[22]	DCM	1.51	-1.22*	-6.46	-3.73	2.73	[23]
	ACN	497 (48)	511	520	0.52	3.21	[24]	ACN	1.17	-1.19	-6.12	-3.76	2.36	[25]
25	ACN	523	547	839	0.015	NA	[26]							
26	ACN	536	556	671	0.884	NA	[27]							
27	ACN	552	577	785	0.854	NA	[27]							
28	ACN	608	NF	---	---	---	[27]							
	MeOH	608	NF	---	---	---	[27]							
	MeOH + $HClO_4$	535	554	641	0.54	NA	[27]							
29	ACN	547	572	799	0.77	NA	[27]							
30	DCM	512 (42)	655	4264	~0.10	NA	[23]	DCM	1.57*	-0.78	-6.52	-4.17	2.35	[23]
31	THF	539 (54)	690	4060	<0.01	NA	[1]	DCM	1.51*	-0.59; -1.63	-6.46	-4.36	2.10	[1]
32	DCM	568 (~34)	NF	---	---	---	[23]	DCM	1.66*	-0.24	-6.61	-4.71	1.90	[23]
33	DCM	570	599	849	0.80	NA	[28]							
34	DCM	631 (102)	664	788	0.93	5.2	[29]	DCM	0.83; 1.68*	-1.08	-5.78	-3.87	1.91	[29]
35	DCM	617 (108)	652	870	0.91	5.8	[29]	DCM	0.78; 1.63*	-1.17	-5.73	-3.78	1.95	[29]
36	$CHCl_3$	542 (140)	549	235	0.96	NA	[30]							
37	$CHCl_3$	579 (202)	583	118	0.96	NA	[31]							
38	$CHCl_3$	652 (314)	661	447	0.90	NA	[30]							
39	$CHCl_3$	673 (288)	683	218	0.86	NA	[31]							
40	$CHCl_3$	671 (313)	680	197	0.91	NA	[30]							
41	$CHCl_3$	662 (316)	671	203	0.97	NA	[30]							
42	DCM	518 (56) / 770 (br)	NF	---	---	---	[23]	DCM	1.24	-0.39; -1.15	-6.19	-4.56	1.63	[23]
43	DCM	482 (~55)	528	1810	Very Low	NA	[32]	DCM	0.95; 1.12	-1.39	-5.90	-3.56	2.34	[32]
44	DCM	516 (36)	546	1065	0.66	NA	[33]							
45	DCM	578 (105)	603	1083	0.97	NA	[34]							

[a] NF = Non-Fluorescent / NA = Non-Available. For compound **43**, only the mention "very low" can be found in the reference regarding the quantum yields.
[b] Reported *vs* SCE. * = Irreversible process. The values reported herein for compounds **23**, **24**, **30**-**32**, **34**, **35**, **42** and **43** were corrected *vs* SCE using Fc^+/Fc = 0.46V in DCM.

Electrochemistry

Figure S.42 – CV of BbF **1** with ferrocene internal reference. (Fc = 0.46 V vs SCE in DCM; Scan rate of 50 mV/s at R.T.)

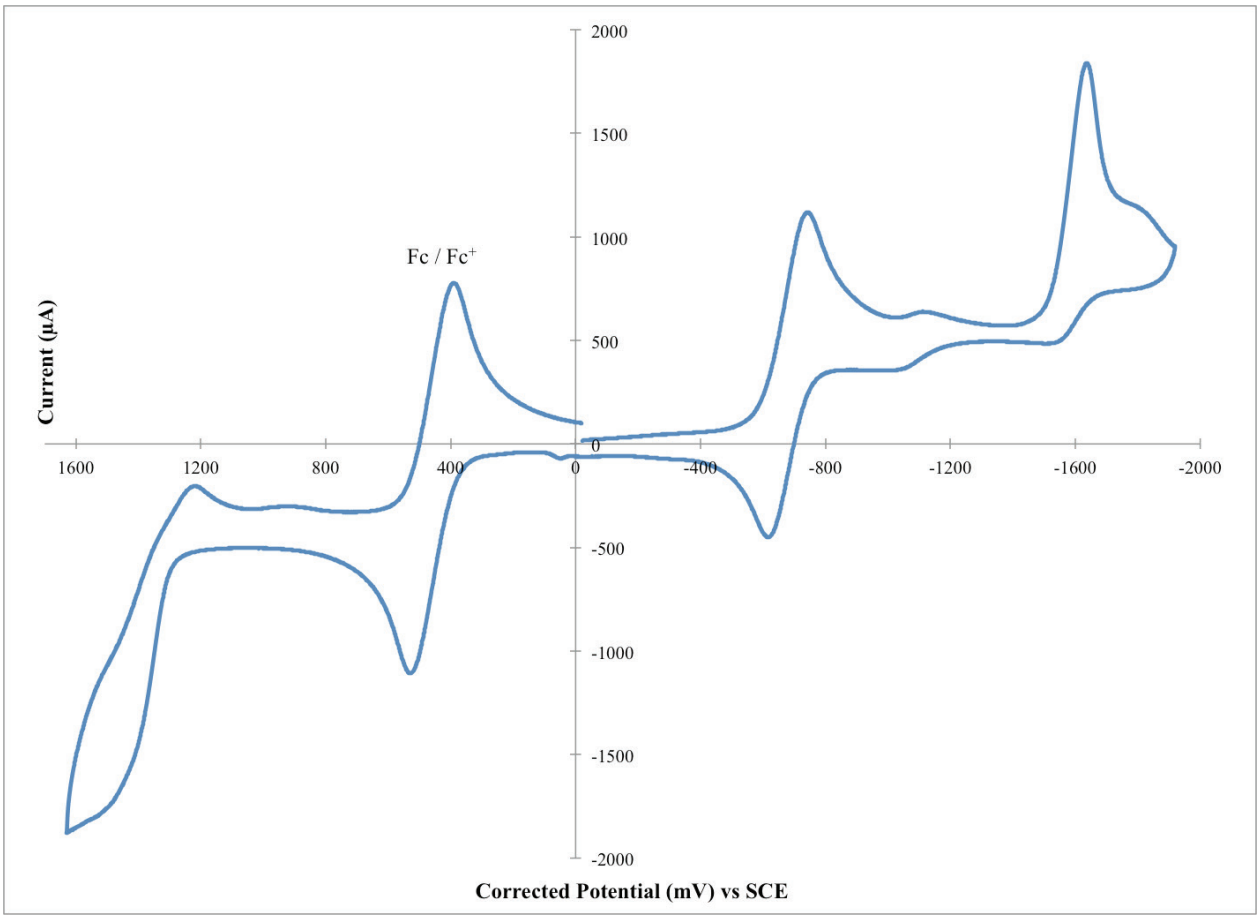

Figure S.43 – DPV of oxidation (top) and reduction (bottom) potentials for BbF **1** with ferrocene internal reference. (0.46 V vs SCE in DCM) (Scan rate of 50 mV/s at R.T.)

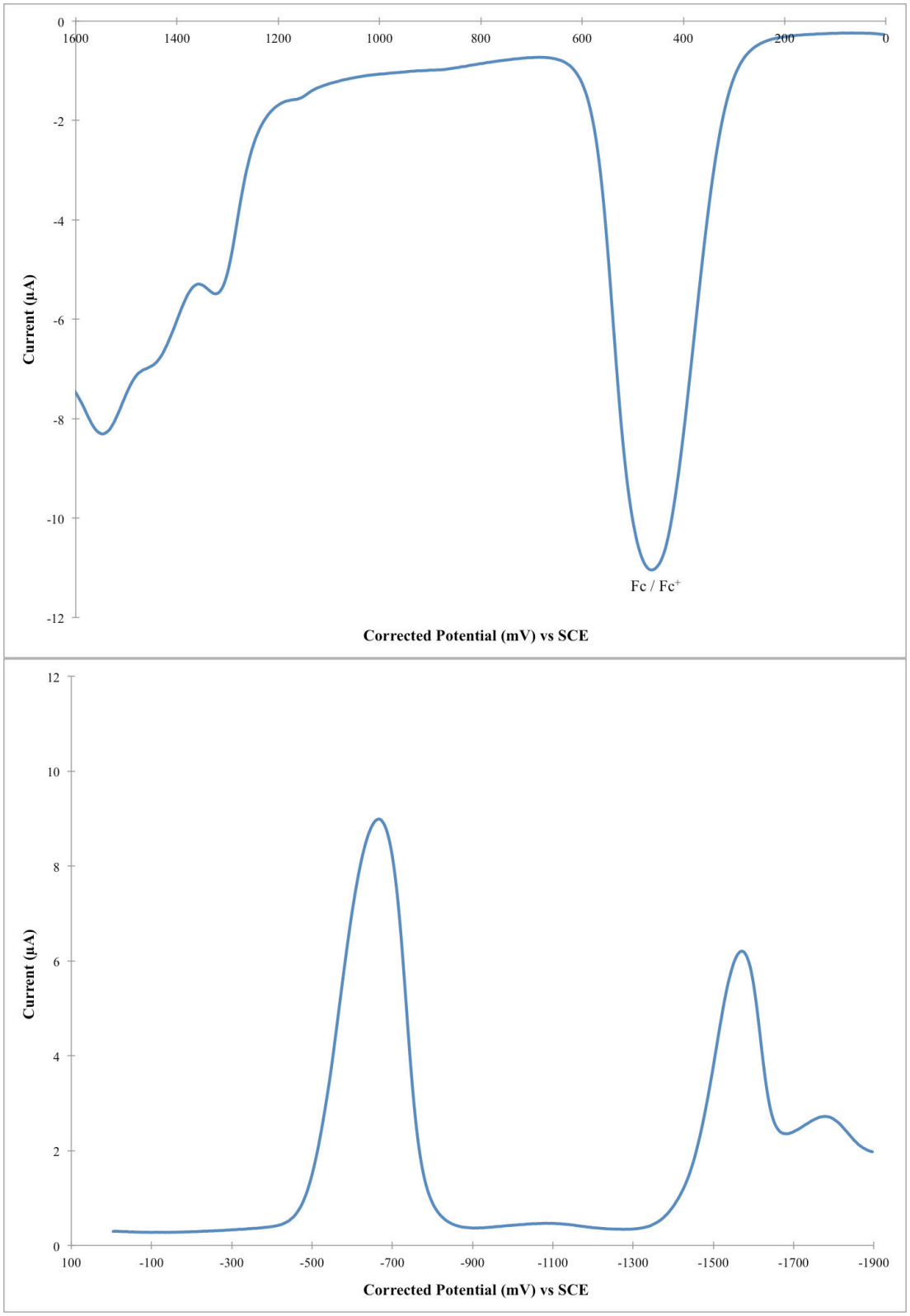

Figure S.44 – CV of BbF **2** with ferrocene internal reference. (Fc = 0.46 V vs SCE in DCM; Scan rate of 50 mV/s at R.T.)

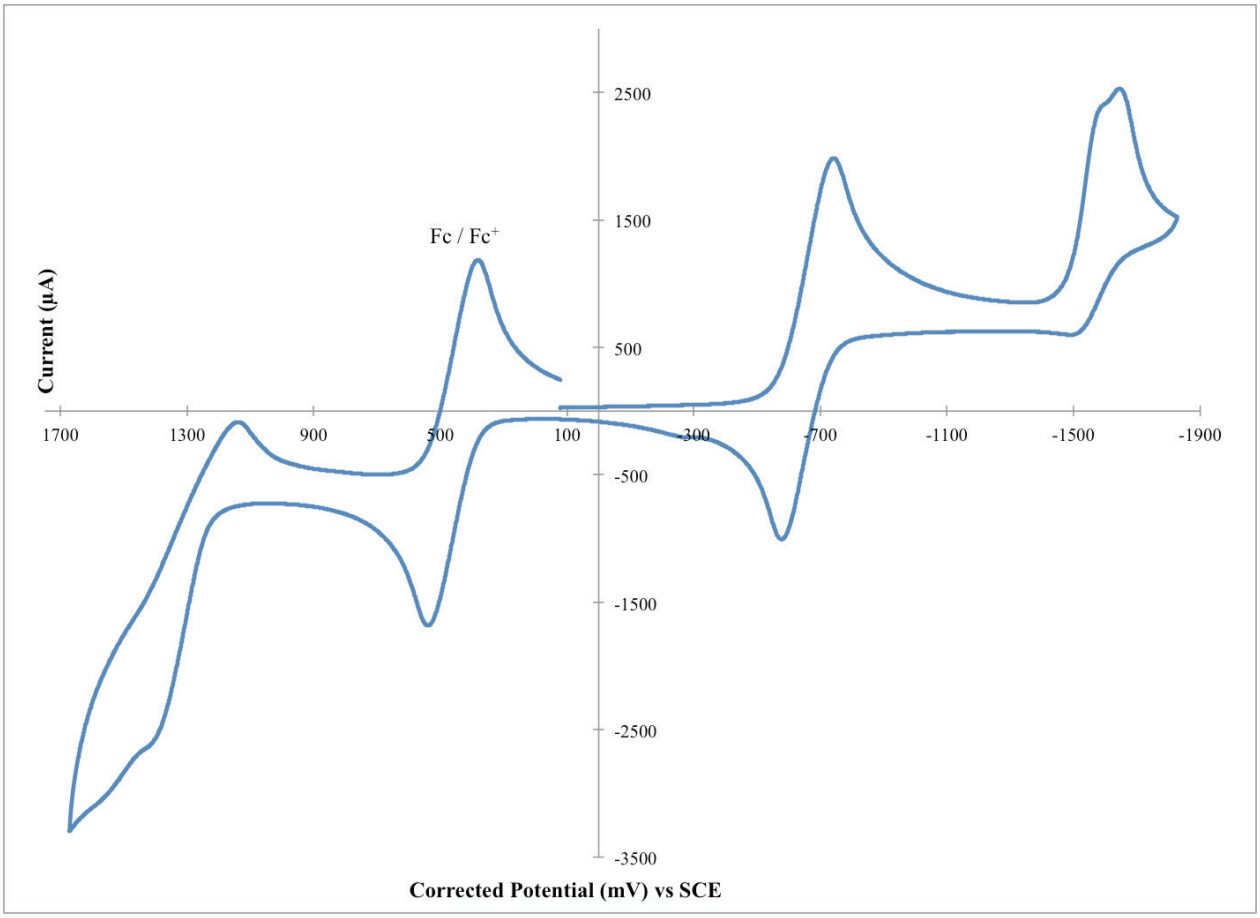

Figure S.45 – DPV of oxidation (top) and reduction (bottom) potentials for BbF **2** with ferrocene internal reference. (0.46 V vs SCE in DCM) (Scan rate of 50 mV/s at R.T.)

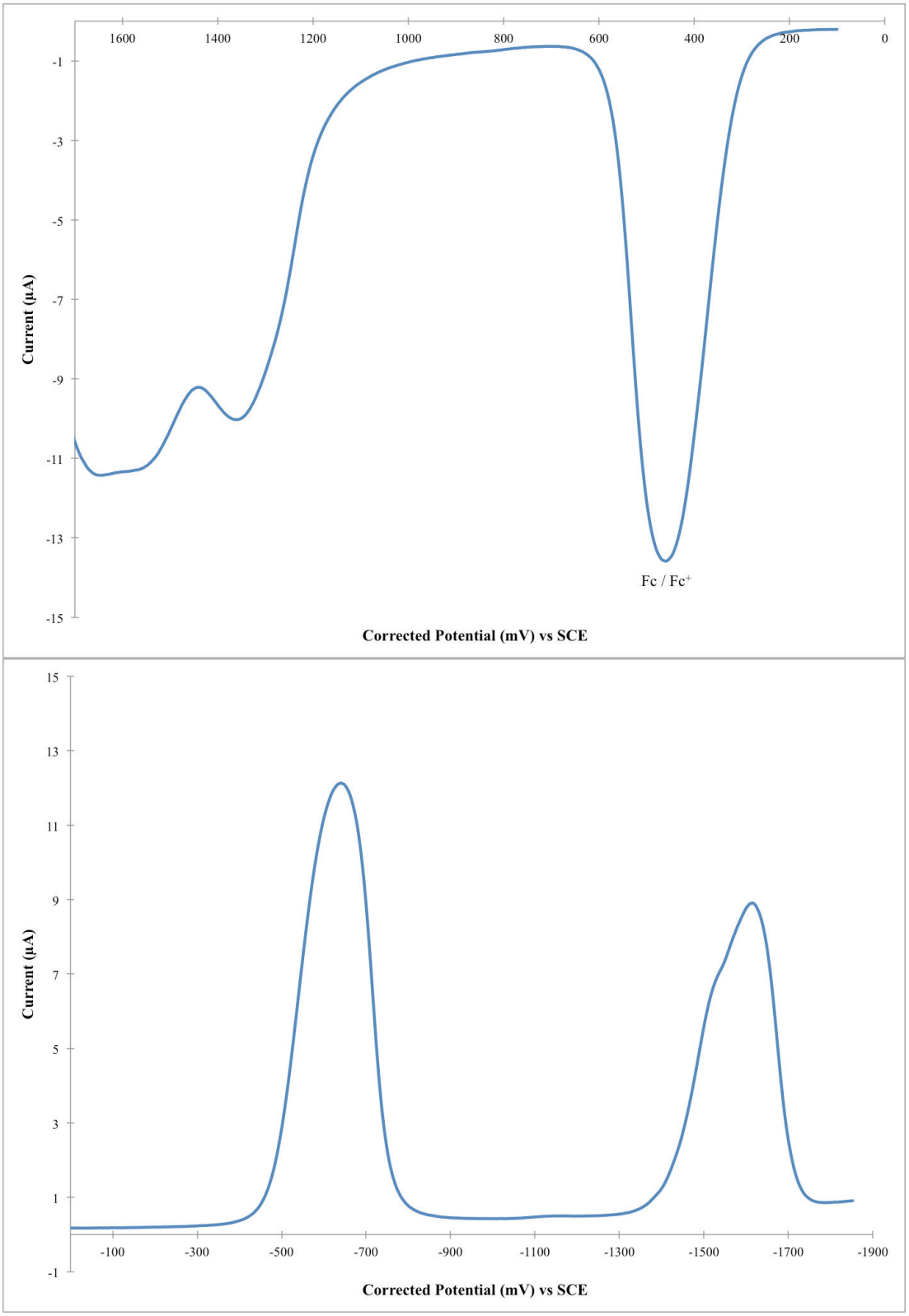

Figure S.46 – CV of BbF **3** with ferrocene internal reference. (Fc = 0.46 V vs SCE in DCM; Scan rate of 50 mV/s at R.T.)

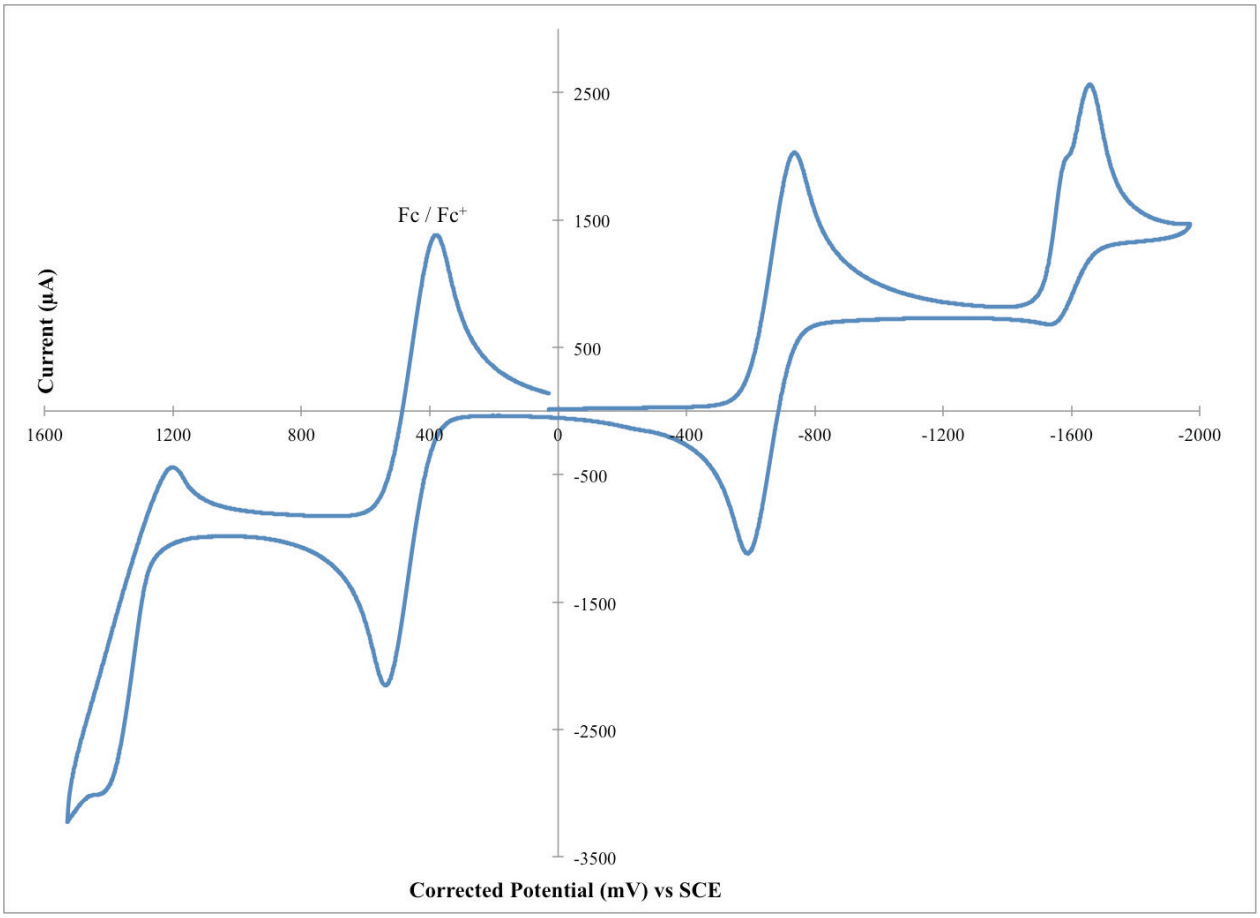

Figure S.47 – DPV of oxidation (top) and reduction (bottom) potentials for BbF **3** with ferrocene internal reference. (0.46 V vs SCE in DCM) (Scan rate of 50 mV/s at R.T.)

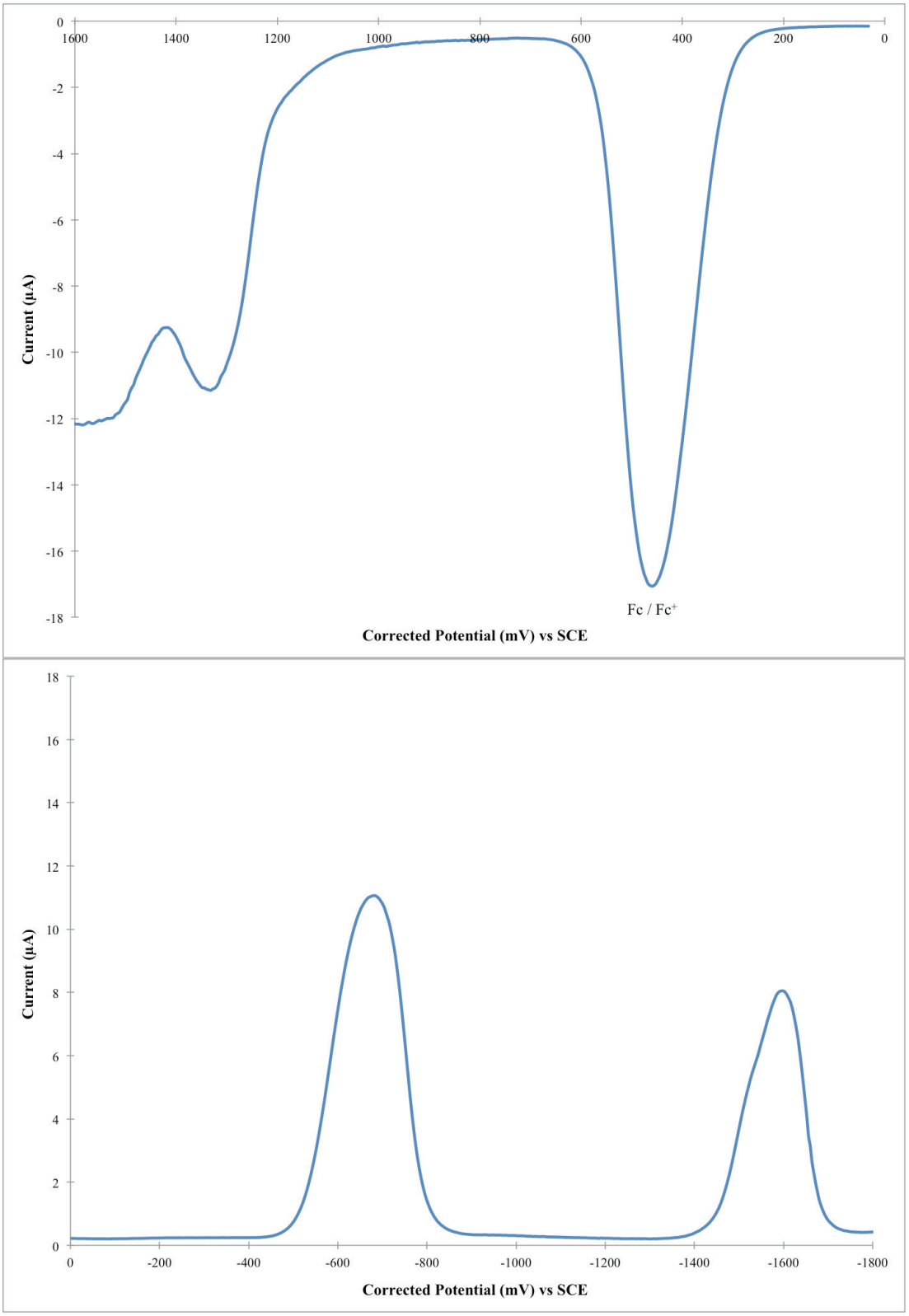

Figure S.48 – CV of BbF **4** with ferrocene internal reference. (Fc = 0.46 V vs SCE in DCM; Scan rate of 50 mV/s at R.T.)

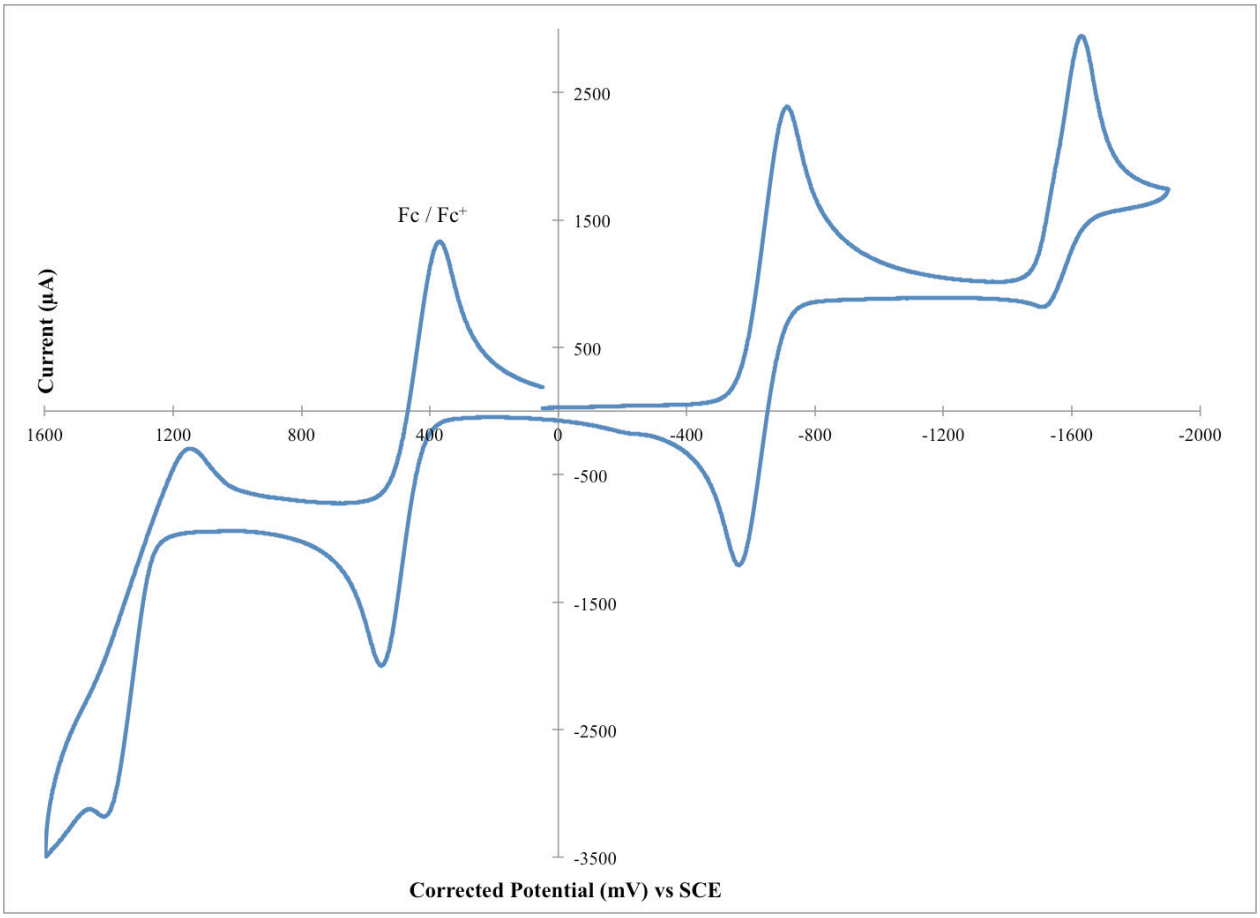

Figure S.49 – DPV of oxidation (top) and reduction (bottom) potentials for BbF **4** with ferrocene internal reference. (0.46 V vs SCE in DCM) (Scan rate of 50 mV/s at R.T.)

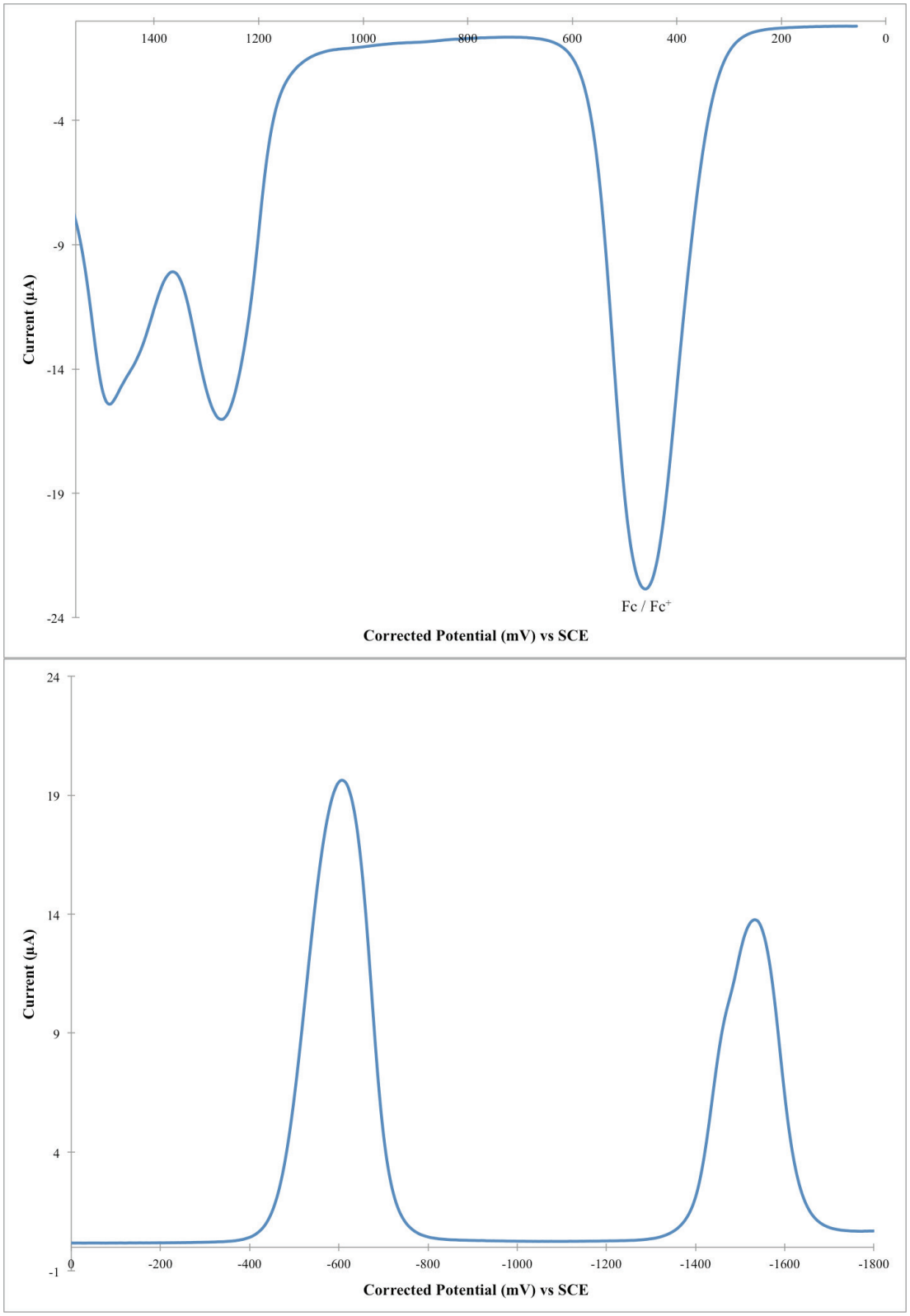

Figure S.50 – CV of BbF **5** with ferrocene internal reference. (Fc = 0.46 V vs SCE in DCM; Scan rate of 50 mV/s at R.T.)

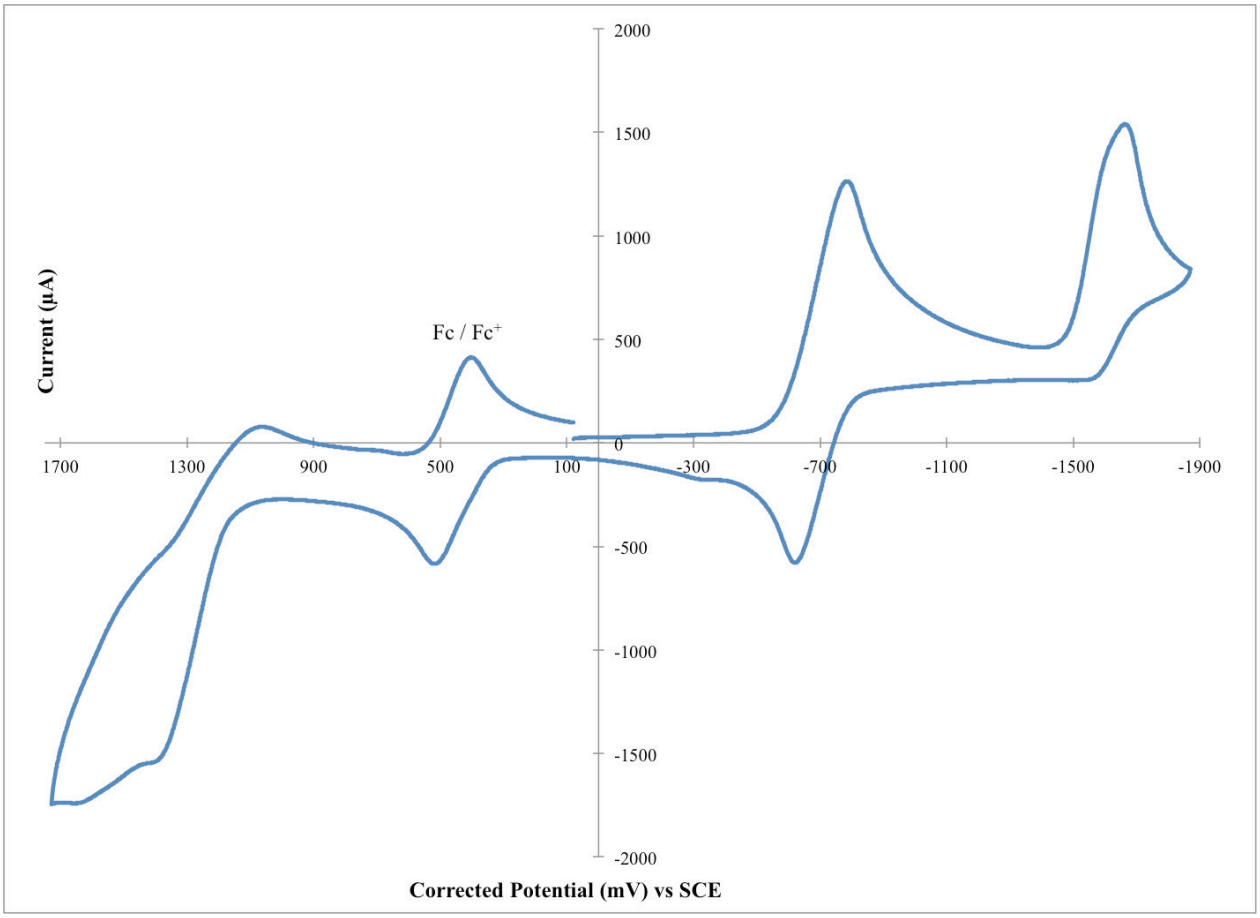

Figure S.51 – DPV of oxidation (top) and reduction (bottom) potentials for BbF **5** with ferrocene internal reference. (0.46 V vs SCE in DCM) (Scan rate of 50 mV/s at R.T.)

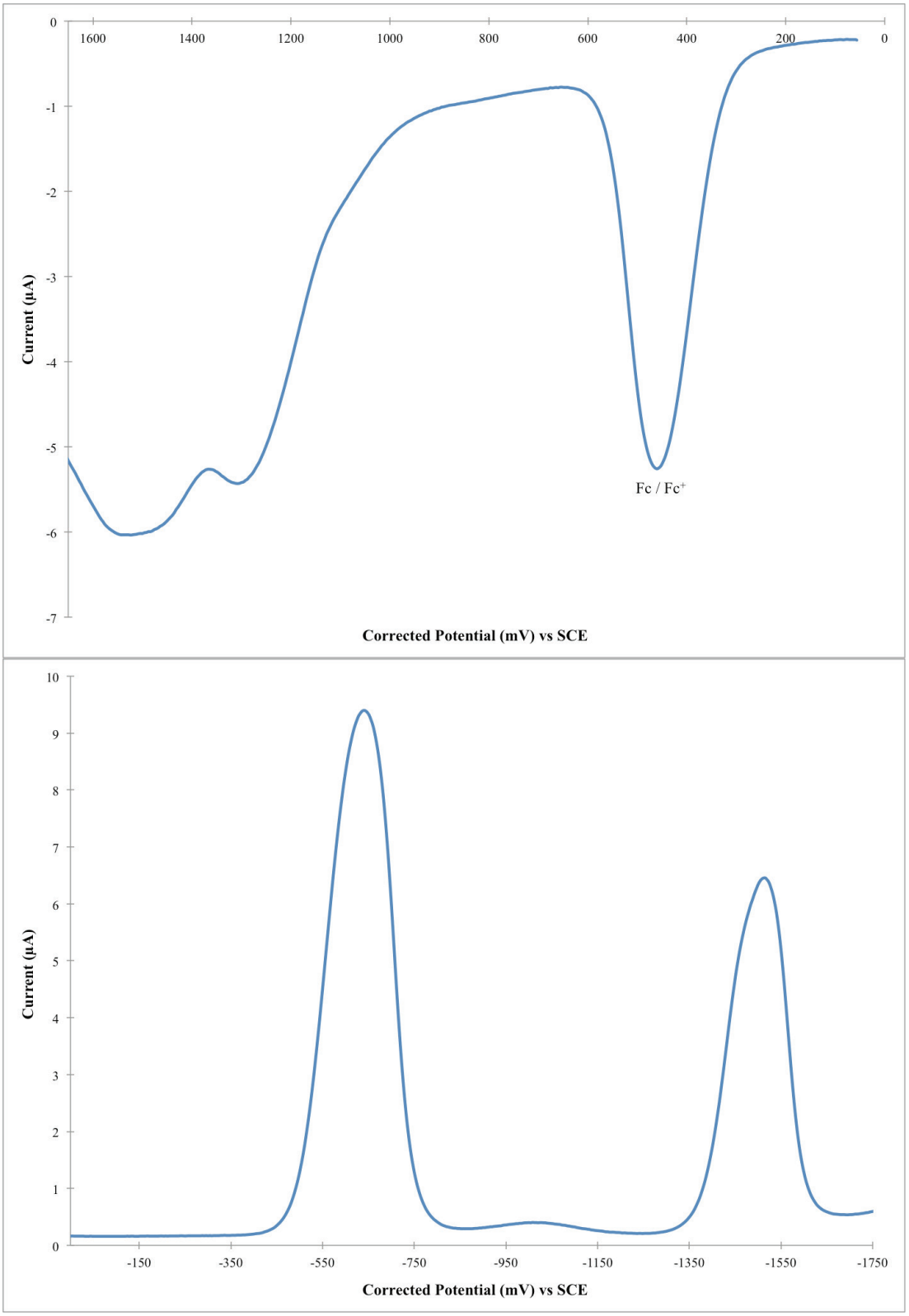

Figure S.52 – CV of BbF **6** with ferrocene internal reference. (Fc = 0.46 V vs SCE in DCM; Scan rate of 50 mV/s at R.T.)

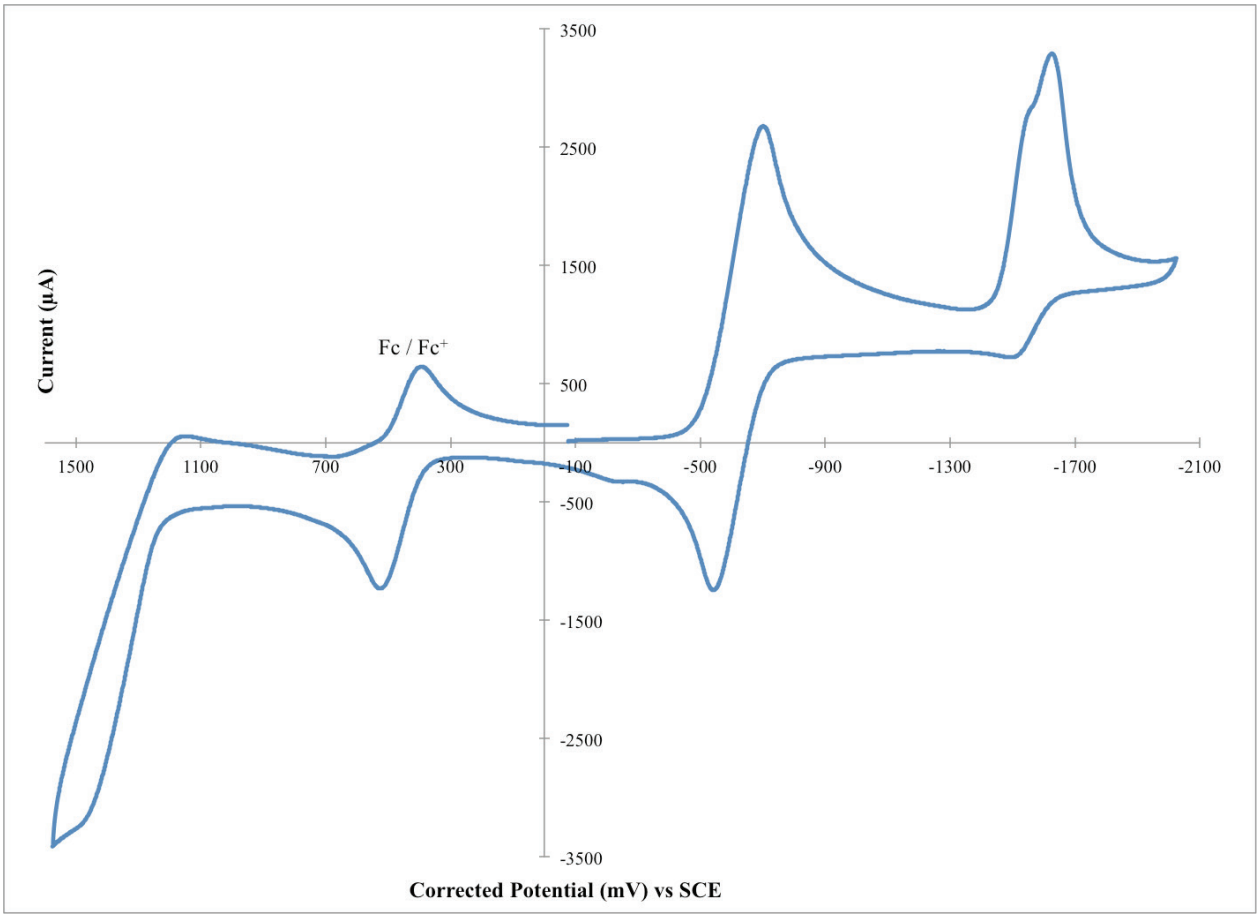

Figure S.53 – DPV of oxidation (top) and reduction (bottom) potentials for BbF **6** with ferrocene internal reference. (0.46 V vs SCE in DCM) (Scan rate of 50 mV/s at R.T.)

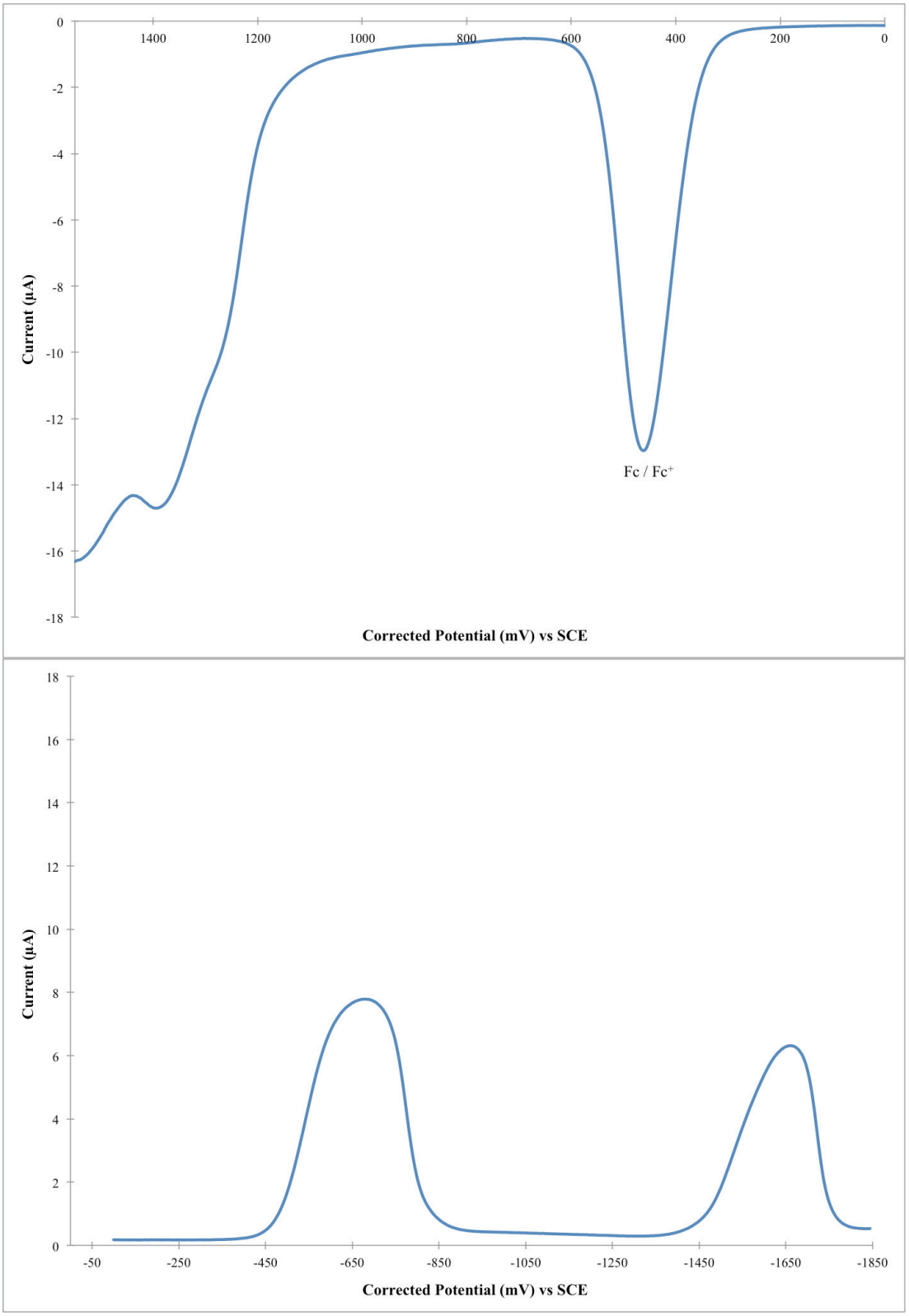

Figure S.54 – CV of BbF **7** with ferrocene internal reference. (Fc = 0.46 V vs SCE in DCM; Scan rate of 50 mV/s at R.T.)

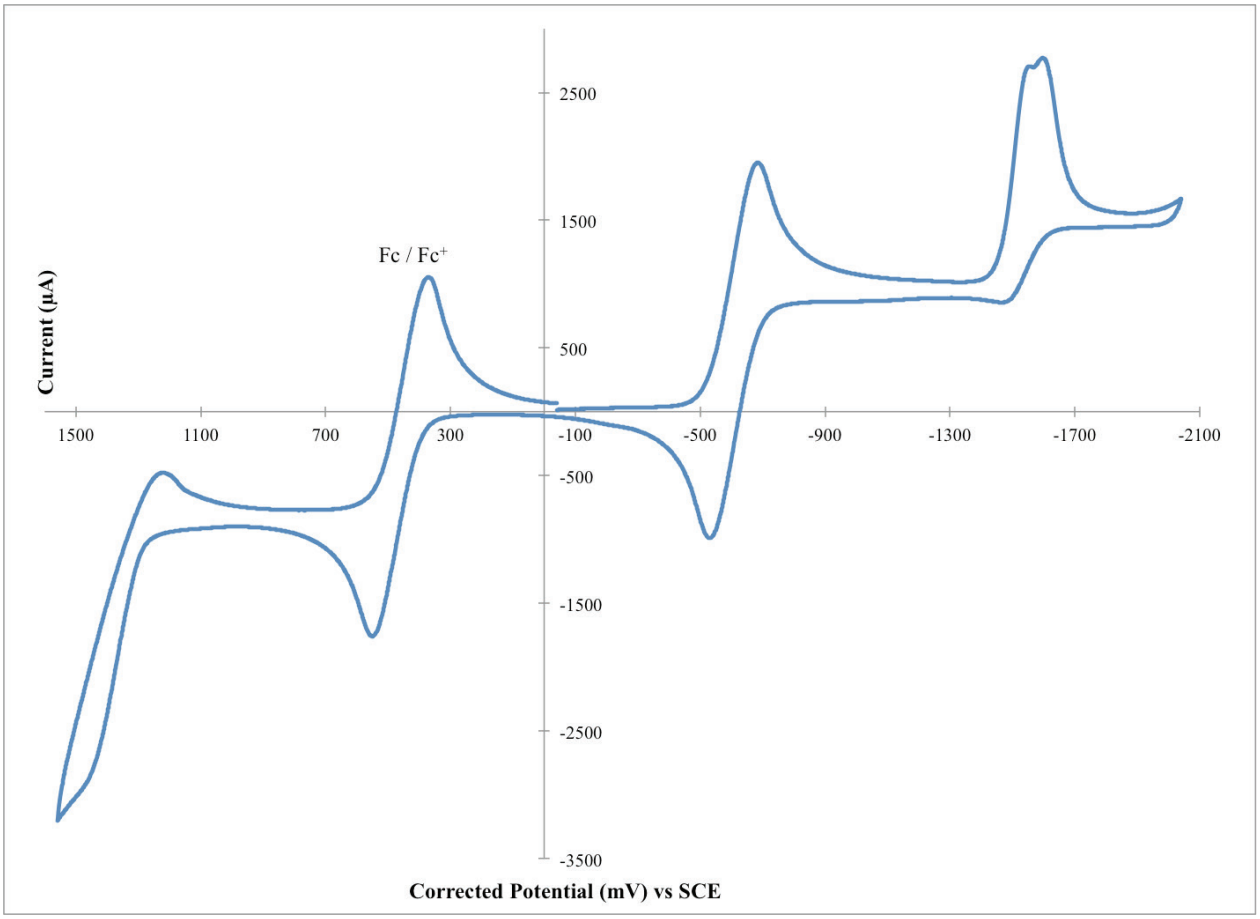

Figure S.55 – DPV of oxidation (top) and reduction (bottom) potentials for BbF **7** with ferrocene internal reference. (0.46 V vs SCE in DCM) (Scan rate of 50 mV/s at R.T.)

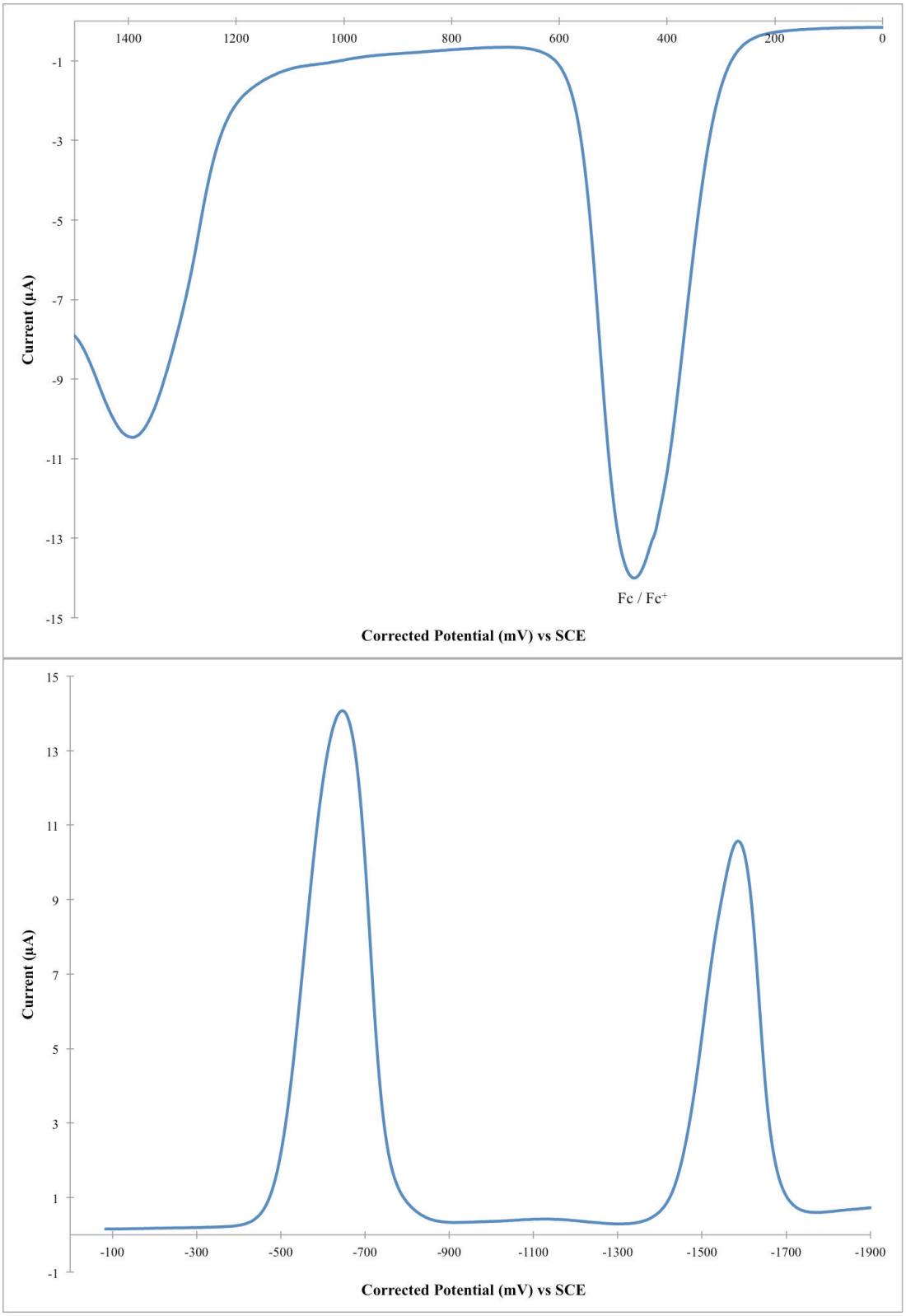

Figure S.56 – CV of BbF **8** with ferrocene internal reference. (Fc = 0.46 V vs SCE in DCM; Scan rate of 50 mV/s at R.T.)

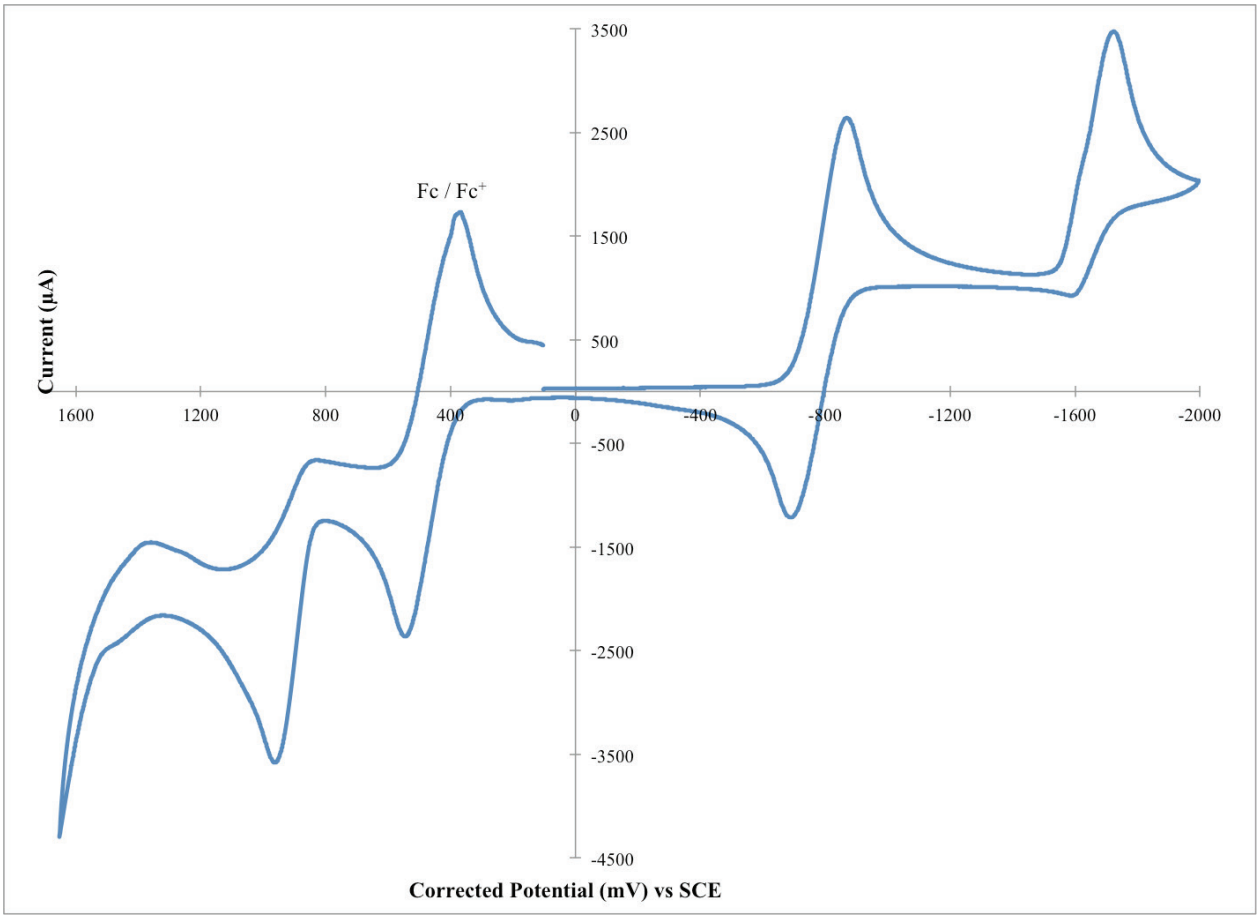

Figure S.57 – DPV of oxidation (top) and reduction (bottom) potentials for BbF **8** with ferrocene internal reference. (0.46 V vs SCE in DCM) (Scan rate of 50 mV/s at R.T.)

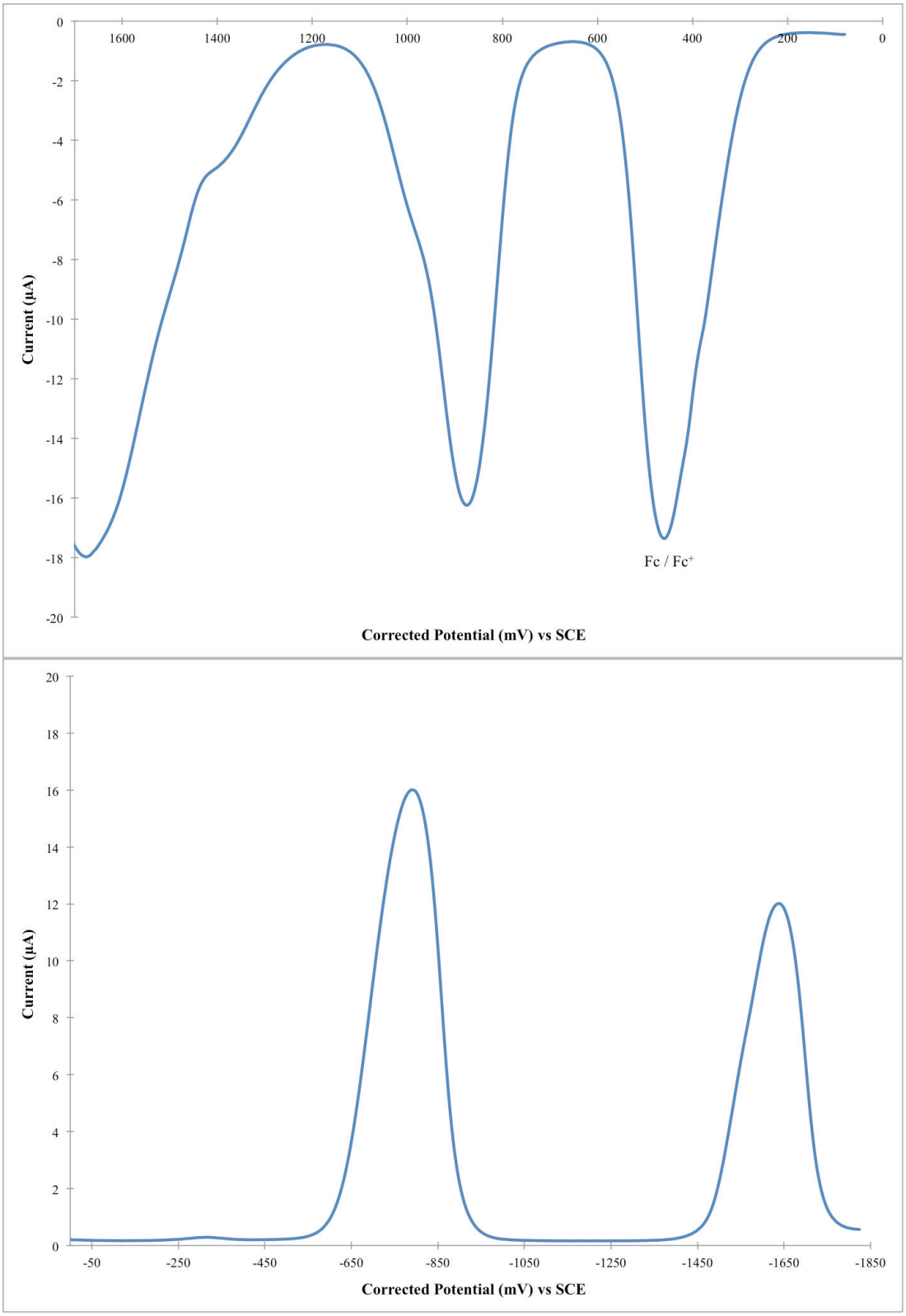

Figure S.58 – CV of BbF **9** with ferrocene internal reference. (Fc = 0.46 V vs SCE in DCM; Scan rate of 50 mV/s at R.T.)

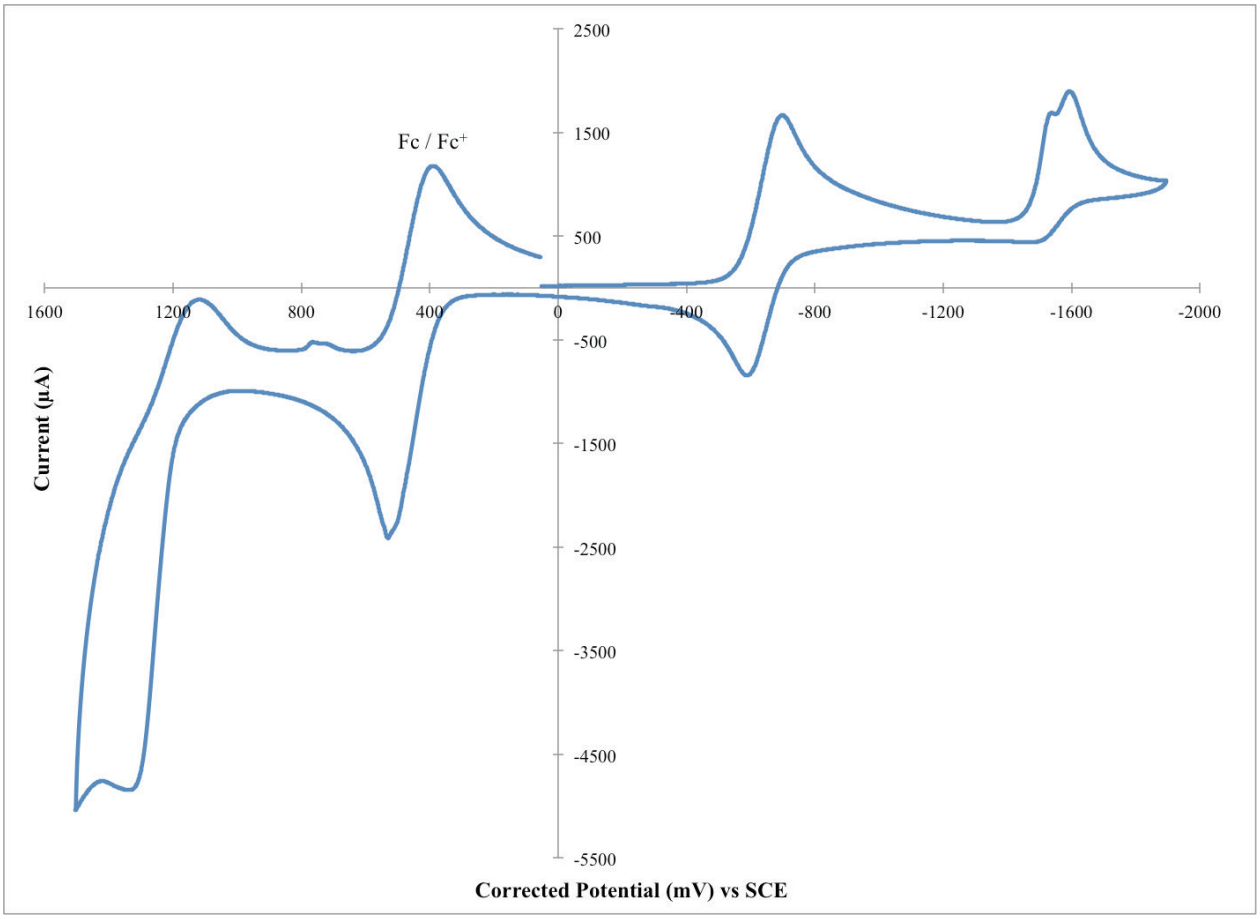

Figure S.59 – DPV of oxidation (top) and reduction (bottom) potentials for BbF **9** with ferrocene internal reference. (0.46 V vs SCE in DCM) (Scan rate of 50 mV/s at R.T.)

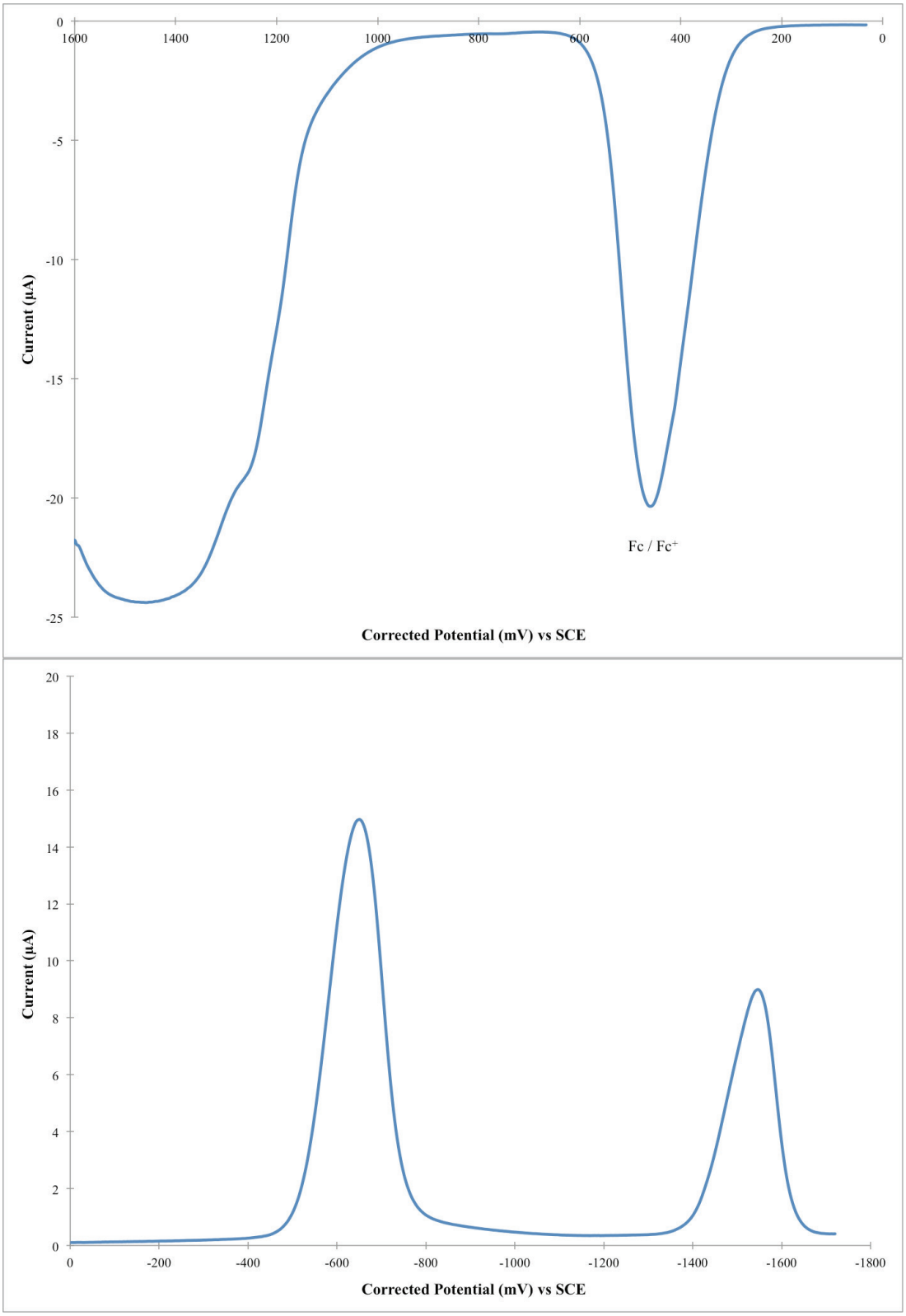

Figure S.60 – CV of BbF **10** with ferrocene internal reference. (Fc = 0.46 V vs SCE in DCM; Scan rate of 50 mV/s at R.T.)

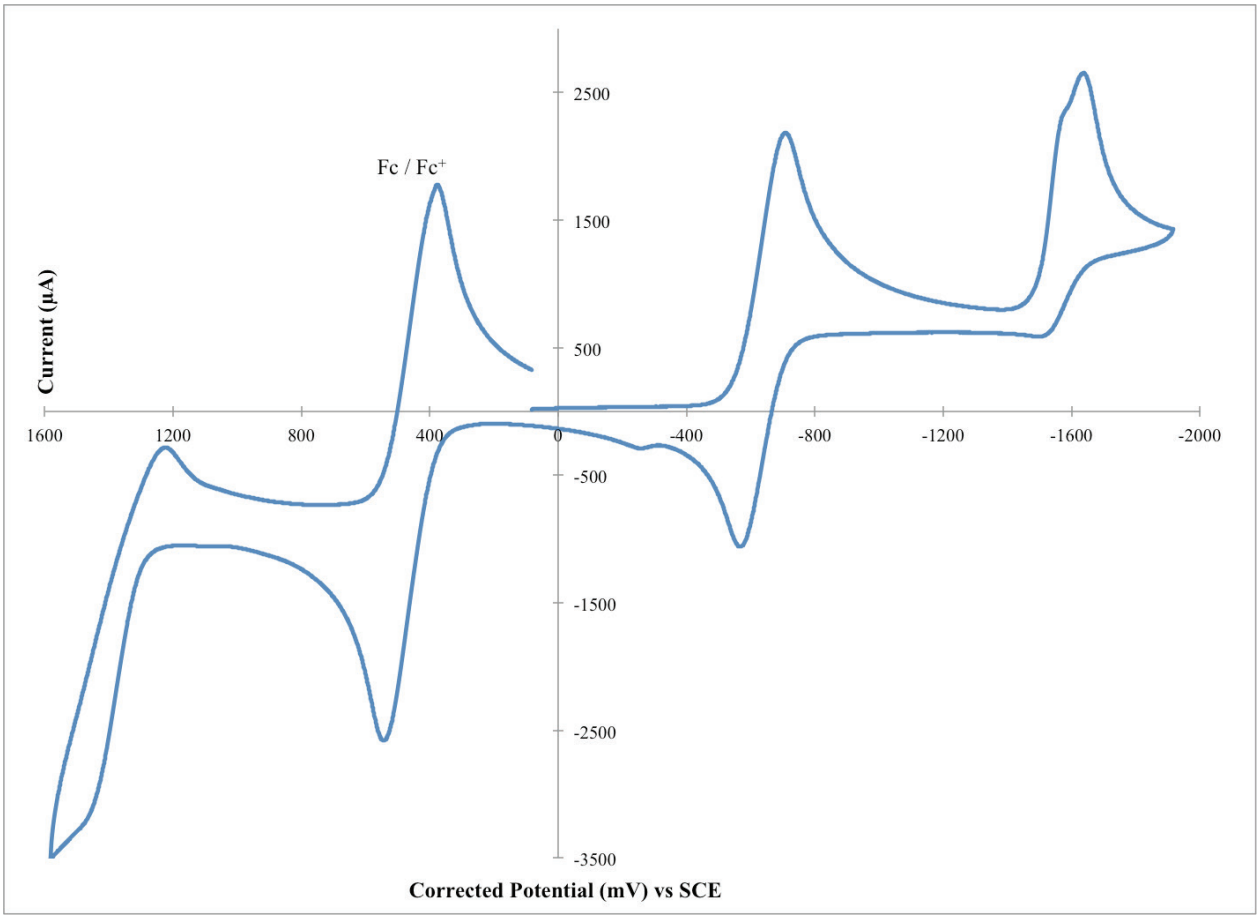

Figure S.61 – DPV of oxidation (top) and reduction (bottom) potentials for BbF **10** with ferrocene internal reference. (0.46 V vs SCE in DCM) (Scan rate of 50 mV/s at R.T.)

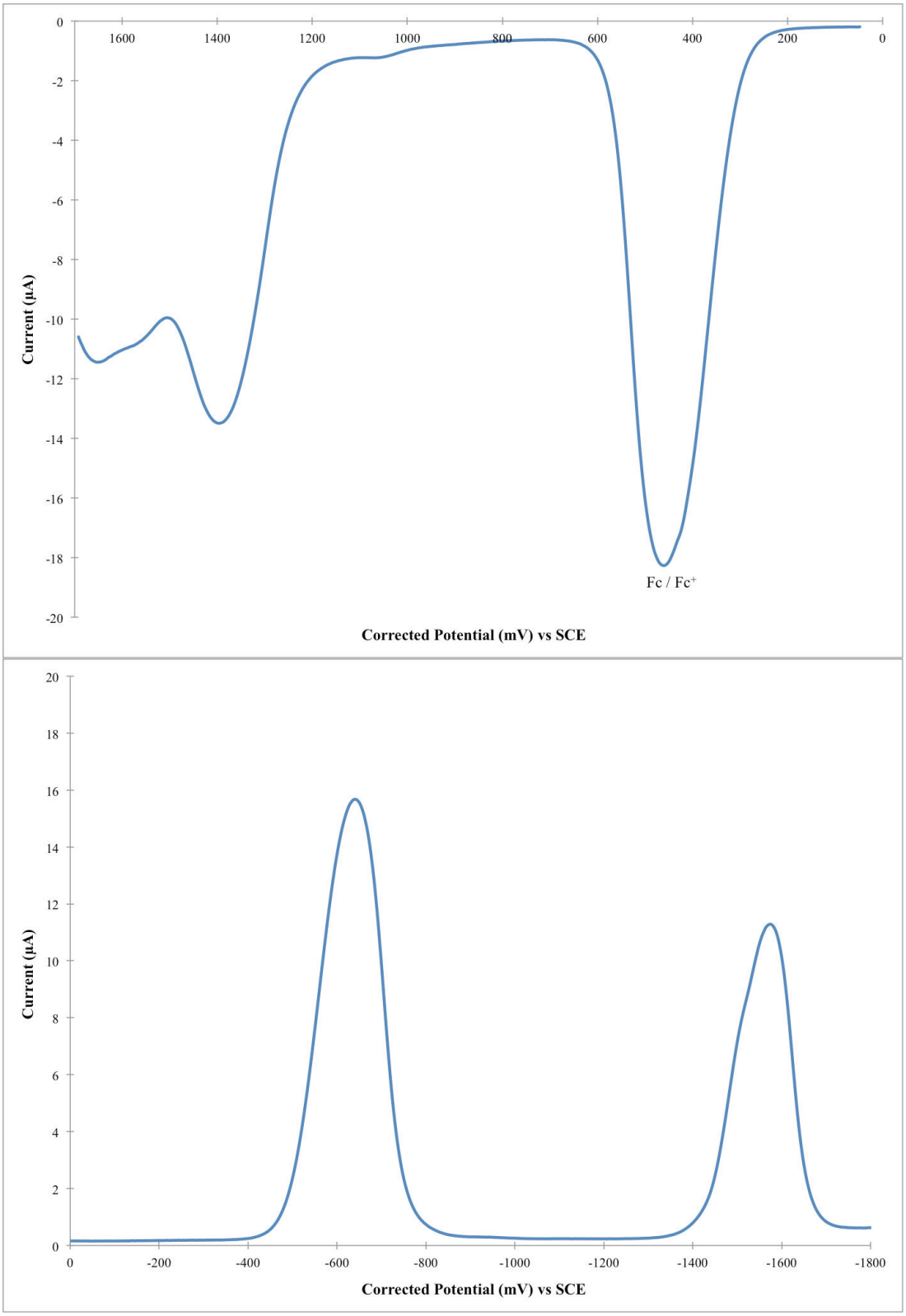

Computational Modelization

Table S.2 – Electronic distribution (%) of frontier molecular orbitals for BbF **1** – **10** as obtained by DFT.

	MO	DPM	Subst	meso	BF2
1	L + 1	48	48	4	1
	LUMO	81	10	8	1
	HOMO	86	11	2	1
	H -1	92	4	1	2
2	L + 1	48	47	4	1
	LUMO	81	11	7	1
	HOMO	82	15	2	0
	H -1	91	5	2	2
3	L + 1	48	46	4	1
	LUMO	81	11	7	1
	HOMO	82	15	2	0
	H -1	91	5	2	2
4	L + 1	48	47	4	1
	LUMO	80	11	7	1
	HOMO	82	15	2	0
	H -1	91	5	2	2
5	L + 1	51	41	8	1
	LUMO	80	12	7	1
	HOMO	70	28	2	0
	H -1	88	7	2	3
6	L + 1	46	49	4	1
	LUMO	82	9	8	1
	HOMO	84	13	2	1
	H -1	82	14	2	2
7	L + 1	54	37	9	1
	LUMO	82	10	8	1
	HOMO	85	12	2	1
	H -1	4	95	0	0
8	L + 1	52	36	11	1
	LUMO	76	16	7	1
	HOMO	40	58	2	0
	H -1	83	12	3	3
9	L + 1	17	82	0	0
	LUMO	79	12	7	1
	HOMO	49	50	2	0
	H -1	76	19	3	2
10	L + 1	13	87	0	0
	LUMO	82	10	8	1
	HOMO	63	34	2	1
	H -1	75	20	2	3

Figure S.62 – Representation of frontier molecular orbital's energy levels (in eV) of BbF **1** – **10** and electronic distribution as obtained by DFT (refer to Scheme 1 for color legend)

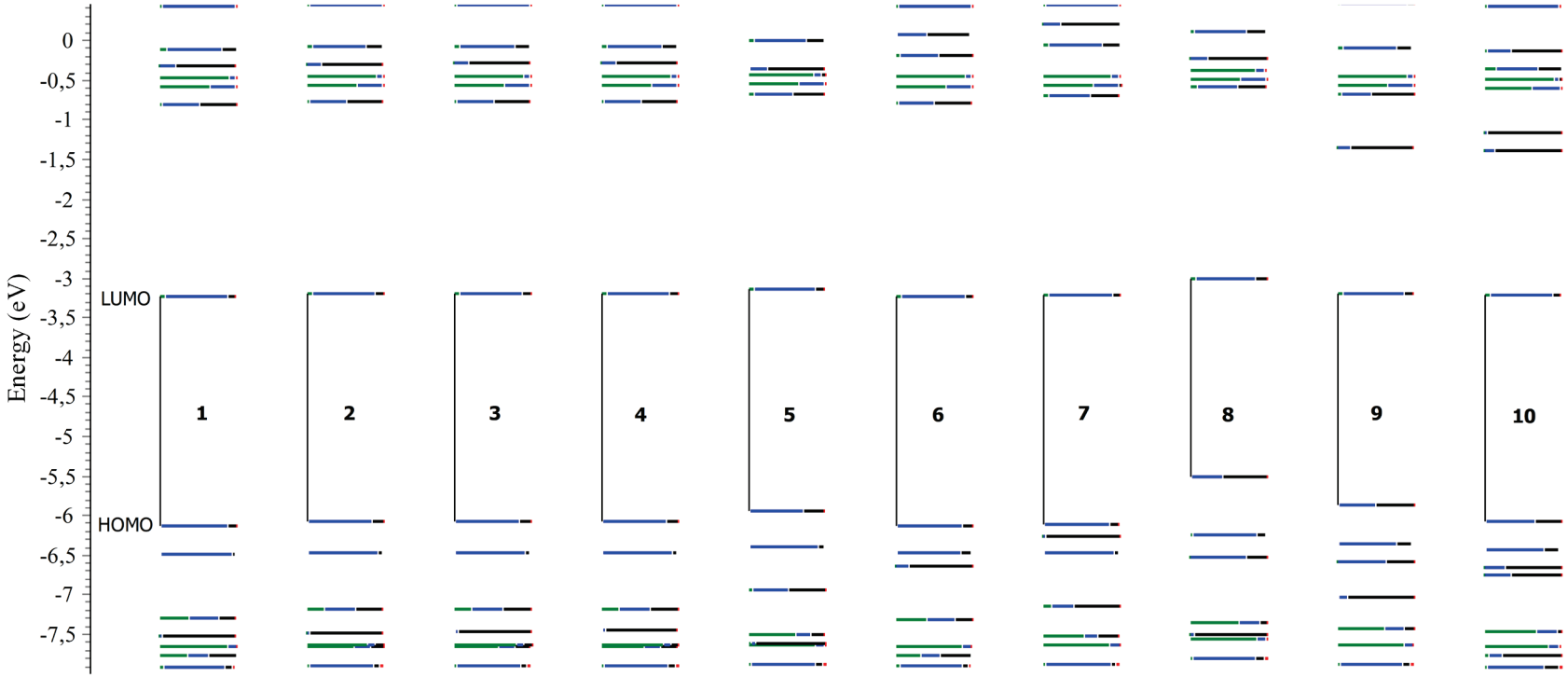

Figure S.63 – BbF **1** experimental absorption spectrum in CH_2Cl_2 vs TD-DFT calculated optical absorption bands (Red = uncorrected; Green = corrected; PCM = CH_2Cl_2).

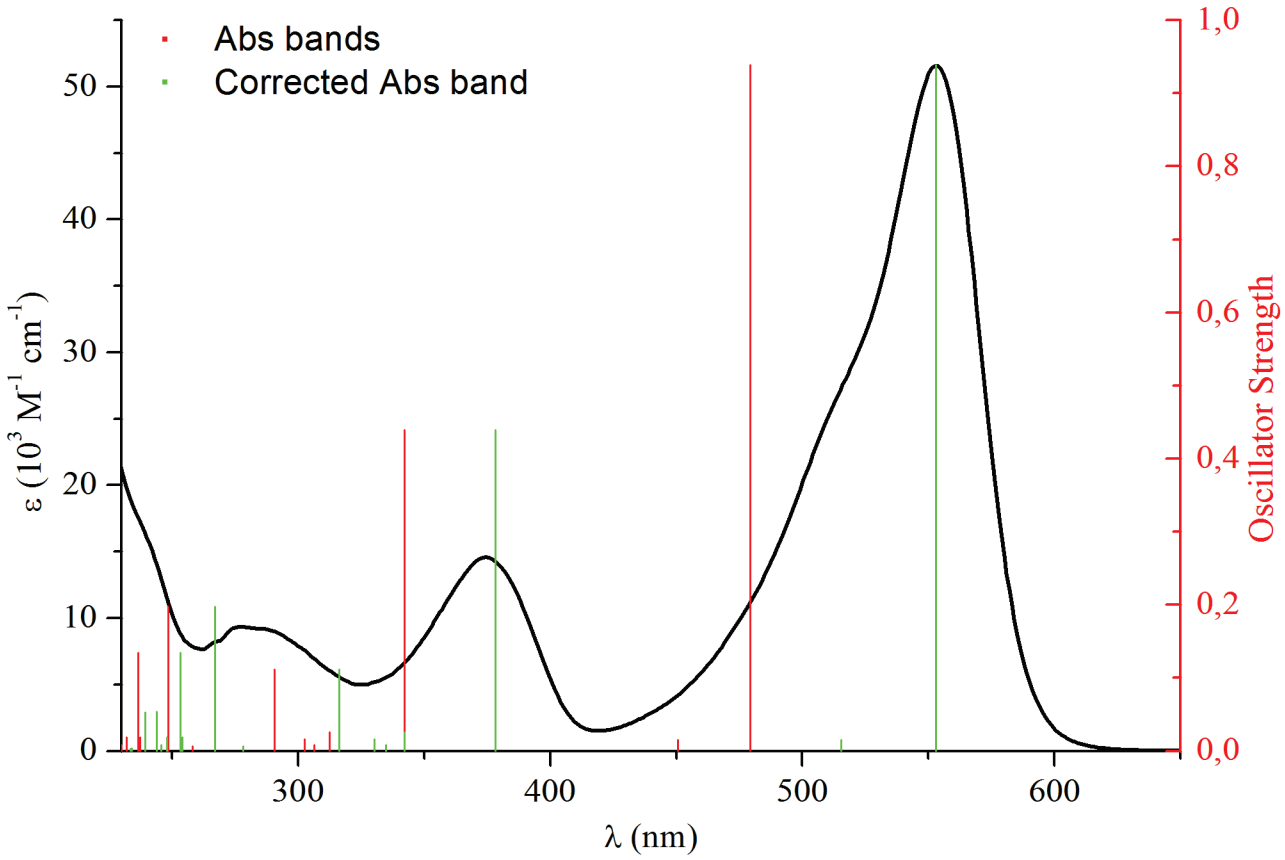

Table S.3 - Assignment of the optical absorption bands for BbF **1** based on TD-DFT calculations

λ, nm				
Observed (ε, x10^3 $M^{-1}cm^{-1}$)	**Calculated** (Osc. Strength)	**Corr.**	**Trans. No.**	**Major contributions to excitation**
553 (52)	479 (0.939)	553	T1	H (99%) -> L
517 (28)	451 (0.015)	515	T2	H-1 (98%) -> L
374 (15)	342 (0.439)	378	T3	H-2 (91%) -> L
	312 (0.026)	342	T4	H-6 (38%), H-5 (15%), H-4 (42%) -> L
	306 (0.008)	335	T5	H-6 (25%), H-5 (10%), H-4 (55%) -> L
	302 (0.016)	330	T6	H-3 (85%) -> L
287 (9.2)	291 (0.111)	316	T7	H-6 (25%), H-5 (65%) -> L
	258 (0.006)	278	T8	H-7 (94%) -> L
277 (9.3)	249 (0.198)	267	T9	H (86%) -> L+1
	237 (0.019)	254	T10	H (86%) -> L+2

Table S.4 – NTO analysis for BbF **1** absorption bands T1 to T10 obtained by TD-DFT (Isovalue = 0.02; PCM = CH_2Cl_2)

Transition / Eigenvalue	**NTO Hole "From"**	**NTO Particle "To"**	**Transition / Eigenvalue**	**NTO Hole "From"**	**NTO Particle "To"**
T1 / 0.99	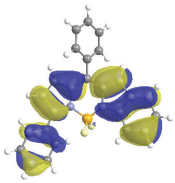	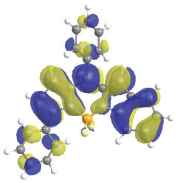	T6 / 0.98	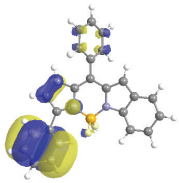	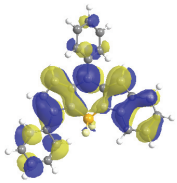
T2 / 0.99	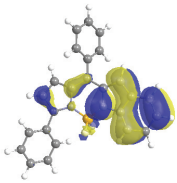	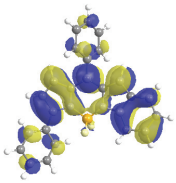	T7 / 0.98	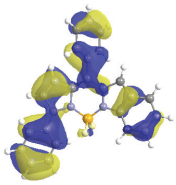	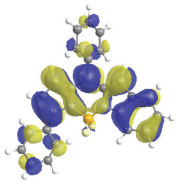
T3 / 0.99	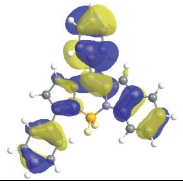	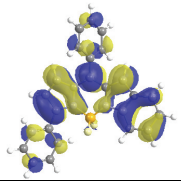	T8 / 0.98	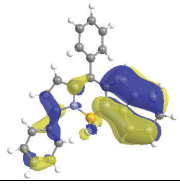	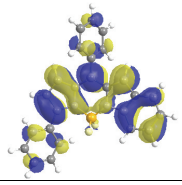
T4 / 0.99	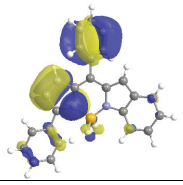	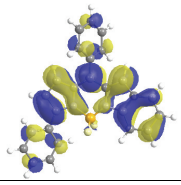	T9 / 0.93	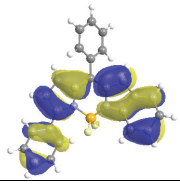	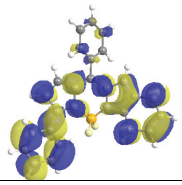
T5 / 0.99	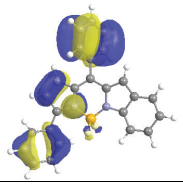	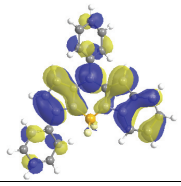	T10 / 0.93	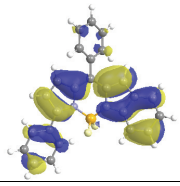	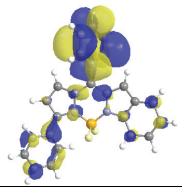

Figure S.64 – BbF **2** experimental absorption spectrum in CH_2Cl_2 vs TD-DFT calculated optical absorption bands (Red = uncorrected; Green = corrected; PCM = CH_2Cl_2).

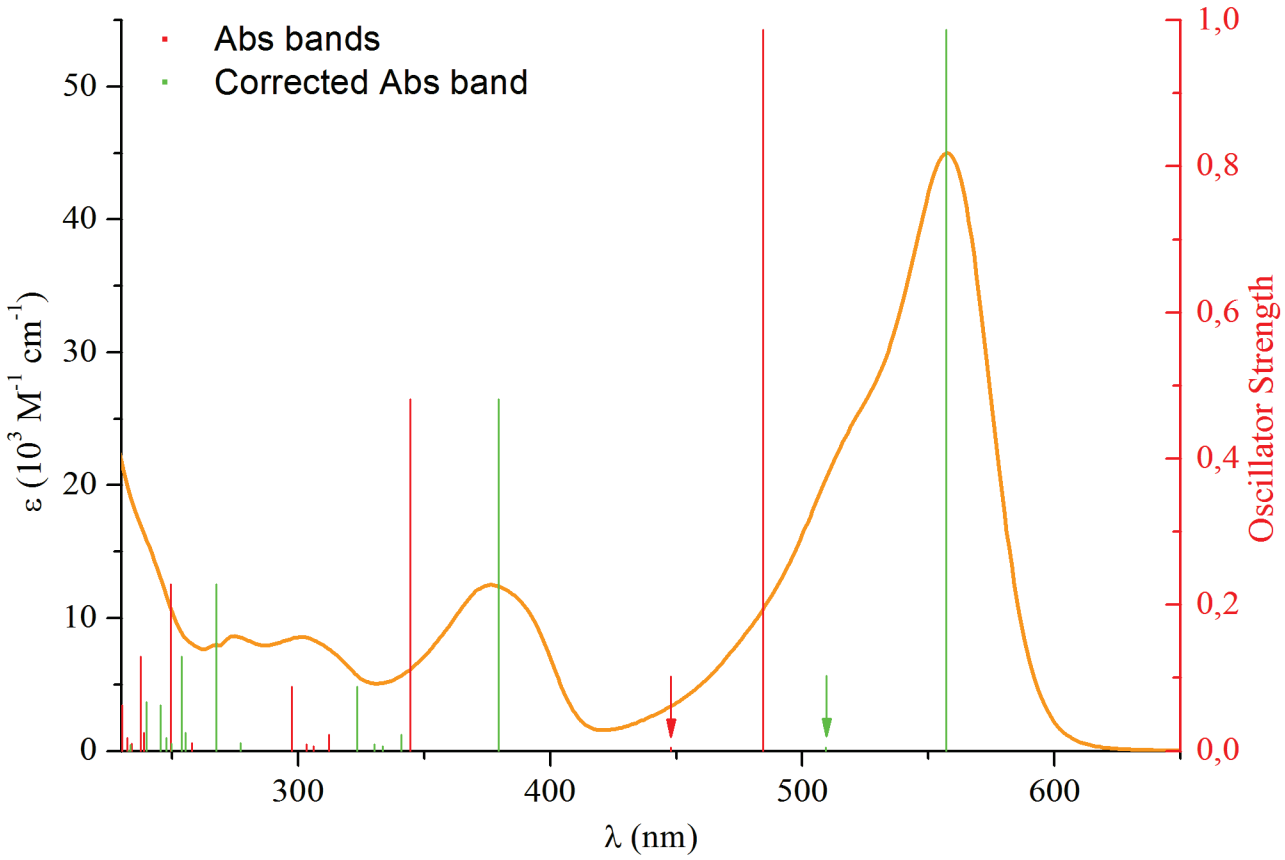

Table S.5 - Assignment of optical absorption bands for BbF **2** based on TD-DFT calculations

λ, nm				
Observed (ε, x10^3 $M^{-1}cm^{-1}$)	**Calculated** (Osc. Strength)	**Corr.**	**Trans. No.**	**Major contributions to excitation**
557 (45)	484 (0.987)	557	T1	H (98%) -> L
521 (25)	448 (0.005)	509	T2	H-1 (97%) -> L
377 (12)	344 (0.482)	380	T3	H-2 (88%) -> L
	312 (0.023)	341	T4	H-6 (39%), H-5 (46%) -> L
	306 (0.007)	334	T5	H-5 (27%), H-4 (58%), H-3 (10%) -> L
302 (8.6)	303 (0.010)	330	T6	H-4 (12%), H-3 (80%) -> L
	297 (0.088)	323	T7	H-6 (51%), H-5 (24%), H-4 (16%) -> L
275 (8.6)	258 (0.011)	277	T8	H-7 (93%) -> L
	250 (0.229)	268	T9	H (87%) -> L+1
	239 (0.025)	255	T10	H (89%) -> L+2

Table S.6 – NTO analysis for BbF **2** absorption bands T1 to T10 obtained by TD-DFT (Isovalue = 0.02; PCM = CH_2Cl_2)

Transition / Eigenvalue	**NTO Hole "From"**	**NTO Particle "To"**		**Transition / Eigenvalue**	**NTO Hole "From"**	**NTO Particle "To"**
T1 / 0.99	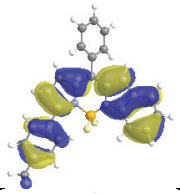	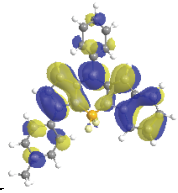		T6 / 0.98	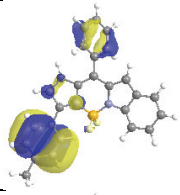	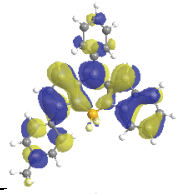
T2 / >0.99	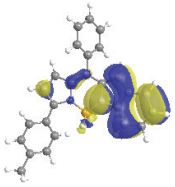	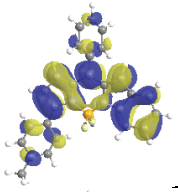		T7 / 0.99	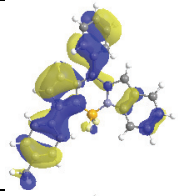	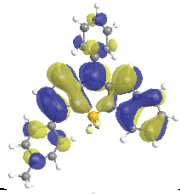
T3 / 0.99	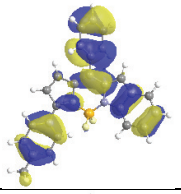	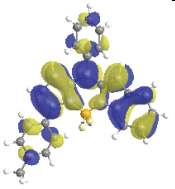		T8 / 0.97	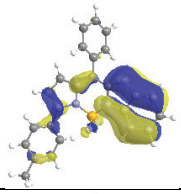	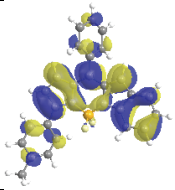
T4 / 0.99	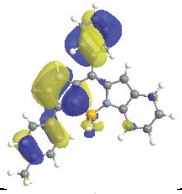	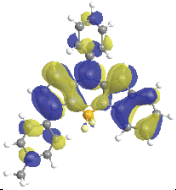		T9 / 0.93	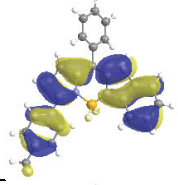	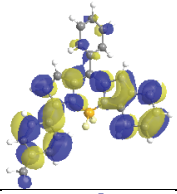
T5 / 0.99	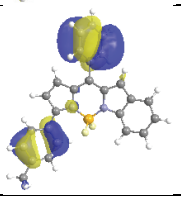	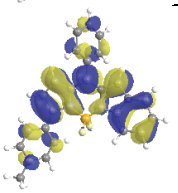		T10 / 0.95	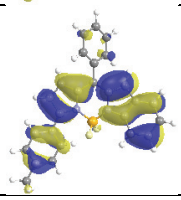	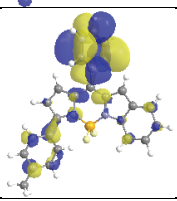

Figure S.65 – BbF **3** experimental absorption spectrum in CH_2Cl_2 vs TD-DFT calculated optical absorption bands (Red = uncorrected; Green = corrected; PCM = CH_2Cl_2).

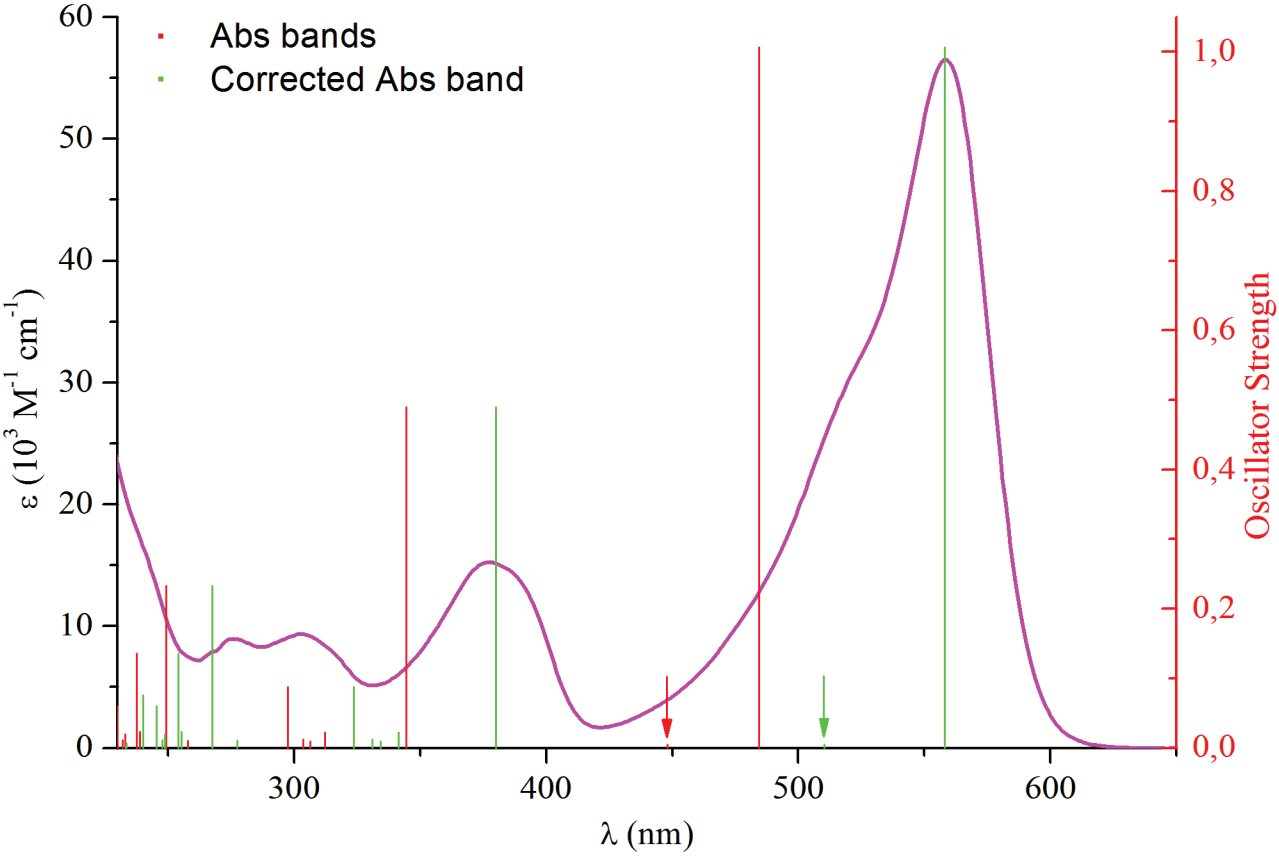

Table S.7 - Assignment of optical absorption bands for BbF **3** based on TD-DFT calculations

λ, nm				
Observed (ε, x10^3 $M^{-1}cm^{-1}$)	**Calculated** (Osc. Strength)	**Corr.**	**Trans. No.**	**Major contributions to excitation**
558 (57)	484 (1.007)	558	T1	H (98%) -> L
523 (31)	448 (0.005)	510	T2	H-1 (97%) -> L
378 (15)	344 (0.490)	380	T3	H-2 (88%) -> L
	312 (0.022)	341	T4	H-6 (39%), H-5 (41%), H-3 (11%) -> L
	306 (0.009)	334	T5	H-5 (31%), H-4 (43%), H-3 (22%) -> L
303 (9.3)	304 (0.012)	331	T6	H-6 (11%), H-4 (23%), H-3 (62%) -> L
	298 (0.088)	324	T7	H-6 (47%), H-5 (24%), H-4 (19%) -> L
276 (9.0)	258 (0.011)	277	T8	H-7 (93%) -> L
	249 (0.233)	268	T9	H (86%) -> L+1
	239 (0.024)	255	T10	H (88%) -> L+2

Table S.8 – NTO analysis for BbF **3** absorption bands T1 to T10 obtained by TD-DFT (Isovalue = 0.02; PCM = CH_2Cl_2)

Transition / Eigenvalue	**NTO Hole "From"**	**NTO Particle "To"**		**Transition / Eigenvalue**	**NTO Hole "From"**	**NTO Particle "To"**
T1 / 0.99	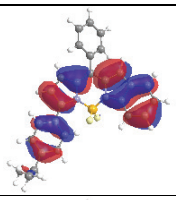	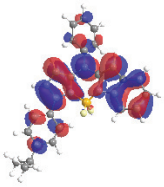		T6 / 0.98	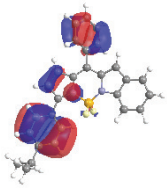	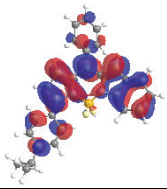
T2 / >0.99	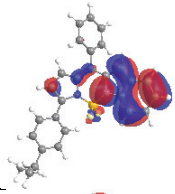	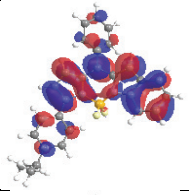		T7 / 0.99	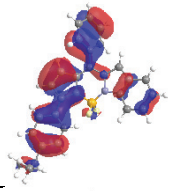	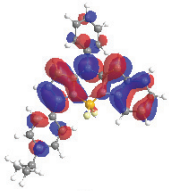
T3 / 0.99	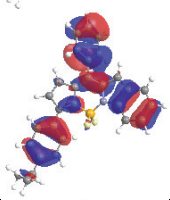	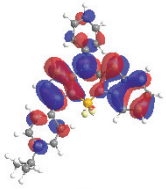		T8 / 0.97	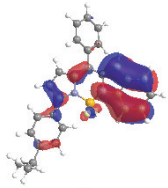	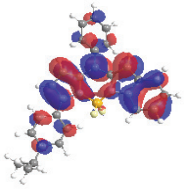
T4 / 0.99	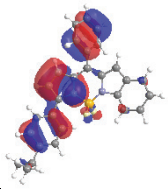	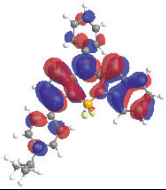		T9 / 0.92	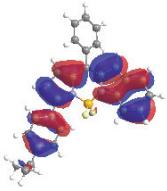	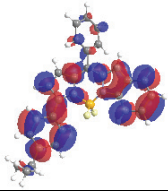
T5 / 0.98	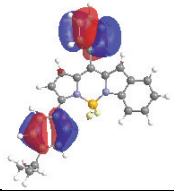	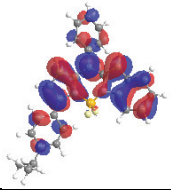		T10 / 0.94	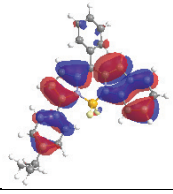	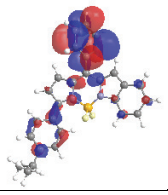

Figure S.66 – BbF **4** experimental absorption spectrum in CH_2Cl_2 vs TD-DFT calculated optical absorption bands (Red = uncorrected; Green = corrected; PCM = CH_2Cl_2).

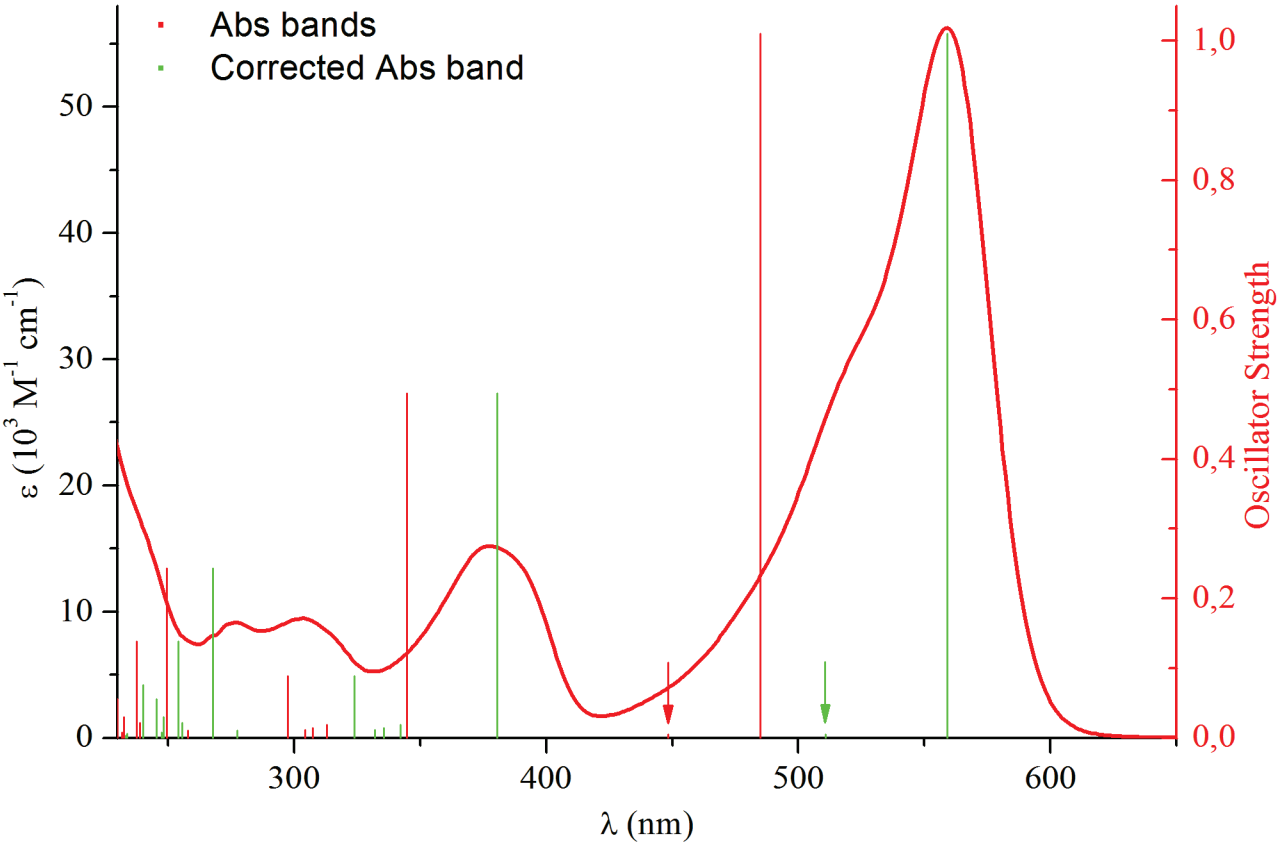

Table S.9 - Assignment of optical absorption bands for BbF **4** based on TD-DFT calculations

λ, nm				
Observed (ε, x10^3 M^{-1}cm^{-1})	**Calculated** (Osc. Strength)	**Corr.**	**Trans. No.**	**Major contributions to excitation**
559 (56)	485 (1.011)	559	T1	H (98%) -> L
525 (32)	448 (0.005)	511	T2	H-1 (97%) -> L
378 (15)	345 (0.494)	380	T3	H-2 (87%) -> L
	313 (0.019)	342	T4	H-6 (33%), H-5 (36%), H-3 (22%) -> L
	307 (0.014)	336	T5	H-5 (32%), H-4 (25%), H-3 (38%) -> L
303 (9.5)	304 (0.012)	332	T6	H-6 (17%), H-4 (42%), H-3 (35%) -> L
	297 (0.089)	324	T7	H-6 (44%), H-5 (26%), H-4 (19%) -> L
277 (9.1)	258 (0.011)	278	T8	H-7 (93%) -> L
	250 (0.243)	268	T9	H (87%) -> L+1
	239 (0.021)	256	T10	H (87%) -> L+2

Table S.10 – NTO analysis for BbF **4** absorption bands T1 to T10 obtained by TD-DFT (Isovalue = 0.02; PCM = CH_2Cl_2)

Transition / Eigenvalue	**NTO Hole "From"**	**NTO Particle "To"**		**Transition / Eigenvalue**	**NTO Hole "From"**	**NTO Particle "To"**
T1 / 0.99	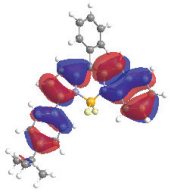	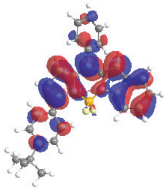		T6 / 0.98	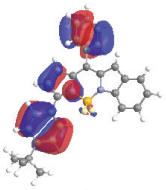	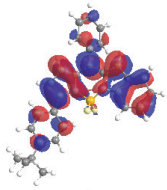
T2 / >0.99	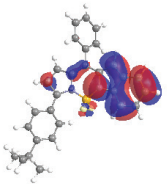	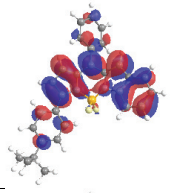		T7 / 0.98	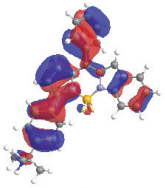	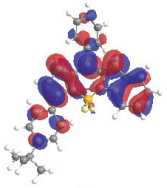
T3 / 0.99	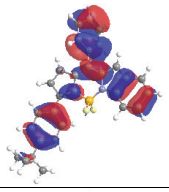	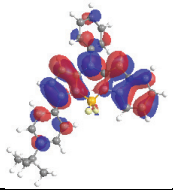		T8 / 0.97	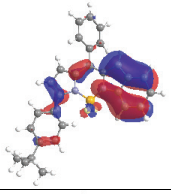	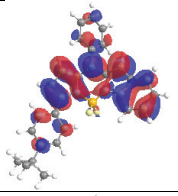
T4 / 0.99	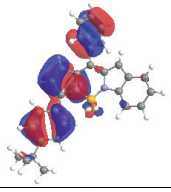	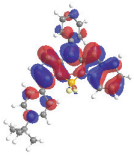		T9 / 0.93	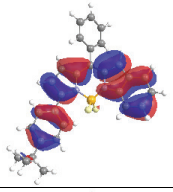	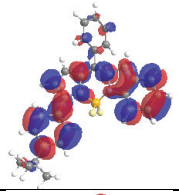
T5 / 0.98	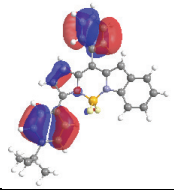	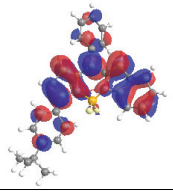		T10 / 0.93	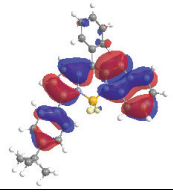	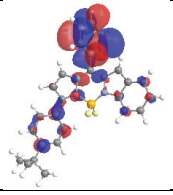

Figure S.67 – BbF **5** experimental absorption spectrum in CH_2Cl_2 vs TD-DFT calculated optical absorption bands (Red = uncorrected; Green = corrected; PCM = CH_2Cl_2).

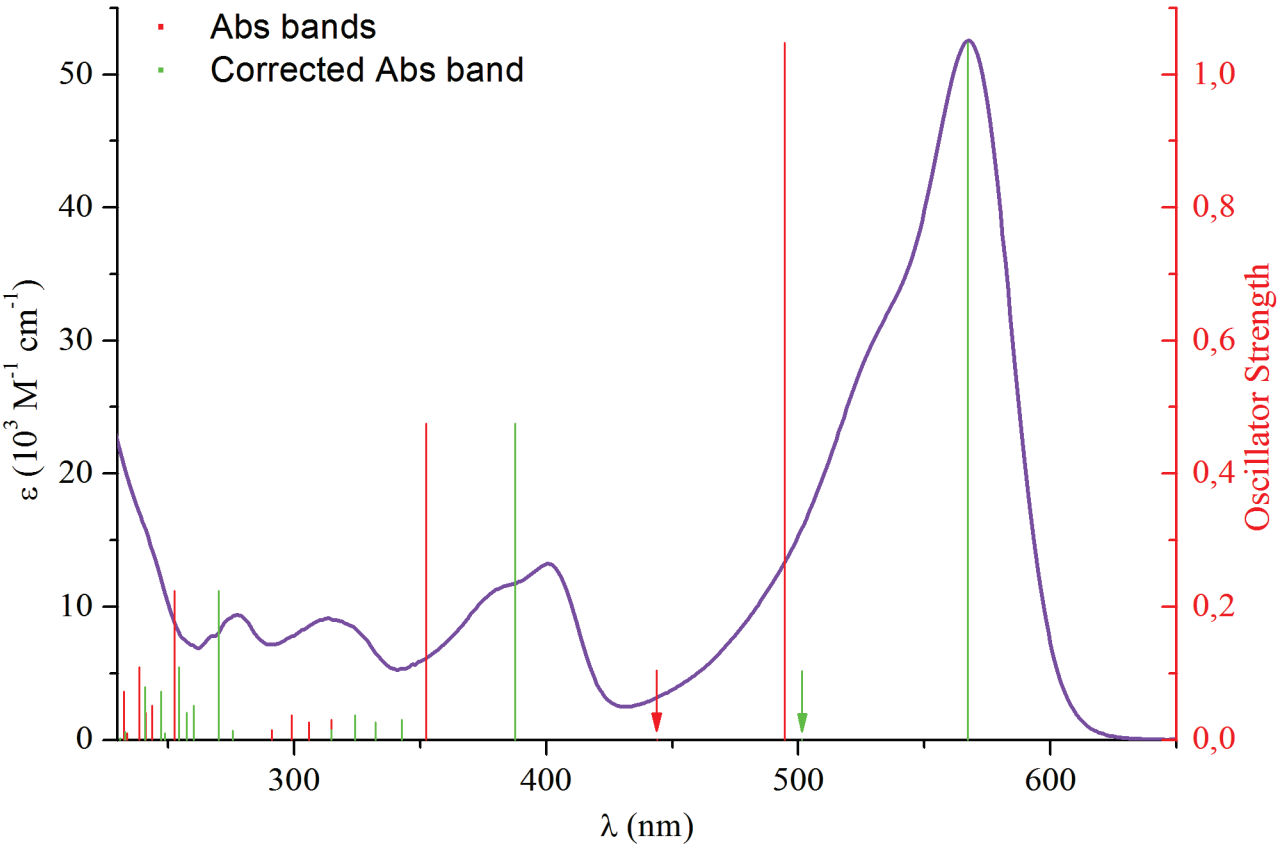

Table S.11 - Assignment of optical absorption bands for BbF **5** based on TD-DFT calculations

λ, nm				
Observed (ε, x10^3 $M^{-1}cm^{-1}$)	**Calculated** (Osc. Strength)	**Corr.**	**Trans. No.**	**Major contributions to excitation**
567 (53)	495 (1.048)	567	T1	H (98%) -> L
537 (33)	444 (0.001)	501	T2	H-1 (96%) -> L
401 (13)	352 (0.475)	388	T3	H-2 (88%) -> L
	315 (0.031)	343	T4	H-3 (78%) -> L
314 (9.1)	306 (0.027)	332	T5	H-6 (23%), H-4 (63%) -> L
	299 (0.037)	324	T6	H-6 (55%), H-5 (13%), H-4 (26%) -> L
	291 (0.015)	315	T7	H-5 (79%) -> L
278 (9.4)	257 (0.014)	276	T8	H-7 (92%) -> L
	253 (0.224)	270	T9	H (88%) -> L+1
	244 (0.052)	260	T10	H (24%) -> L+2; H -> L+4 (51%)

Table S.12 – NTO analysis for BbF **5** absorption bands T1 to T10 obtained by TD-DFT (Isovalue = 0.02; PCM = CH_2Cl_2)

Transition / Eigenvalue	**NTO Hole "From"**	**NTO Particle "To"**		**Transition / Eigenvalue**	**NTO Hole "From"**	**NTO Particle "To"**
T1 / 0.99	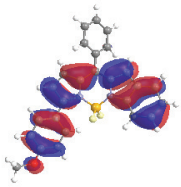	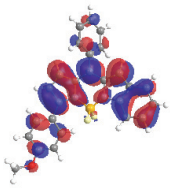		T6 / 0.99	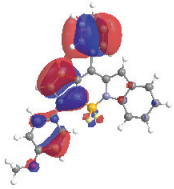	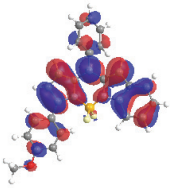
T2 / >0.99	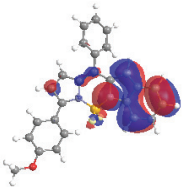	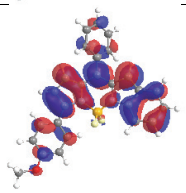		T7 / 0.96	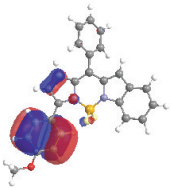	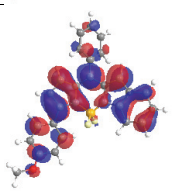
T3 / 0.99	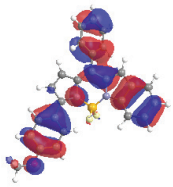	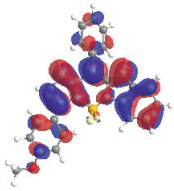		T8 / 0.97	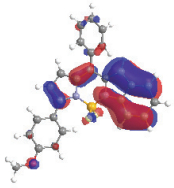	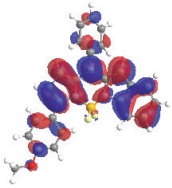
T4 / 0.99	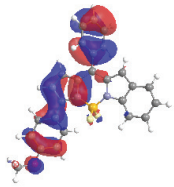	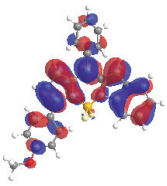		T9 / 0.91	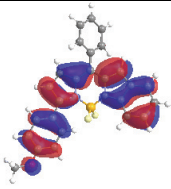	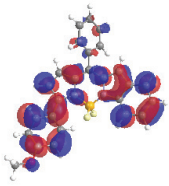
T5 / 0.99	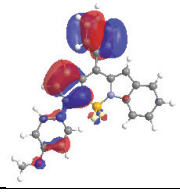	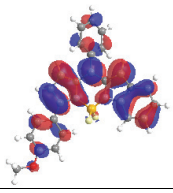		T10 / 0.80	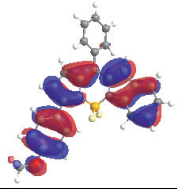	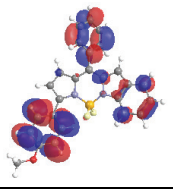

Figure S.68 – BbF **6** experimental absorption spectrum in CH_2Cl_2 vs TD-DFT calculated optical absorption bands (Red = uncorrected; Green = corrected; PCM = CH_2Cl_2).

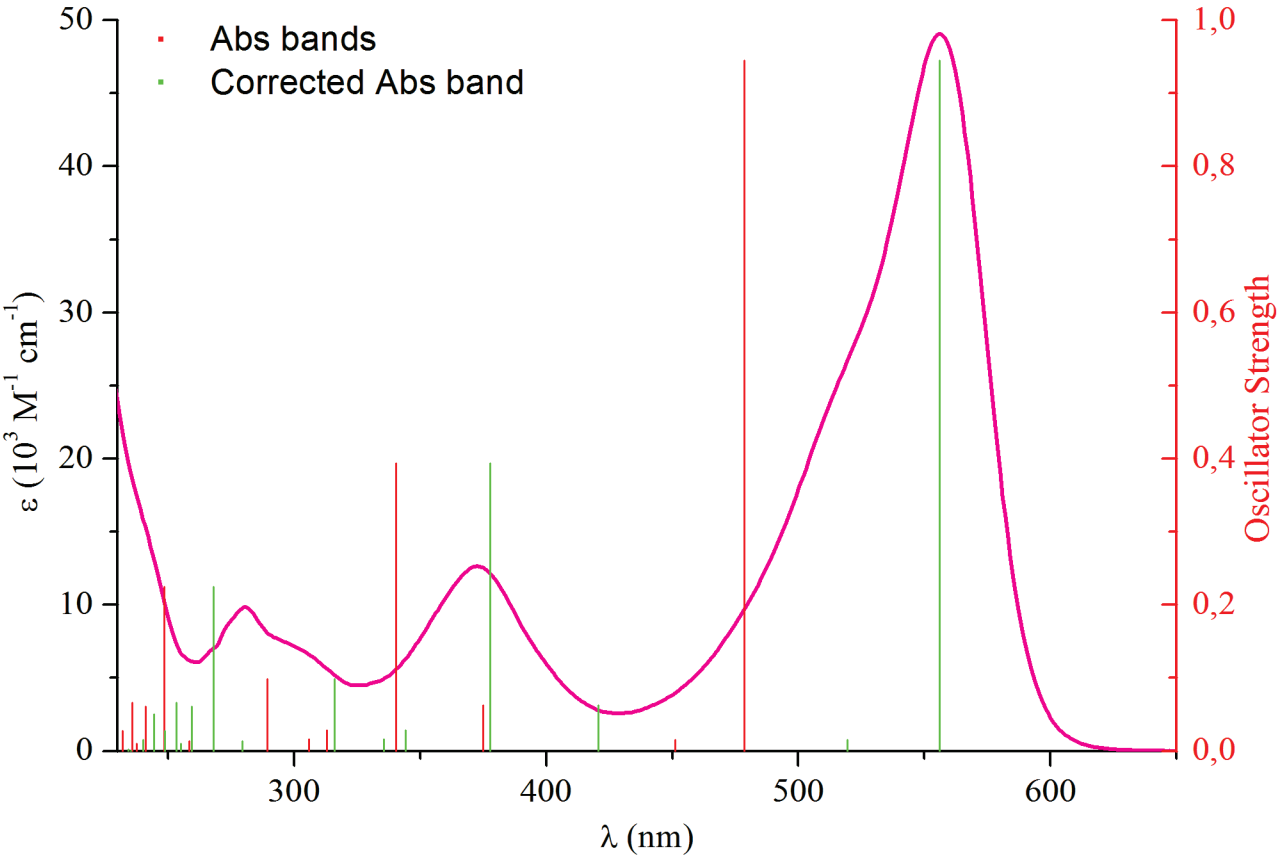

Table S.13 - Assignment of optical absorption bands for BbF **6** based on TD-DFT calculations

λ, nm				
Observed (ε, x10^3 $M^{-1}cm^{-1}$)	**Calculated** (Osc. Strength)	**Corr.**	**Trans. No.**	**Major contributions to excitation**
556 (49)	479 (0.946)	556	T1	H (99%) -> L
520 (27)	451 (0.016)	519	T2	H-1 (96%) -> L
373 (13)	375 (0.063)	421	T3	H-2 (96%) -> L
	340 (0.394)	378	T4	H-3 (91%) -> L
	313 (0.028)	344	T5	H-6 (36%), H-5 (11%), H-4 (51%) -> L
	306 (0.016)	336	T6	H-6 (39%), H-5 (12%), H-4 (47%) -> L
303 (6.9)	289 (0.099)	316	T7	H-6 (21%), H-5 (69%) -> L
281 (9.8)	259 (0.014)	280	T8	H-7 (92%) -> L
	249 (0.225)	268	T9	H (82%) -> L+1
	241 (0.061)	259	T10	H-8 (15%) -> L; H-2 (36%) -> L+1; H (12%) -> L+4

Table S.14 – NTO analysis for BbF **6** absorption bands T1 to T10 obtained by TD-DFT (Isovalue = 0.02; PCM = CH_2Cl_2)

Transition / Eigenvalue	**NTO Hole "From"**	**NTO Particle "To"**	**Transition / Eigenvalue**	**NTO Hole "From"**	**NTO Particle "To"**
T1 / 0.99	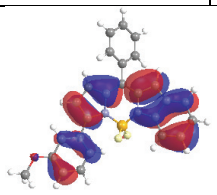	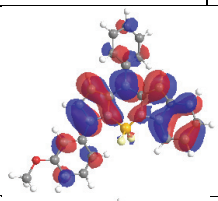	T6 / 0.99	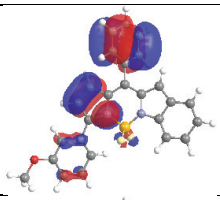	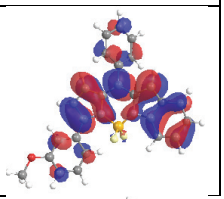
T2 / 0.99	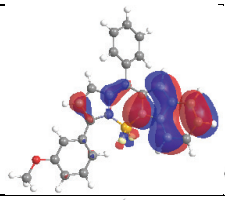	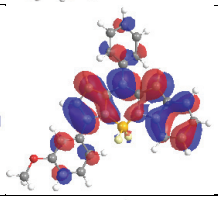	T7 / 0.98	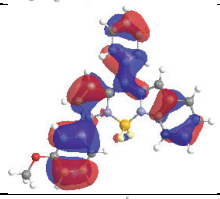	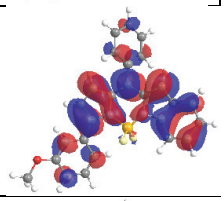
T3 / 0.99	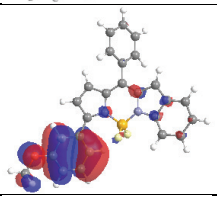	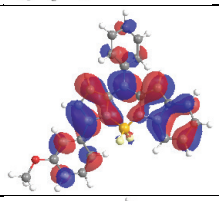	T8 / 0.97	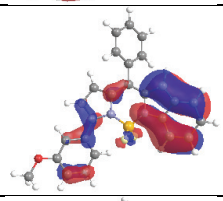	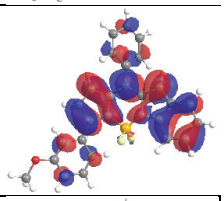
T4 / 0.99	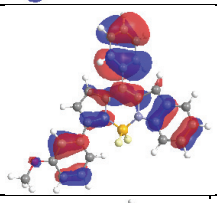	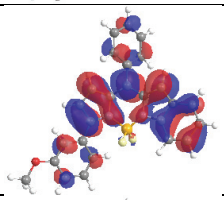	T9 / 0.90	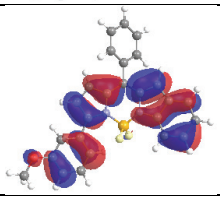	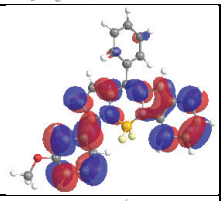
T5 / 0.99	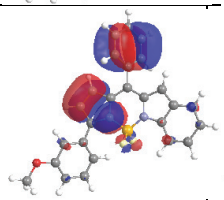	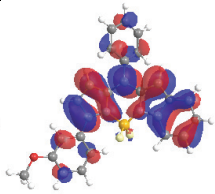	T10 / 0.52	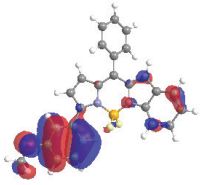	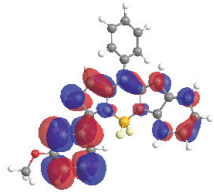

Figure S.69 – BbF **7** experimental absorption spectrum in CH_2Cl_2 vs TD-DFT calculated optical absorption bands (Red = uncorrected; Green = corrected; PCM = CH_2Cl_2).

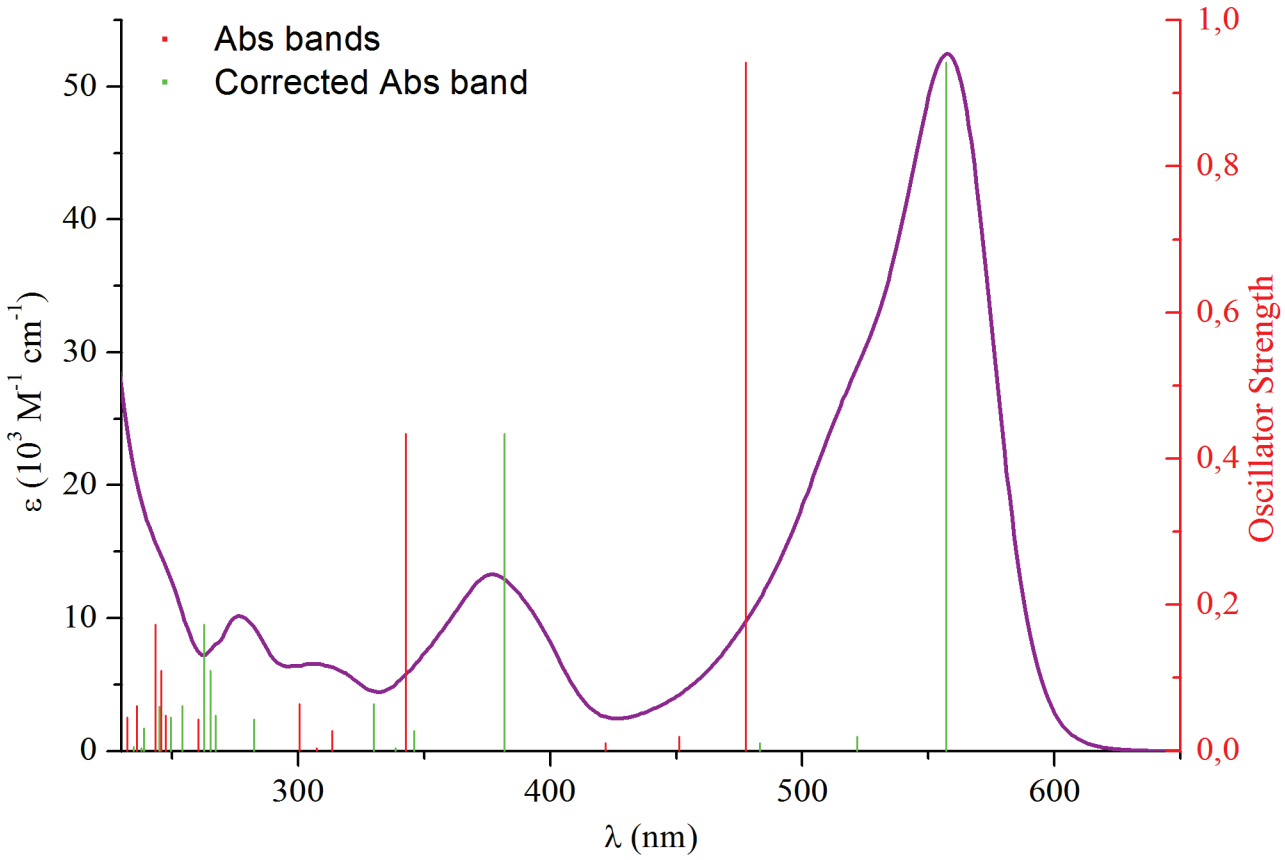

Table S.15 - Assignment of optical absorption bands for BbF **7** based on TD-DFT calculations

λ, nm				
Observed (ε, x10^3 $M^{-1}cm^{-1}$)	**Calculated** (Osc. Strength)	**Corr.**	**Trans. No.**	**Major contributions to excitation**
557 (52)	477 (0.942)	557	T1	H (99%) -> L
522 (29)	451 (0.020)	522	T2	H-2 (97%) -> L
	422 (0.011)	483	T3	H-1 (98%) -> L
377 (13)	343 (0.434)	382	T4	H-4 (19%), H-3 (77%) -> L
	314 (0.027)	346	T5	H-6 (44%), H-5 (36%), H-4 (16%) -> L
	308 (0.004)	339	T6	H-5 (54%), H-4 (31%) -> L
307 (6.5)	300 (0.065)	330	T7	H-6 (46%), H-4 (29%), H-3 (14%) -> L
	260 (0.044)	282	T8	H-7 (87%) -> L
277 (10)	248 (0.049)	267	T9	H-1 (64%) -> L+1; H-1 (12%) -> L+4
	246 (0.110)	265	T10	H (80%) -> L+1

Table S.16 – NTO analysis for BbF **7** absorption bands T1 to T10 obtained by TD-DFT (Isovalue = 0.02; PCM = CH_2Cl_2)

Transition / Eigenvalue	**NTO Hole "From"**	**NTO Particle "To"**	**Transition / Eigenvalue**	**NTO Hole "From"**	**NTO Particle "To"**
T1 / 0.99	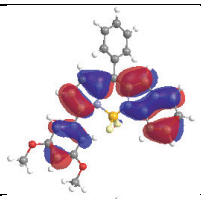	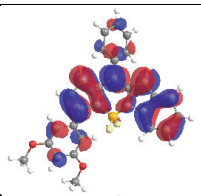	T6 / 0.94	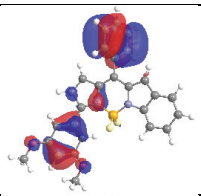	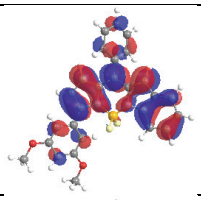
T2 / >0.99	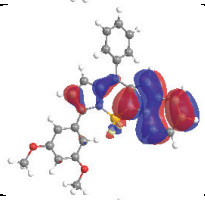	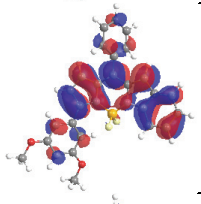	T7 / 0.93	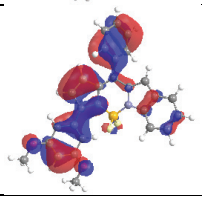	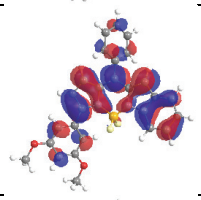
T3 / 0.99	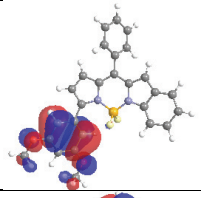	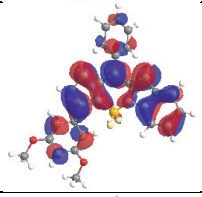	T8 / 0.90	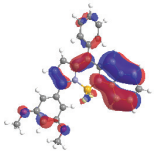	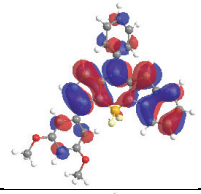
T4 / 0.99	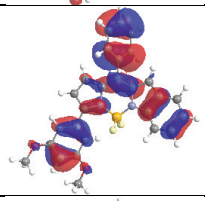	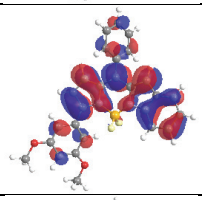	T9 / 0.86	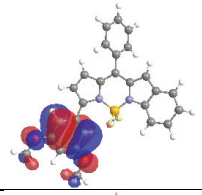	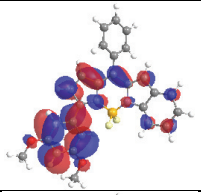
T5 / 0.99	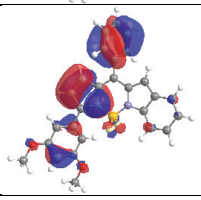	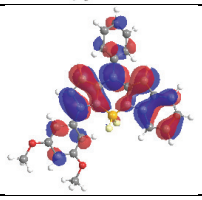	T10 / 0.95	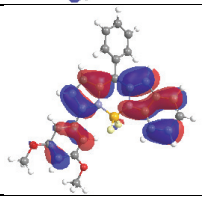	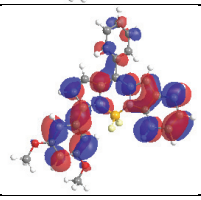

Figure S.70 – BbF **8** experimental absorption spectrum in CH_2Cl_2 vs TD-DFT calculated optical absorption bands (Red = uncorrected; Green = corrected; PCM = CH_2Cl_2).

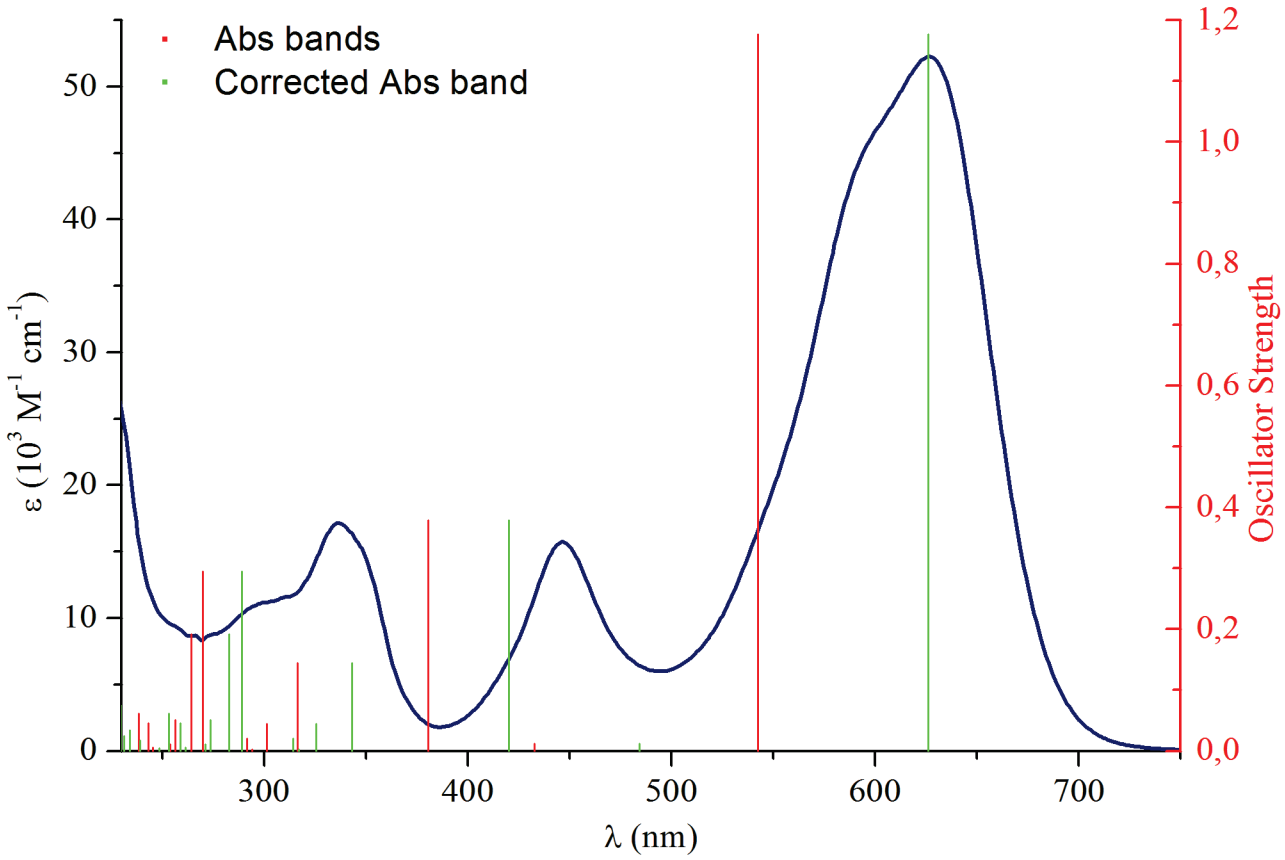

Table S.17 - Assignment of optical absorption bands for BbF **8** based on TD-DFT calculations

λ, nm				
Observed (ε, x10^3 $M^{-1}cm^{-1}$)	**Calculated** (Osc. Strength)	**Corr.**	**Trans. No.**	**Major contributions to excitation**
626 (52)	542 (1.177)	626	T1	H (98%) -> L
597 (46)	---	---	---	
446 (16)	433 (0.013)	484	T2	H-2 (18%), H-1 (81%) -> L
	381 (0.379)	420	T3	H-2 (77%), H-1 (18%) -> L
336 (17)	317 (0.145)	343	T4	H-3 (94%) -> L
	301 (0.045)	325	T5	H-6 (52%), H-5 (28%), H-4 (17%) -> L
	294 (0.003)	317	T6	H-5 (58%), H-4 (31%) -> L
301 (11)	292 (0.021)	314	T7	H-6 (40%), H-5 (12%), H-4 (40%) -> L
	270 (0.295)	289	T8	H (72%) -> L+1; H (15%) -> L+4
	264 (0.191)	283	T9	H (17%) -> L+1; H (61%) -> L+4
	256 (0.051)	274	T10	H-7 (88%) -> L

Table S.18 – NTO analysis for BbF **8** absorption bands T1 to T10 obtained by TD-DFT (Isovalue = 0.02; PCM = CH_2Cl_2)

Transition / Eigenvalue	**NTO Hole "From"**	**NTO Particle "To"**		**Transition / Eigenvalue**	**NTO Hole "From"**	**NTO Particle "To"**
T1 / 0.99	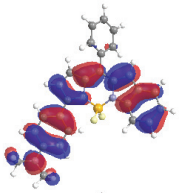	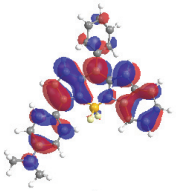		T6 / 0.94	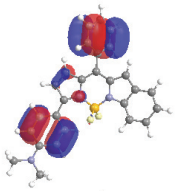	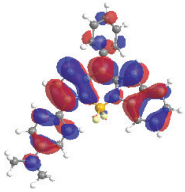
T2 / >0.99	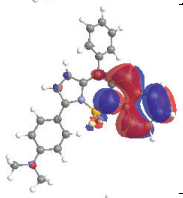	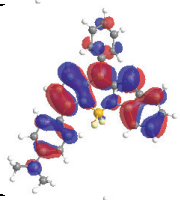		T7 / 0.93	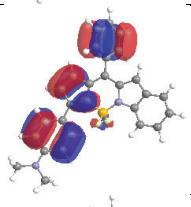	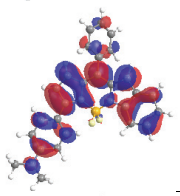
T3 / 0.99	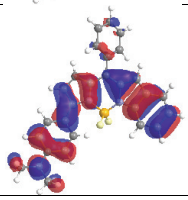	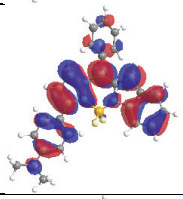		T8 / 0.90	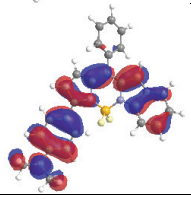	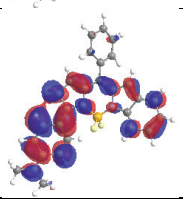
T4 / 0.99	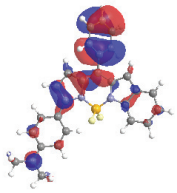	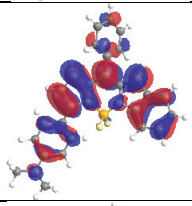		T9 / 0.86	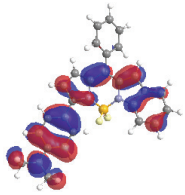	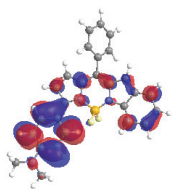
T5 / 0.99	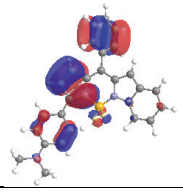	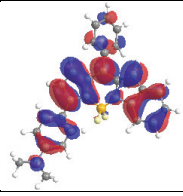		T10 / 0.95	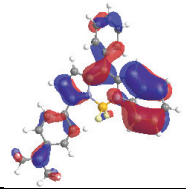	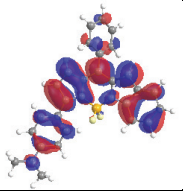

Figure S.71 – BbF **9** experimental absorption spectrum in CH_2Cl_2 vs TD-DFT calculated optical absorption bands (Red = uncorrected; Green = corrected; PCM = CH_2Cl_2).

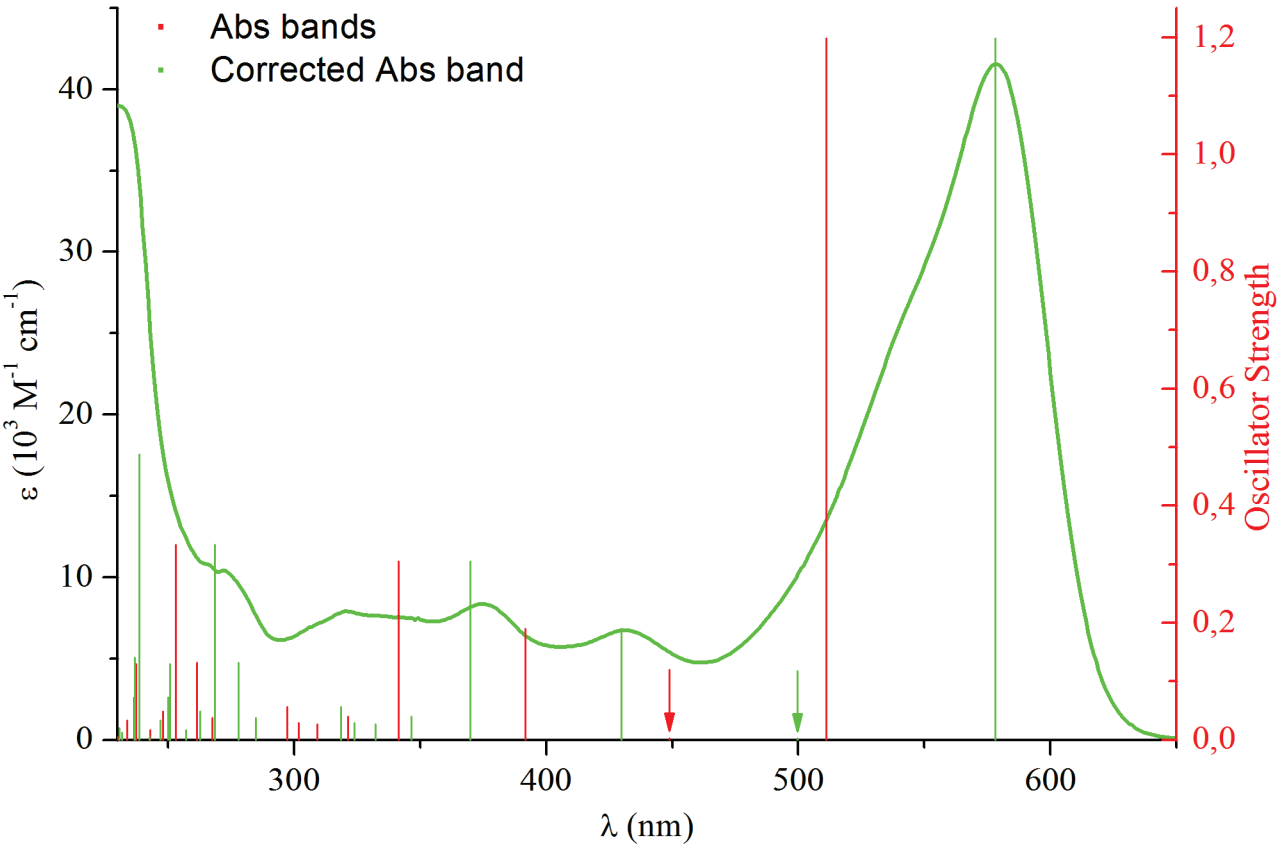

Table S.19 - Assignment of optical absorption bands for BbF **9** based on TD-DFT calculations

λ, nm				
Observed (ε, x10^3 $M^{-1}cm^{-1}$)	**Calculated** (Osc. Strength)	**Corr.**	**Trans. No.**	**Major contributions to excitation**
578 (42)	511 (1.198)	578	T1	H (97%) -> L
548 (28)	449 (0.002)	500	T2	H-2 (27%), H-1 (71%) -> L
431 (6.7)	392 (0.191)	430	T3	H-2 (67%), H-1 (27%) -> L
375 (8.3)	341 (0.305)	370	T4	H-4 (20%), H-3 (73%) -> L
321 (7.9)	321 (0.040)	347	T5	H-4 (71%), H-3 (15%) -> L
	309 (0.027)	332	T6	H-6 (31%), H-5 (63%) -> L
	302 (0.029)	324	T7	H-6 (57%), H-5 (34%) -> L
	297 (0.056)	319	T8	H (72%) -> L+1
272 (10)	268 (0.038)	285	T9	H-3 (25%) -> L+1; H (47%) -> L+2
	262 (0.132)	278	T10	H-8 (12%), H-7 (80%) -> L

Table S.20 – NTO analysis for BbF **9** absorption bands T1 to T10 obtained by TD-DFT (Isovalue = 0.02; PCM = CH_2Cl_2)

Transition / Eigenvalue	**NTO Hole "From"**	**NTO Particle "To"**	**Transition / Eigenvalue**	**NTO Hole "From"**	**NTO Particle "To"**
T1 / 0.99	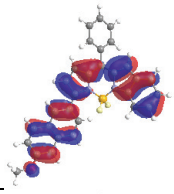	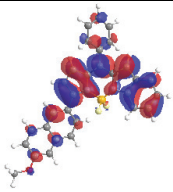	T6 / 0.97	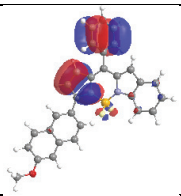	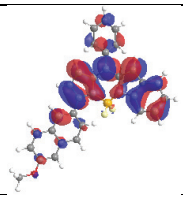
T2 / >0.99	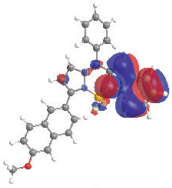	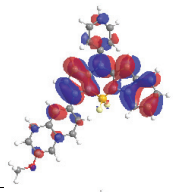	T7 / 0.92	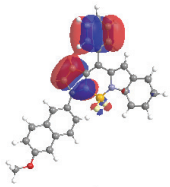	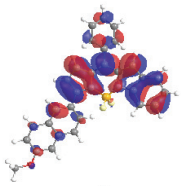
T3 / 0.99	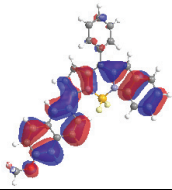	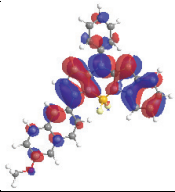	T8 / 0.81	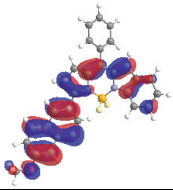	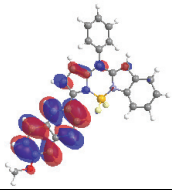
T4 / 0.96	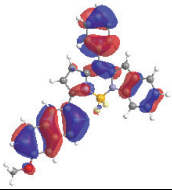	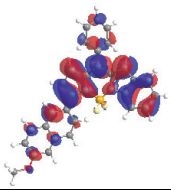	T9 / 0.65	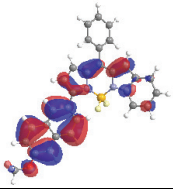	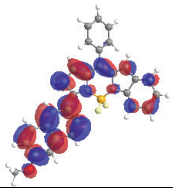
T5 / 0.93		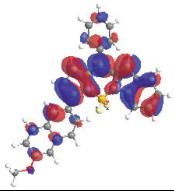	T10 / 0.95	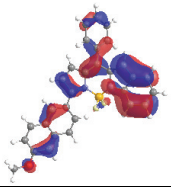	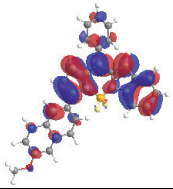

Figure S.72 – BbF **10** experimental absorption spectrum in CH_2Cl_2 vs TD-DFT calculated optical absorption bands (Red = uncorrected; Green = corrected; PCM = CH_2Cl_2).

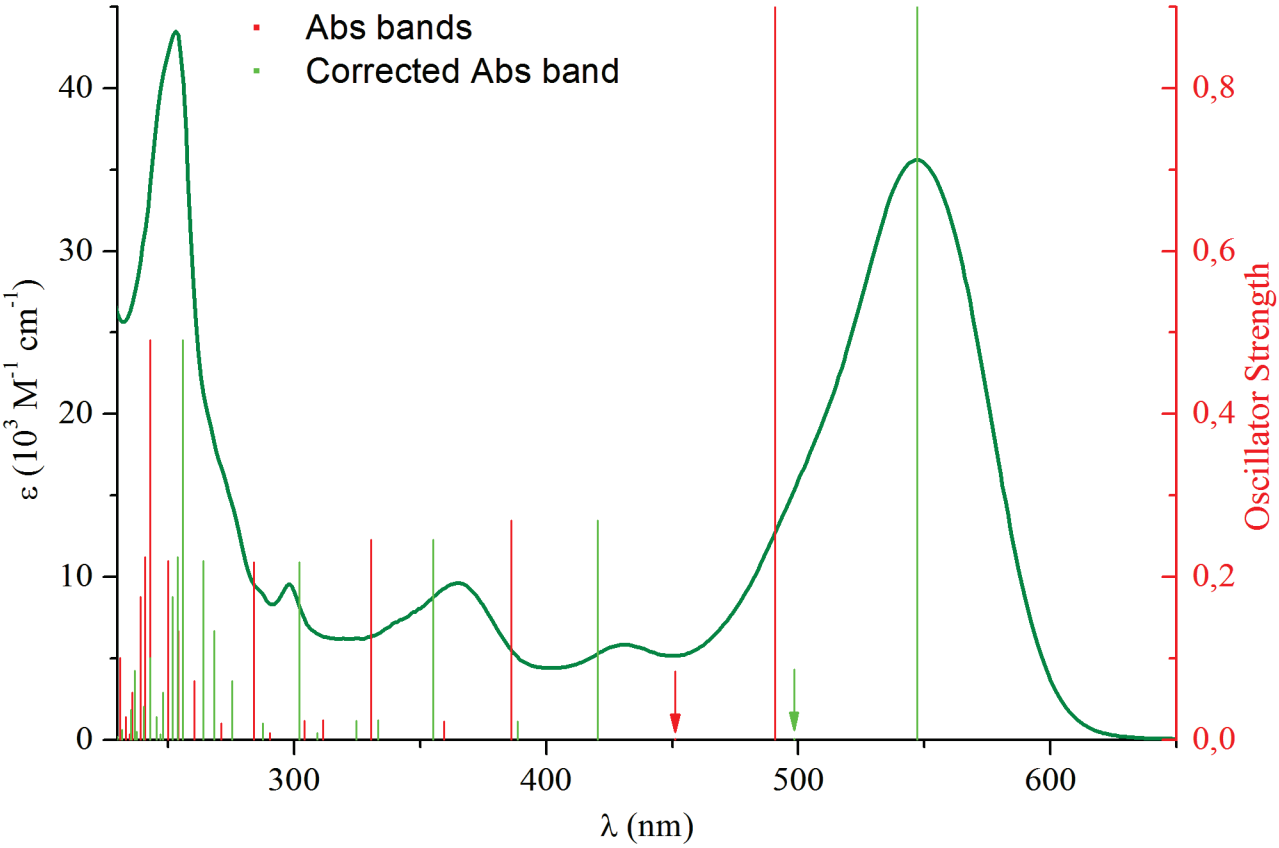

Table S.21 - Assignment of optical absorption bands for BbF **10** based on TD-DFT calculations

λ, nm				
Observed (ε, x10^3 $M^{-1}cm^{-1}$)	**Calculated** (Osc. Strength)	**Corr.**	**Trans. No.**	**Major contributions to excitation**
547 (36)	491 (0.901)	547	T1	H (97%) -> L
511 (20)	451 (0.001)	498	T2	H-1 (83%) -> L
431 (5.8)	386 (0.269)	420	T3	H-3 (32%), H-2 (49%), H-1 (16%) -> L
365 (9.6)	359 (0.022)	389	T4	H-3 (58%), H-2 (38%) -> L
	330 (0.246)	355	T5	H-4 (95%) -> L
	312 (0.024)	333	T6	H-7 (33%), H-5 (62%) -> L
	304 (0.023)	325	T7	H-7 (49%), H-6 (13%), H-5 (36%) -> L
298 (9.5)	290 (0.008)	309	T8	H-3 (15%), H-2 (17%) -> L+1
				H-1 (11%), H (38%) -> L+2
	284 (0.218)	302	T9	H (73%) -> L+1
273 (16)	271 (0.020)	287	T10	H-7 (14%), H-6 (77%) -> L

Table S.22 – NTO analysis for BbF **10** absorption bands T1 to T10 obtained by TD-DFT (Isovalue = 0.02; PCM = CH_2Cl_2)

Transition / Eigenvalue	**NTO Hole "From"**	**NTO Particle "To"**	**Transition / Eigenvalue**	**NTO Hole "From"**	**NTO Particle "To"**
T1 / 0.99	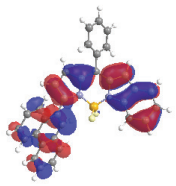	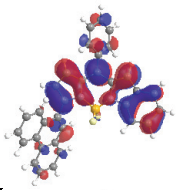	T6 / 0.99	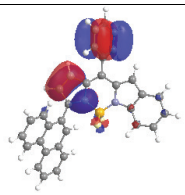	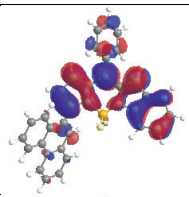
T2 / >0.99	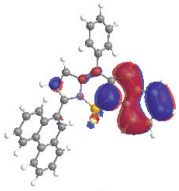	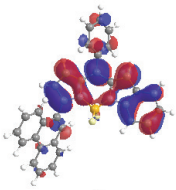	T7 / 0.99	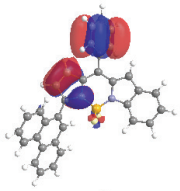	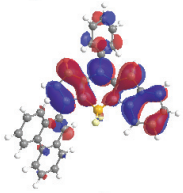
T3 / 0.99	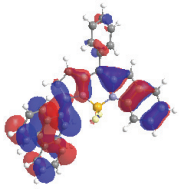	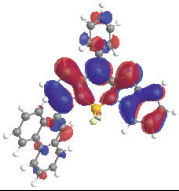	T8 / 0.63	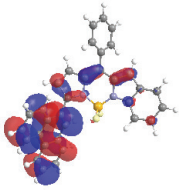	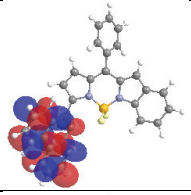
T4 / 0.99	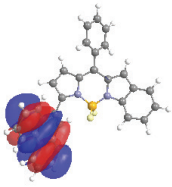	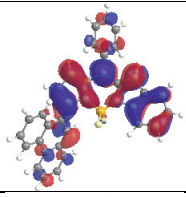	T9 / 0.88	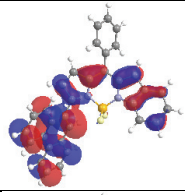	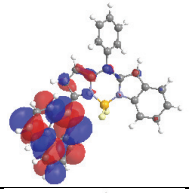
T5 / 0.99	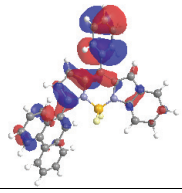	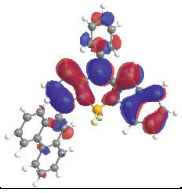	T10 / 0.96	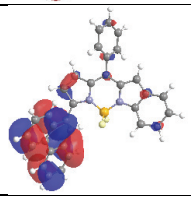	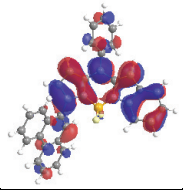

Table S.23 – Selected bond lengths (Å) and angles (°) for BbF **1**, **5**, **8** and **9** calculated by DFT.[a]

	1	**5**	**8**	**9** [b]
Bond lengths				
F1-B1	1.396 (-0.001)	1.397 (+0.004)	1.399 (-0.004)	1.397 (+0.016)
F2-B1	1.383 (+0.005)	1.384 (=)	1.386 (=)	1.384 (-0.018)
N1-B1	1.532 (-0.005)	1.531 (-0.003)	1.530 (+0.001)	1.532 (+0.010)
N2-B1	1.566 (-0.002)	1.565 (-0.002)	1.562 (-0.009)	1.565 (-0.007)
N1-C1	1.361 (-0.011)	1.362 (-0.014)	1.364 (-0.014)	1.361 (-0.014)
N1-C8	1.377 (-0.010)	1.377 (-0.004)	1.376 (-0.007)	1.377 (-0.014)
N2-C10	1.393 (-0.013)	1.394 (-0.021)	1.396 (-0.012)	1.394 (-0.010)
N2-C13	1.345 (-0.002)	1.346 (-0.013)	1.351 (-0.008)	1.346 (-0.001)
C8-C9	1.412 (-0.014)	1.414 (-0.011)	1.418 (-0.014)	1.413 (-0.016)
C9-C10	1.385 (+0.003)	1.382 (=)	1.378 (-0.003)	1.384 (=)
C13-C14	1.462 (-0.008)	1.454 (-0.012)	1.444 (-0.008)	1.457 (-0.010)
C_{Subst}-O1/N3	---	1.344 (-0.064)	1.355 (-0.003)	1.349 (-0.015)
Angles				
C1-N1-B1	126.6 (-0.1)	126.5 (+0.1)	126.2 (+0.6)	126.4 (-0.2)
C13-N2-B1	129.4 (+0.5)	129.5 (-0.6)	129.6 (+0.1)	129.4 (+0.5)
F1-B1-F2	110.1 (-0.4)	109.9 (+0.4)	109.6 (-0.3)	110.0 (-0.2)
F1-B1-N1	109.3 (-0.9)	109.3 (-0.2)	109.1 (-0.4)	109.3 (-2.0)
F1-B1-N2	109.4 (+1.1)	109.5 (-0.9)	109.8 (=)	109.5 (-1.5)
F2-B1-N1	110.6 (+0.1)	110.6 (+1.5)	110.4 (-0.3)	110.6 (+1.2)
F2-B1-N2	110.5 (-0.3)	110.5 (-0.9)	110.5 (+0.7)	110.4 (+2.2)
N1-B1-N2	106.9 (+0.5)	107.0 (-0.3)	107.4 (+0.3)	107.0 (+0.3)
Tilt angles between planes of the pyrrole and the benzo[b]-fused pyrrolic rings				
	8.9 (-6.4)	8.8 (-1.5)	7.5 (+3.3)	8.9 (-1.0)
Tilt angle between planes of the pyrrole ring and proximal aryl				
	36.3 (-0.7)	32.3	25.9 (-3.3)	33.3 (+9.6)
Tilt angles between the DPM moiety and the aryl rings				
meso-Ph	57.6 (+9.3)	58.0 (+6.9)	58.4 (+6.2)	57.4 (+10)
Ar proximal	40.5 (-2.8)	36.6 (+8.9)	29.6 (-2.7)	37.5 (-10.3)

[a] Atom numbering following the one used for X-ray crystallography (Refer to Figure 6). Difference with corresponding X-ray structure given in parenthesis. [b] Atom numbering following the one used for X-ray crystallography, except for F1 assigned to the fluoride doing an H-bond with H19 in order to be consistent with other calculated structures.

Table S.24 – Selected bond lengths (Å) and angles (°) for BbF **2-4**, **6**, **7** and **10** calculated by DFT.

	2	**3**	**4**	**6**	**7**	**10**
Bond lengths						
F1-B1	1.396	1.396	1.396	1.396	1.395	1.394
F2-B1	1.383	1.383	1.383	1.382	1.382	1.382
N1-B1	1.532	1.532	1.532	1.533	1.534	1.535
N2-B1	1.565	1.566	1.566	1.566	1.567	1.565
N1-C1	1.361	1.361	1.361	1.361	1.360	1.360
N1-C8	1.377	1.377	1.377	1.377	1.377	1.378
N2-C10	1.394	1.394	1.394	1.393	1.393	1.392
N2-C13	1.345	1.345	1.345	1.345	1.344	1.341
C8-C9	1.412	1.413	1.413	1.412	1.412	1.412
C9-C10	1.385	1.384	1.384	1.385	1.385	1.386
C13-C14	1.459	1.459	1.459	1.463	1.464	1.467
C_{Subst}-O1/N3	1.498	1.510	1.525	1.352	1.351/2	---
Angles						
C1-N1-B1	126.5	126.6	126.5	126.4	126.4	126.5
C13-N2-B1	129.4	129.4	129.4	129.3	129.4	128.4
F1-B1-F2	110.1	110.1	110.1	110.2	110.3	110.2
F1-B1-N1	109.3	109.3	109.3	109.2	109.2	109.4
F1-B1-N2	109.4	109.4	109.4	109.5	109.5	109.6
F2-B1-N1	110.6	110.6	110.6	110.5	110.5	110.9
F2-B1-N2	110.5	110.5	110.5	110.5	110.5	110.3
N1-B1-N2	106.9	106.9	106.9	106.9	106.8	106.4
Tilt angles between planes of the pyrrole and the benzo[b]-fused pyrrolic rings						
	8.8	8.9	8.8	8.6	8.8	8.7
Tilt angle between planes of the pyrrole ring and proximal aryl						
	34.7	35.0	34.7	37.0	37.8	57.8
Tilt angles between the DPM moiety and the aryl rings						
meso-Ph	57.7	57.7	57.7	57.5	58.1	57.0
Ar proximal	38.9	39.3	38.9	41.0	42.0	61.6

Table S.25 – Intramolecular H-bonding for BbF **1**, **5**, **8** and **9** calculated by DFT.[a]

D-H···A	**D-H**	**H···A**	**D···A**	**< D-H···A**
1				
C19-H19···F1	1.081	2.124	3.219	143.2
2				
C19-H19···F1	1.081	2.119	3.058	143.6
3				
C19A-H19A···F1	1.081	2.121	3.216	143.7
4				
C19-H19···F1	1.081	2.120	3.059	143.7
5				
C19A-H19A···F1	1.081	2.102	3.050	144.8
6				
C19-H19···F2	1.080	2.123	3.049	142.1
7				
C19-H19···F2	1.080	2.126	3.042	141.0
8				
C19-H19···F1	1.080	2.082	3.041	146.3
9				
C19-H19···F2	1.081	2.102	3.051	145.0
10				
C19-H19···F2	1.083	2.259	3.025	126.0

[a] Distances in Å and angles in °.

X-ray Diffraction Measurements and Structure Determination

Crystallographic data were collected at 100 K for **1** and at 105K for **5**, **8** and **9** from single crystal samples that were mounted on a loop fiber (refer to Synthetic Methods section for specific crystallization conditions). Data were collected using a Bruker D8 Venture diffractometer configured with a Metal Jet liquid-metal source (Ga Kα λ=1.34Å), a Helios MX Mirror optics and a Photon 100 CMOS-based area detector. The crystal-to-detector distance was 4.0 cm and the data collection was carried out in 1024 x 1024 pixel mode. The initial unit cell parameters were determined by a least-squares fit of the angular setting of strong reflections, collected by a 52.0 degree scan in 104 frames over three different parts of the reciprocal space.

For data collection, determination of cell parameters, cell refinement, and data reduction *APEX2* and *SAINT* were used.[35] Absorption corrections were applied using *SADABS*.[36] Structure solution was performed using direct methods with *SHELXT* and refined on F^2 by full-matrix least squares using *SHELXL2014*.[37, 38] The absence of twinning was investigated using TWINRotMat from PLATON.[39] The material was prepared for publication using Mercury and *OLEX2*.[40, 41] Figures were generated using ORTEP3 and POV-Ray.[42, 43]

For all the structures, all non-H atoms were refined by full-matrix least-squares with anisotropic displacement parameters. The H-atoms were included in calculated positions and treated as riding atoms: aromatic C—H 0.95 Å, methyl C—H 0.98 Å, with $U_{iso}(H) = k \times U_{eq}$ (parent C-atom), where k = 1.2 for the aromatic H-atoms and 1.5 for the methyl H-atoms.

Excellent sets of data were obtained for the four compounds. The use of the SIMU restraint was necessary for BbF **5** in order to model the disordered *para*-methoxyphenyl pointing toward each of the two fluoride atoms as two components and the occupancy of each part was determined to be in a 53:47 ratio using a least-square refined free variable.

Data were deposited in CCDC under the deposit numbers: CCDC 1418610 – 1418613. The alerts given by the checkCIF/ PLATON routine are commented in the crystallographic information files (cifs) of the corresponding compounds.

Table S.26 – Solid-state structure and refinement data for BbF **1**, **5**, **8** and **9**.

	1	**5**	**8**	**9**
Empirical formula	$C_{25}H_{17}BN_2F_2$	$C_{26}H_{19}BF_2N_2O$	$C_{27}H_{22}BF_2N_3$	$C_{30}H_{21}BF_2N_2O$
Formula weight	394.21	424.24	437.28	474.30
Temperature (K)	100	105	105	105
Crystal system	orthorhombic	monoclinic	orthorhombic	orthorhombic
Space group	Pbca	$P2_1/c$	$P2_12_12_1$	$Pna2_1$
Unit Cell: *a* (Å)	12.2509(7)	20.5702(9)	7.5580(2)	7.6330(2)
b (Å)	7.8383(4)	12.2670(5)	10.8156(3)	18.6828(4)
c (Å)	39.829(2)	7.9969(4)	25.7212(8)	15.7103(4)
α (°)	90	90	90	90
β (°)	90	99.415(3)	90	90
γ (°)	90	90	90	90
V (Å^3)	3824.6(4)	1990.7(2)	2102.6(1)	2240.4(1)
Z	8	4	4	4
d_{calc} (g/cm^3)	1.369	1.416	1.381	1.406
μ (mm^{-1})	0.489	0.521	0.488	0.504
F(000)	1632.0	880.0	912.0	984.0
2θ range (°)	3.86 to 121.356	7.326 to 121.666	5.978 to 121.31	6.396 to 121.202
Reflections collected	38065	30340	33147	34104
Independent reflections	4375	4579	4803	5130
GoF	1.043	1.025	1.047	1.073
Final R indexes [I>=2σ (I)]	R_1 = 0.0488, wR_2 = 0.1122	R_1 = 0.0504, wR_2 = 0.1160	R_1 = 0.0277, wR_2 = 0.0721	R_1 = 0.0304, wR_2 = 0.0644
Final R indexes [all data]	R_1 = 0.0685, wR_2 = 0.1215	R_1 = 0.0717, wR_2 = 0.1287	R_1 = 0.0278, wR_2 = 0.0723	R_1 = 0.0360, wR_2 = 0.0664
Largest diff. peak and hole (e/Å^3)	0.39 and -0.19	0.36 and -0.48	0.25 and -0.16	0.20 and -0.12
Flack parameter	---	---	0.025(17)	0.03(6)

Table S.27 – Selected bond lengths (Å) and angles (°) for BbF **1**, **5**, **8** and **9**.

	1	**5**	**8**	**9**
Bond lengths (Å)				
F1-B1	1.397(2)	1.393(2)	1.403(2)	1.381(3)
F2-B1	1.378(2)	1.384(2)	1.386(2)	1.402(2)
N1-B1	1.537(2)	1.534(2)	1.529(2)	1.522(3)
N2-B1	1.568(2)	1.567(2)	1.571(2)	1.572(3)
N1-C1	1.372(2)	1.376(2)	1.378(2)	1.375(2)
N1-C8	1.387(2)	1.381(2)	1.383(2)	1.391(2)
N2-C10	1.406(2)	1.415(2)	1.408(2)	1.404(2)
N2-C13	1.347(2)	1.359(2)	1.359(2)	1.347(3)
C8-C9	1.426(2)	1.425(2)	1.432(2)	1.429(2)
C9-C10	1.382(2)	1.382(2)	1.381(2)	1.384(3)
C13-C14	1.470(2)	1.466(2)	1.452(2)	1.467(3)
C-X in proximal Ar	---	1.408(2) (C17-01)	1.358(2) (C17-N3)	1.364(3) (C22-O1)
Angles (°)				
C1-N1-B1	126.7(1)	126.4(1)	125.6(1)	126.6(2)
C13-N2-B1	128.9(1)	130.1(1)	129.5(1)	128.9(2)
F1-B1-F2	110.5(1)	109.5(1)	109.9(1)	110.2(2)
F1-B1-N1	110.2(1)	110.6(1)	109.5(1)	111.3(2)
F1-B1-N2	108.3(1)	109.0(1)	109.8(1)	111.0(2)
F2-B1-N1	110.5(1)	109.1(1)	110.7(1)	109.4(2)
F2-B1-N2	110.8(1)	111.4(1)	109.8(1)	108.2(2)
N1-B1-N2	106.4(1)	107.3(1)	107.1(1)	106.7(2)
Dihedral angles (°)				
C12-C13-C14-C15	-34.6(2)	-18.9(4) / 11.6(3) [a]	-27.7(2)	39.5(3)
C8-C9-C_i-C_j	49.3(2) (C20-C21)	49.6(2) (C21-C22)	53.3(2) (C22-C23)	-49.0(2) (C25-C26)
Tilt angles (°) between planes of the pyrrole and the benzo[b]-fused pyrrolic rings				
	15.3(1)	10.3(1)	4.2(1)	9.9(1)
Tilt angle (°) between planes of the pyrrole ring and proximal aryl				
	37.0(1)	23.0(2) / 18.4(1) [a]	29.2(1)	42.9(1)
Tilt angles (°) between the DPM moiety and aryl rings				
meso-Ph	48.3(1)	51.1(1)	52.2(1)	47.4(1)
Ar proximal	43.3(1)	27.7(2) / 14.1(1) [a]	32.3(1)	47.8(1)

[a] Two angles given, corresponding to the two disordered positions of the *para*-methoxyphenyl.

Table S.28 – Intramolecular H-bonding for BbF **1**, **5**, **8** and **9**.

D-H···A	**D-H**	**H···A**	**D···A**	**< D-H···A**
1				
C19-H19···F1	0.950	2.352(1)	3.166(2)	143.5(1)
5				
C19A-H19A···F1	0.950	2.080(1)	2.948(4)	150.7(2)
C19B-H19B···F2	0.950	1.933(1)	2.788(5)	148.5(2)
8				
C19-H19···F1	0.950	2.227(1)	3.077(2)	148.4(1)
9				
C19-H19···F2	0.950	2.351(1)	3.137(2)	139.8(1)

[a] Distances in Å and angles in °.

References

1. Wakamiya, A.; Murakami, T.; Yamaguchi, S., *Chem. Sci.* **2013,** *4*, 1002-1007.
2. Rieth, R. D.; Mankad, N. P.; Calimano, E.; Sadighi, J. P., *Org. Lett.* **2004,** *6*, 3981-3983.
3. Verdoes, M.; Hillaert, U.; Florea, B. I.; Sae-Heng, M.; Risseeuw, M. D. P.; Filippov, D. V.; van der Marel, G. A.; Overkleeft, H. S., *Bioorg. Med. Chem. Lett.* **2007,** *17*, 6169-6171.
4. Wen, J.; Qin, S.; Ma, L.-F.; Dong, L.; Zhang, J.; Liu, S.-S.; Duan, Y.-S.; Chen, S.-Y.; Hu, C.-W.; Yu, X.-Q., *Org. Lett.* **2010,** *12*, 2694-2697.
5. Aliev, I. A.; Almamedova, D. T.; Gasanov, B. R.; Mikhaleva, A. I., *Chem. Heterocycl. Compd.* **1984,** *20*, 1117-1119.
6. Ohri, R. V.; Radosevich, A. T.; Hrovat, K. J.; Musich, C.; Huang, D.; Holman, T. R.; Toste, F. D., *Org. Lett.* **2005,** *7*, 2501-2504.
7. Gao, W.-C.; Jiang, S.; Wang, R.-L.; Zhang, C., *Chem. Commun.* **2013,** *49*, 4890-4892.
8. Connelly, N. G.; Geiger, W. E., *Chem. Rev.* **1996,** *96*, 877-910.
9. Le Guennic, B.; Maury, O.; Jacquemin, D., *Phys. Chem. Chem. Phys.* **2012,** *14*, 157-164.
10. Frisch, M. J.; Trucks, G. W.; Schlegel, H. B.; Scuseria, G. E.; Robb, M. A.; Cheeseman, J. R.; Scalmani, G.; Barone, V.; Mennucci, B.; Petersson, G. A.; Nakatsuji, H.; Caricato, M.; Li, X.; Hratchian, H. P.; Izmaylov, A. F.; Bloino, J.; Zheng, G.; Sonnenberg, J. L.; Hada, M.; Ehara, M.; Toyota, K.; Fukuda, R.; Hasegawa, J.; Ishida, M.; Nakajima, T.; Honda, Y.; Kitao, O.; Nakai, H.; Vreven, T.; J. A. Montgomery, J.; Peralta, J. E.; Ogliaro, F.; Bearpark, M.; Heyd, J. J.; Brothers, E.; Kudin, K. N.; Staroverov, V. N.; Kobayashi, R.; Normand, J.; Raghavachari, K.; Rendell, A.; Burant, J. C.; Iyengar, S. S.; Tomasi, J.; Cossi, M.; Rega, N.; Millam, J. M.; Klene, M.; Knox, J. E.; Cross, J. B.; Bakken, V.; Adamo, C.; Jaramillo, J.; Gomperts, R.; Stratmann, R. E.; Yazyev, O.; Austin, A. J.; Cammi, R.; Pomelli, C.; Ochterski, J. W.; Martin, R. L.; Morokuma, K.; Zakrzewski, V. G.; Voth, G. A.; Salvador, P.; Dannenberg, J. J.; Dapprich, S.; Daniels, A. D.; Farkas, Ö.; Foresman, J. B.; Ortiz, J. V.; Cioslowski, J.; Fox, D. J. *Gaussian 09 Revision D.01*, Gaussian Inc.: Wallingford CT 2009.
11. Perdew, J. P.; Burke, K.; Ernzerhof, M., *Phys. Rev. Lett.* **1996,** *77*, 3865-3868.
12. Perdew, J. P.; Burke, K.; Ernzerhof, M., *Phys. Rev. Lett.* **1997,** *78*, 1396.
13. Adamo, C.; Barone, V., *J. Chem. Phys.* **1999,** *110*, 6158-6169.
14. Tomasi, J.; Mennucci, B.; Cammi, R., *Chem. Rev.* **2005,** *105*, 2999-3093.
15. Boese, A. D.; Martin, J. M. L., *J. Chem. Phys.* **2004,** *121*, 3405-3416.
16. Dennington, R.; Keith, T.; Millam, J.; Eppinnett, K.; Hovell, W. L.; Gilliland, R. *GaussView Version 3.09*, Semichem Inc.: Shawnee Mission KS, 2003.
17. O'Boyle, N. M.; Tenderholt, A. L.; Langner, K. M., *J. Comp. Chem.* **2008,** *29*, 839-845.
18. Chemissian, a computer program to analyze and visualize quantum-chemical calculations, by L. Skripnikov. For the current version, see http://www.chemissian.com
19. Lakshmi, V.; Shaikh, M.; Ravikanth, M., *J. Fluoresc.* **2013,** *23*, 519-525.
20. Richards, V. J.; Gower, A. L.; Smith, J. E. H. B.; Davies, E. S.; Lahaye, D.; Slater, A. G.; Lewis, W.; Blake, A. J.; Champness, N. R.; Kays, D. L., *Chem. Commun.* **2012,** *48*, 1751-1753.
21. Yu, C.; Jiao, L.; Yin, H.; Zhou, J.; Pang, W.; Wu, Y.; Wang, Z.; Yang, G.; Hao, E., *Eur. J. Org. Chem.* **2011,** 5460-5468.
22. Wang, L.; Zhang, Y.; Xiao, Y., *RSC Adv.* **2013,** *3*, 2203-2206.
23. Ni, Y.; Zeng, W.; Huang, K.-W.; Wu, J., *Chem. Commun.* **2013,** *49*, 1217-1219.
24. Guzow, K.; Kornowska, K.; Wiczk, W., *Tetrahedron Lett.* **2009,** *50*, 2908-2910.
25. Gabe, Y.; Ueno, T.; Urano, Y.; Kojima, H.; Nagano, T., *Anal. Bioanal. Chem.* **2006,** *386*, 621-626.

26. Wang, L.; Verbelen, B.; Tonnele, C.; Beljonne, D.; Lazzaroni, R.; Leen, V.; Dehaen, W.; Boens, N., *Photochem. Photobiol. Sci.* **2013,** *12*, 835-847.
27. Verbelen, B.; Boodts, S.; Hofkens, J.; Boens, N.; Dehaen, W., *Angew. Chem., Int. Ed.* **2015,** *54*, 4612-4616.
28. Yu, C.; Xu, Y.; Jiao, L.; Zhou, J.; Wang, Z.; Hao, E., *Chem. Eur. J.* **2012,** *18*, 6437-6442.
29. Tomimori, Y.; Okujima, T.; Yano, T.; Mori, S.; Ono, N.; Yamada, H.; Uno, H., *Tetrahedron* **2011,** *67*, 3187-3193.
30. Umezawa, K.; Matsui, A.; Nakamura, Y.; Citterio, D.; Suzuki, K., *Chem. Eur. J.* **2009,** *15*, 1096-1106.
31. Umezawa, K.; Nakamura, Y.; Makino, H.; Citterio, D.; Suzuki, K., *J. Am. Chem. Soc.* **2008,** *130*, 1550-1551.
32. Maeda, C.; Todaka, T.; Ema, T., *Org. Lett.* **2015,** *17*, 3090-3093.
33. Bochkov, A. Y.; Akchurin, I. O.; Dyachenko, O. A.; Traven, V. F., *Chem. Commun.* **2013,** *49*, 11653-11655.
34. Zatsikha, Y. V.; Yakubovskyi, V. P.; Shandura, M. P.; Dubey, I. Y.; Kovtun, Y. P., *Tetrahedron* **2013,** *69*, 2233-2238.
35. Bruker *APEX2 and SAINT*, Bruker AXS Inc.: Madison, Wisconsin, USA., 2007.
36. Bruker *SADABS and TWINABS*, Bruker AXS Inc.: Madison, Wisconsin, USA., 2001.
37. Sheldrick, G. M., *Acta Crystallogr., Sect. A* **2008,** *64*, 112-122.
38. Sheldrick, G. M., *Acta Crystallogr., Sect. A* **2015,** *71*, 3-8.
39. Spek, A. L., *Acta Crystallogr., Sect. D* **2009,** *65*, 148-155.
40. CCDC *Mercury 3.1 - 3.3*, 2001-2013.
41. Dolomanov, O. V., Bourhis, L. J., Gildea, R. J., Howard, J. A. K., Puschmann, H., *J. Appl. Cryst.* **2009,** *42*, 339-341.
42. Farrugia, L. J., *J. Appl. Crystallogr.* **1997,** *30*, 565.
43. *POV-Ray* Persistence of Vision Pty. Ltd., retrieved from http://www.povray.org/download/: 2004.